To the Graduate Council:

I am submitting herewith a dissertation written by Spyros Michael Spyrou entitled "Attachment of Low-Energy Electrons (0-10 eV) to Polyatomic Molecules." I have examined the final copy of this dissertation for form and content and recommend that it be accepted in partial fulfillment of the requirements for the degree of Doctor of Philosophy, with a major in Physics.

L. G. Christophorou

L. G. Christophorou, Major Professor

We have read this dissertation and recommend its acceptance:

Sivata Mukherjee

Linda R. Painter

T. Franklin Williams

Solon Georghiou

Accepted for the Council:

Carolyn Swinkel

The Graduate School

# ATTACHMENT OF LOW-ENERGY ELECTRONS (0-10 eV) TO POLYATOMIC MOLECULES

A Dissertation

Presented for the

Doctor of Philosophy

Degree

The University of Tennessee, Knoxville

Spyros Michael Spyrou

December 1983

To my wife Chrysanthi

and my daughters Marina and Sophia

ACKNOWLEDGMENTS

I would like to express my sincere thanks to Dr. L. G. Christophorou for his continuous guidance, encouragement and support during the years of my graduate studies.

I wish also to express my thanks to J. G. Carter for technical assistance, to V. E. Anderson for computational help, to Dr. J. L. Adcock of The University of Tennessee for synthesizing some of the compounds used in the present study, to Dr. D. L. McCorkle of The University of Tennessee, and to Dr. I. Sauers, Dr. S. R. Hunter and all the members of the Atomic, Molecular and High Voltage Physics Group of the Oak Ridge National Laboratory for their advice and in many ways assistance in the course of this work.

The financial support of an assistantship from The University of Tennessee Physics Department throughout the years of my graduate studies is gratefully acknowledged. Appreciation is also acknowledged to the Health and Safety Research Division of Oak Ridge National Laboratory for providing the facilities and support for this research.

Finally, I would like to especially thank my wife, Chrysanthi, for her encouragement, support and patience during my graduate studies.

## ABSTRACT

Attachment of low-energy electrons (0-10 eV) to six normal perfluoroalkanes [n-$C_NF_{2N+2}$(N = 1-6)], three isomeric perfluoroalkanes (i-$C_4F_{10}$, i-$C_5F_{12}$, neo-$C_5F_{12}$), one cyclic perfluorocarbon (c-$C_5F_{10}$), four fluoroethers ($CF_3OCF_3$, $CF_3OCF_2H$, $CF_2HOCF_2H$, and $CF_3OCH_3$), two fluorosulphides ($CF_3SCF_3$ and $CF_3SCH_3$), and the freon $CClF_3$ has been studied using a time-of-flight mass spectrometer. The molecules n-$C_NF_{2N+2}$ (N = 4-6), i-$C_4F_{10}$, i-$C_5F_{12}$, neo-$C_5F_{12}$, and c-$C_5F_{10}$ were found to attach electrons dissociatively and/or nondissociatively. The autodetachment lifetimes, $\tau_a$, of the long-lived metastable parent and fragment anions of all these molecules were measured. Additionally, for those long-lived anions whose cross section was large, the variation of $\tau_a$ with incident electron energy was measured. On the other hand, for the lower normal perfluoroalkanes (N=1-3), the fluoroethers, the fluorosulphides, and the $CClF_3$ molecules studied, only fragment negative ions were observed. The relative cross sections for all observed negative ions have been measured and corrected for the finite width of the electron pulse using an unfolding procedure. Possible fragmentation mechanisms of the dissociative negative ion states (NISs) leading to the production of the observed fragment anions have been suggested and discussed. From the appearance onsets of a number of fragment negative ions, various bond dissociation energies, heats of formation, and electron affinities of certain fragments have been determined and are reported. The separation times of the dissociating fragments and the autodetachment lifetimes of the extremely short-lived ($\sim 10^{-15}$ s) and

dissociating NISs of $CF_4$ and $C_2F_6$ were estimated. The effect of molecular size and geometry and the effect of atomic substitution in a molecule on its electron attaching properties are discussed in relation to the position of the observed NISs and to the relative intensities of the parent and fragment anions.

A high temperature (300-900 K) electron swarm apparatus was constructed and used to study the effect of temperature on the electron attachment to the molecule $CClF_3$. The electron attachment rate constant, $k_a(\langle\varepsilon\rangle)$, of this molecule was measured as a function of temperature. The swarm-unfolding technique was used to determine the attachment cross section, $\sigma_a(\varepsilon)$, from the measured $k_a(\langle\varepsilon\rangle)$ at all the temperatures studied. The enhancement of $k_a(\langle\varepsilon\rangle)$ with T is discussed and rationalized.

TABLE OF CONTENTS

## LIST OF TABLES

## LIST OF FIGURES

# CHAPTER I

# INTRODUCTION

## I. GENERAL CONSIDERATIONS

The interaction of low-energy electrons with atoms and molecules to form negative ions is a field of immense interest both for fundamental and practical reasons and as such it has known enormous and continuous progress over the last two decades. Negative ion studies and more generally the knowledge on electron-molecule interactions by their transdisciplinary nature have stimulated the advancement of broad areas of physics, chemistry, and biology. Of equal importance is also the application of this knowledge in many areas of technology and energy, chemical and electrical engineering, life and radiation sciences, space, atmosphere, and the environment.

The existing literature in this field is voluminous. For a detailed treatment of the various aspects of the subject and for references to previous work in this area, the reader may refer to the recent review by Christophorou (1983). In this chapter a brief but comprehensive outline of the electron attachment processes is given, and the importance of negative ion studies is highlighted. Also, the present work is outlined and its significance is indicated.

# II. PROCESSES OF ELECTRON ATTACHMENT TO MOLECULES

## A. Modes of Production of Negative Ions

Negative ions can be formed in either the gaseous or condensed phase through the collision of either a free electron or a bound electron with a molecule. The negative ions so formed may live for times ranging from $\sim 10^{-15}$ to $>10^{-2}$ s and the process of their formation is strongly dependent on the environment (Christophorou and Siomos, 1983). The bound-electron capture by molecules includes the cases which are referred to invariably as charge exchange, chemi-ionization, ion-pair formation or collisional ionization. Free electron attachment to molecules may be of resonance or nonresonance character. Nonresonance processes include cases like ion-pair formation (Christophorou, 1971; Massey, 1976), free-electron capture by dipolar molecules (Christophorou, 1971; Christophorou et al., 1983; Lane, 1980) and free-electron capture by molecular clusters (Wegener, 1974). Resonance electron attachment is the most significant mode of electron capture by molecules. The remainder of the discussion in this section will be devoted to the resonance processes.

## B. Resonance Electron Attachment to Molecules

Resonance electron attachment processes are characterized by the fact that they occur at low energies (< 20 eV), they take place over a narrow range of incident electron energies and are generally discussed within the formalism of resonance scattering theory and the formation of transient negative ions. Resonances can be classified into four categories according to the mechanism by which the incident electron is

temporarily trapped by the molecule (Christophorou et al., 1983; Bardsley and Mandl, 1968; Schulz, 1973): (1) shape or single-particle resonances, (2) core-excited shape resonances (type II), (3) nuclear-excited Feshbach resonances, and (4) electron-excited Feshbach (core-excited type I) resonances.

In both the shape and the core-excited shape resonances the trapping mechanism is a potential barrier which is the combined effect of the attractive polarization potential between the neutral molecule and the incident electron and the repulsive centrifugal potential arising from the relative motion of the two bodies. The difference between these two types of resonances is whether the ground or an excited electronic state of the target molecule is involved in the attachment mechanism. For both resonances the negative ion state (NIS) lies above the neutral ground (for the former) or, respectively, excited (for the latter) state, and therefore the electron affinity (EA) of the molecule is negative.

In a Feshbach resonance, the incident electron loses energy to the target molecule and thus has insufficient energy to escape until some energy is regained from the target. In the nuclear-excited Feshbach resonance the incident electron loses its energy to the nuclear motion of the target, while in the electron-excited Feshbach resonance the electron excites electronically (and/or vibrationally and rotationally) the target molecule. Contrary to the shape resonances, in the Feshbach resonances the NISs lie below the corresponding neutral ground (for the former) or, respectively, excited (for the latter) state, and thus they are characterized by positive EA. Knowledge on the number and energies

of NISs is normally obtained from electron scattering and transmission experiments. Similar knowledge can be acquired also from electron beam and electron swarm techniques as in the present work (see Chapters III to VI).

Within the formalism of the resonance scattering theory the interaction of a slow electron of energy $\varepsilon$, $e(\varepsilon)$, with a polyatomic molecule AB...CD (G; v = 0) in its ground electronic state G and predominantly in its lowest (v = 0) vibrational state of excitation, is considered as proceeding through the formation of a transient ion $AB...CD^{-}*$ (G or E) in either the field of the ground (G) or excited (E) electronic state with a capture cross section $\sigma_c(\varepsilon)$. The initial formation of $AB...CD^{-}*$ and the ensuing decomposition channels may be represented as (Christophorou, 1980; Christophorou et al., 1983)

$$e(\varepsilon) + AB...CD(G;\ v=0) \xrightarrow{\sigma_c(\varepsilon)} AB...CD^{-}*(G \text{ or } E) \left\{ \begin{array}{ll} AB...CD + e(\varepsilon) & \text{(I-1)} \\ AB...CD^{(*)} + e(\varepsilon') & \text{(I-2)} \\ \left.\begin{array}{l} AB^{(*)} + CD^{-} \\ \cdots\cdots\cdots\cdots \\ \{AB...C\}^{(*)} + D^{-} \end{array}\right\} & \text{(I-3a)} \\ \left.\begin{array}{l} \text{or} \\ AB^{(*)} + CD^{-}* \\ \qquad \left\{ \begin{array}{l} \hookrightarrow CD^{(*)} + e \\ \hookrightarrow C^{(*)} + D^{-} \end{array} \right. \end{array}\right\} & \begin{array}{l} \text{(I-3b)} \\ \text{(I-3c)} \end{array} \\ AB...CD^{-} + \text{energy} & \text{(I-4)} \end{array} \right.$$

where $\varepsilon'(<\varepsilon)$ is the energy of the scattered electron. The asterisk indicates excess internal energy and the asterisk in parentheses indicates possible increase in the internal energy of the corresponding species. Reactions (I-1) and (I-2) are, respectively, indirect elastic

and inelastic electron scattering. Reaction (I-3a) is dissociative attachment producing stable fragment negative ions; for a polyatomic molecule this process can lead to simultaneous multiple fragmentation. Reactions (I-3b) and (I-3c) are dissociative attachment processes producing metastable negative ion fragment(s) which are subject to autodetachment and/or autodissociation. Finally, reaction (I-4) represents parent negative ion formation which is possible when the electron affinity, EA(AB...CD), of AB...CD is positive (>0 eV) and the excess internal energy is removed, usually by collisions of $AB...CD^{-}*$ with another body. In this study, we used time-of-flight mass spectrometry to explore channels (I-3a) and (I-3b). In addition, the relative cross sections for formation and the autodetachment lifetimes $\tau_a$ of those anions which were long lived ($\tau_a > 10^{-6}$ s) have been measured. Channel (I-4) can be probed in a high-pressure swarm experiment which, however, was used only for a part of this work in conjunction with high temperature studies (Chapter VI).

In molecules, nuclear and electronic motion are separable in the Born-Oppenheimer approximation and application of the Franck-Condon principle permits electron attachment to molecules to proceed by vertical transitions between potential-energy curves (surfaces) from the equilibrium positions of the atoms. The Franck-Condon region and other pertinent parameters for resonance dissociative and non-dissociative electron attachment processes and the energy dependences of the respective cross sections for a diatomic or diatomic-like molecule AX are illustrated schematically in Figure I-1 (from Christophorou et al., 1983). The widths of the potential energy curves of $AX^{-}*$ were

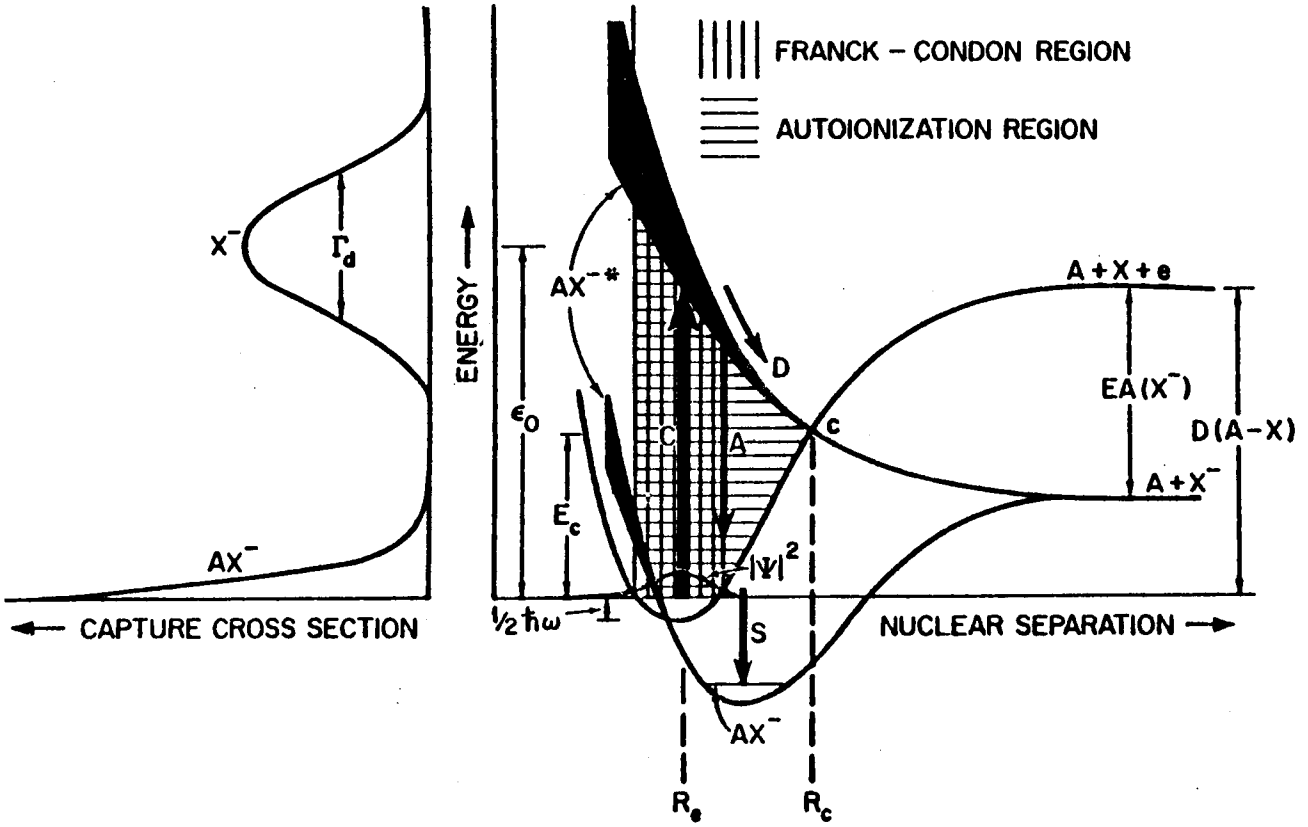


Figure I-1. Schematic diagrams illustrating the pertinent parameters for resonance dissociative and nondissociative electron attachment processes and the energy dependencies of the respective cross sections. (From Christophorou et al., 1983.)

drawn progressively larger the smaller the value of R to illustrate the increased probability of autodetachment with decreasing R. The magnitude, energy position and shape of the cross section functions provide most useful information on the state $AX^-$. As stated earlier [Reaction (I-4)] and is shown in the figure, for $AX^-$ to be formed, EA(AX) must be positive and the transient anion must be stabilized, whereas dissociative attachment does not require stabilization.

## C. A Theoretical Treatment of Electron Attachment

1. Molecular parent negative ions. It has been established that many complex polyatomic molecules have very large electron attachment cross sections at thermal and near-thermal energies (<0.5 eV) and their parent anions have long lifetimes (see Christophorou, 1971, 1978 and Christophorou et al., 1983). To reconcile the large cross sections and the long lifetimes, Compton et al. (1966), Klots (1967), and Christophorou et al. (1973, 1977) assumed that the excess energy of the anion (comprised of the molecule's electron affinity and the captured electron's kinetic energy) is rapidly distributed among its many internal degrees of freedom, thus delaying the time required for the metastable anion to return to a configuration which will lead to autodetachment. Although it is difficult to assess quantitatively the complete—and equally probable—randomization of the excess energy among all the vibrational degrees of freedom (De Copro et al., 1971; De Copro and Franklin, 1971; Franklin, 1976; Compton et al. (1966), Klots (1967) and Christophorou et al. (1973, 1977 and 1983) used this hypothesis to relate the rate for the capture and the autodetachment

processes through the principle of detailed balance and with the aid of unimolecular reaction rate theory (see Robinson and Holbrook, 1972; Forst, 1973) derived expressions relating $\tau_a$, $\sigma_a(\varepsilon)$, EA, N (number of degrees of freedom), and $\nu_i$ (the vibrational frequencies of the molecule). The derived expressions allow a qualitative understanding of long-lived negative ions as well as of the energy dependence of $\tau_a$ on incident electron energy. A more comprehensive theoretical understanding is, however, needed.

2. Dissociative electron attachment. Dissociative attachment has been treated within the resonance attachment formalism by a number of authors (Bardsley et al., 1964, 1966; O'Malley, 1966; Chen, 1967; Chen and Peacher, 1967). Much of the theory, however, deals with the case of diatomic molecules, and its application to polyatomic molecules is only possible when polyatomic structures can be considered—as far as dissociative attachment is concerned—as diatomic-like (see Chapter III). Within this theory the cross section, $\sigma_{da}(\varepsilon)$, for dissociative attachment as a function of electron energy, $\varepsilon$, is equal to the product of the cross section, $\sigma_c(\varepsilon)$, for capture of the electron by the molecule to form the metastable negative ion intermediate and the probability, $p(\varepsilon)$, that the transient negative ion will decay via dissociative attachment, viz.,

$$\sigma_{da}(\varepsilon) = \sigma_c(\varepsilon)p(\varepsilon) \ . \qquad \text{(I-5)}$$

O'Malley (1966) calculated an expression for $\sigma_{da}(\varepsilon)$ for a diatomic molecule AX initially in its lowest vibrational level ($v = 0$) and with

a purely repulsive ion state $AX^{-}*$ (upper curve in Figure I-1) given by

$$\sigma_{da}(\varepsilon)_{v=0} = \underbrace{\frac{4\pi^{3/2}}{(2m/\hbar^2)\varepsilon}\frac{\overline{g}\,\Gamma_{\overline{a}}}{\Gamma_d}\exp\left[\frac{\Gamma_a^2 - 4(\overline{\varepsilon}_0 - \varepsilon)^2}{\Gamma_d^2}\right]}_{\sigma_c(\varepsilon)} \underbrace{e^{-\rho(\varepsilon)}}_{p(\varepsilon)} \qquad \text{(I-6)}$$

In Equation (I-6) m is the electron mass, $\hbar$ is Planck's constant divided by $2\pi$, $\overline{g}$ is a statistical factor, $\Gamma_a$ is the total autodetachment width, $\Gamma_{\overline{a}}$ is the partial autodetachment width, $\Gamma_d$ is the dissociative attachment resonance width, $\overline{\varepsilon}_0 = \varepsilon_0 + 1/2\ \hbar\omega$ (see Figure I-1), $\varepsilon_0$ is the true electron energy at the peak of $\sigma_{da}(\varepsilon)$ and $1/2\ \hbar\omega$ is the zero-point energy. The quantity $e^{-\rho(\varepsilon)}$, defined explicitly (Bardsley et al., 1964, 1966; Chen, 1966; O'Malley, 1966) by

$$e^{-\rho(\varepsilon)} = \exp\left[-\int_{R_\varepsilon}^{R_c}\frac{\Gamma_a(R)}{\hbar v(R)}\,dR\right] \simeq \exp(-\tau_s/\overline{\tau}_a)\ , \qquad \text{(I-7)}$$

is the survival probability of $AX^{-}*$. That is, the probability that $AX^{-}*$ will not autoionize while separating from the point of formation by capture of an electron with energy $\varepsilon$ at an internuclear separation $R_\varepsilon$ to the point c (Figure I-1) at an internuclear separation $R_c$ where the potential energy curves of AX and $AX^{-}*$ cross. For $R > R_c$, $AX^{-}*$ will dissociate with unit efficiency [$p(\varepsilon) = 1$]. The $\tau_s$ is the separation time needed for $A\text{-}X^{-}$ to separate from $R_\varepsilon$ to $R_c$, given by

$$\tau_s = \int_{R_\varepsilon}^{R_c}\frac{dR}{v(R)}\ , \qquad \text{(I-8)}$$

where $v(R)$ is the relative velocity of separation of A and $X^-$ and $\bar{\tau}_a$ ($= \hbar/\bar{\Gamma}_a$) is the mean autoionization lifetime of $AX^{-}*$.

In Chapter III, Section IVA, Equation (I-6) is used under certain assumptions to calculate the $\bar{\tau}_a$ for two of the molecules studied.

## III. BASIC AND APPLIED SIGNIFICANCE OF NEGATIVE ION STUDIES

Negative ions are important in a large number of basic and applied areas. The reader may refer to a review of these in the recent works of Massey et al. (1982) and Christophorou and Hunter (1983). The discussion in this section only touches on some of these applications.

Free low-energy electrons are ever present and/or can be produced in a variety of ways (e.g., through interaction of radiation with matter, field ionization, thermally, chemically, etc.) in various physical, chemical or biological systems. The essence of the significance of the electron attachment processes to various applications may then be easily understood. Some applications require the preventing of the attachment of these electrons. On the other hand, some other applications require thermalization of the electrons through negative ion formation or more generally the monitoring of their number density and energy distribution. For example, in tailoring good gaseous dielectrics for use in high-voltage applications, one is looking for electron capturing gas molecules which can prevent the initiation of the avalanche by removing the free electrons. The development of better gaseous insulators is today an area of enormous interest and applications (Christophorou et al., 1982a). On the other hand, in a

laser device or in an electrical discharge lamp or in a gas-filled radiation detector (Christophorou and Hunter, 1983), gaseous mixtures are required which should not attach electrons but instead must have other desirable properties. In a diffuse-discharge opening switch, for example, a gas mixture is required which among other properties is desired to be a good conductor at low E/N (density reduced electric field) and a very good electron attacher (insulator) at high E/N values.

A recently developed technique where electron attachment plays an important role is the so-called negative ion chemical ionization mass spectrometry (e.g., Field, 1980, and Dougherty, 1981) which seems promising for high detection sensitivity and selectivity. Relevant to this application is also the use of electron attaching molecules as tagging materials for detection of explosives (Christophorou et al., 1982b).

The role of negative ions in the atmosphere and the environment is important and diverse also. Negative ions influence the basic character of the ionosphere (e.g., see Danilov, 1970; Ferguson, 1968, 1969, 1974), may contribute to the destruction of atmospheric ozone (e.g., see McConnell and Schiff, 1978), and clusters of these ions constitute condensation nuclei with climatic consequences and other health effects (e.g., see Castelman and Keesee, 1981).

Another interesting area in which the role of electrons and anions is undeniable is biological science. Albert Szent-Gyorgui (1968) characterizes the electron as the fuel of life and addresses the role of intermolecular transfer in cellular regulation, defense and cancer.

Christophorou (1971, Chapter 9) and Christophorou and Hunter (1983) review the physicochemical foundation of biological action, the possible role of dissociative attachment in the toxic action of some molecules, the possible correlation of carcinogenicity and electrophilicity of molecules, the use of molecules of high affinity in radiosensitizers and radiopharmaceuticals and other interesting aspects of the problem.

Examples of other applications of negative ion formation are: Isotope separation for fission generators (e.g., see Chen and Chantry, 1979), chemical accelerators (Greene et al., 1975), radiocarbon dating using electrostatic accelerators and detection of $^{14}C^-$ (Bennett et al., 1977), inhibition of flames, plasmas and arcs (e.g., see Creitz, 1961; Mills, 1968), plasma etching (e.g., see Coburn and Winters, 1979), ozone production (Phelps, 1979), magnetohydrodynamics and plasma fusion, electrical power generation, communication, space and defense (see Massey et al., 1982, Vol. 3, for a review), and so on.

Concerning the contribution to basic studies, negative ions provided a means for probing molecular structure and obtaining information on many molecular parameters. In the following chapters we describe in detail how negative ion data were used to yield various thermochemical data (e.g., bond dissociation energies, electron affinities, heats of formation of radicals and molecules), negative ion potential energy curves, number and position of negative ion states, separation times of dissociating fragments and autodetachment lifetimes of extremely short-lived ($\sim 10^{-15}$ s) and dissociating NISs.

## IV. OUTLINE AND SIGNIFICANCE OF THE PRESENT WORK

The present work consists of experimental studies and analyses of attachment of low-energy (0-10 eV) electrons to four groups of molecules:

1. The normal perfluoroalkanes n-$C_NF_{2N+2}$ (N = 1-6).
2. The isomeric perfluoroalkanes i-$C_4F_{10}$, i-$C_5F_{12}$, neo-$C_5F_{12}$ and c-$C_5F_{10}$.
3. The fluoroethers $CF_3OCF_3$, $CF_3OCF_2H$, $CF_2HOCF_2H$, and $CF_3OCH_3$) and the fluorosulphides $CF_3SCF_3$ and $CF_3SCH_3$.
4. The freon $CCIF_3$.

In Chapter II the experimental apparatuses and procedures used in the present work are discussed.

In Chapters III, IV, and V the results and analysis are presented for the molecules of the 1st, 2nd and 3rd group of molecules, respectively. All the molecules were studied in a time-of-flight mass spectrometer (TOFMS) at room temperature and the results are compared with the results of a swarm study whenever available. The objective of the TOF mass spectrometric study was to study "all" the negative ions which could be observed below 10 eV and also to measure the auto-detachment lifetimes of those anions which were long lived. From the deduction of these data (e.g., nature of negative ions observed, their relative intensities, fragmentation mechanisms leading to the formation of the fragment anions) the gaining of an insight into the nature of the attachment processes to polyatomic molecules was intended.

Chapter VI contains the results of a room temperature TOF mass spectrometric study and a high temperature swarm study of $CClF_3$. The objective of the high temperature swarm study was to examine the effect of internal excitation of the molecule on its electron attaching properties.

Finally, in Chapter VII the results of the present work are summarized and possible future studies are indicated.

The study of the above molecules was motivated by practical as well by intrinsic interest. Some of these molecules have high dielectric strengths and can be used as gaseous insulators, especially in combination with other gases. Other possible uses indicated are for diffuse-discharge switches, plasma etching, gas-filled radiation detectors, etc. As it has been pointed out in Section II, no theory applicable to electron attachment to polyatomic molecules is available. Existing theories for dissociative attachment were derived only for diatomic or diatomic-like molecules. There is therefore a need to overcome the shortcomings of the theory and still being able to get a deeper insight into the electron attachment processes in polyatomic molecules. In this work the approach was to study a series of similar compounds and observe how small changes in a complex molecule may affect its electron attaching properties. Thus, in the first group of the molecules studied the molecular size was changed. The molecules of the second group are also similar differing only in the geometrical arrangement of the constituent atoms in the molecule. In the third group of molecules the effect of substituting one atom by another of a

different kind in the molecule on negative ion formation was examined. Finally, the study of $CClF_3$ was undertaken to examine the effect of internal excitation of the molecule on its electron attaching properties.

# CHAPTER II

## EXPERIMENTAL METHODS AND PROCEDURES

In this chapter the experimental methods and the analytical procedures for the two techniques (electron beam and electron swarm) used in the present study are discussed. In the introductory section a comparison of the two techniques is presented. In the next section the time-of-flight mass spectrometer is discussed in more detail with emphasis on the improvements of the experiment by interfacing it to a PDP-11 computer. In the final section a description is given of the swarm technique along with a description of a new swarm apparatus which was built for high temperature electron attachment studies. A considerable amount of time was invested in refining the apparatus, although this will not be reflected in the extent of the measurements obtained by this technique.

### I. INTRODUCTION

A great variety of experimental techniques can be employed to study electron attachment to molecules. The choice of a specific technique pertains to the particular application of interest. For the present study a time-of-flight (TOF) mass spectrometer and a high temperature electron attachment swarm apparatus were used. In this chapter both experimental methods are discussed. The basic operating principles of both techniques have been employed for many years. Consequently, the discussion will be directed mostly to those aspects of

the apparatuses and procedures which have been innovated during this work. At the same time those experimental features which pertain to the understanding and interpretation of the experimental results will be given particular emphasis.

In order to have a better perspective of the two experimental methods of the present work, and how they compare between themselves and also with other techniques used for negative ion studies, it is probably worth to mention how the various techniques relate to the lifetime, $\tau_a$, of the negative ions. Christophorou (1971, 1978) classified the metastable atomic and molecular negative ions with regard to their lifetimes broadly as (a) extremely short lived ($10^{-15} \lesssim \tau_a \lesssim 10^{-12}$ s), (b) moderately short lived ($\sim 10^{-12} \lesssim \tau_a \lesssim 10^{-6}$ s), and (c) long lived ($\tau_a > 10^{-6}$ s). The basis of this classification entails to the experimental method employed to determine $\tau_a$: low-energy electron scattering techniques for (a), high pressure electron swarm studies for (b), and TOF mass spectrometry and ion cyclotron resonance techniques for (c). Of course the various techniques can be grouped into categories not only according to the magnitude of the $\tau_a$, but also according to other important quantities they can measure, like electron attachment cross sections and rate constants, electron energy loss, types of molecular ion products resulting from electron attachment, kinetic energy of fragment ions, etc. The different techniques have been discussed and reviewed by various authors (e.g., Christophorou, 1971; Christophorou et al., 1983; Massey, 1976).

The TOF mass spectrometer is a powerful technique with a number of distinct advantages. The electron beam interacts with the molecule being studied under single collision conditions (pressure: $10^{-4}$ to $10^{-7}$ Torr). This provides a direct way of obtaining information on the various products of the electron-molecule interactions. The long-lived negative ions formed following the electron attachment are mass analyzed fairly easily, their relative intensities as a function of the incident electron energy can be monitored, and at times the kinetic energies of the dissociative attachment fragments at ambient or higher temperatures are measured. The spread of the electron energy in the beam can vary from a few to a few hundred millivolts depending on the type of the electron source [Retarding Potential Difference (RPD), electron monochromatic or electrostatic source]. The autodetachment lifetimes of metastable long-lived ions can be measured and the variation of $\tau_a$ as a function of incident electron energy can be observed. Negative ion species which live shorter than a microsecond cannot be observed in a TOF mass spectrometer. Also quite generally beam experiments do not provide accurate means of measuring the absolute attachment cross section.

In an electron swarm experiment the pressures employed (a few Torr to ∿50,000 Torr) are much higher than those in a beam experiment. Short-lived ($\tau_a < 10^{-6}$ s) negative ion states, which in a beam experiment could not be observed, can be stabilized by collision in a swarm experiment and thus can be probed. Variation of the pressure can also provide a means for studying the pressure dependence of electron

attachment processes. These facts have to be kept in mind when one compares results obtained by the beam and the swarm techniques. A difficulty, however, associated with the fact that the swarm technique utilizes high pressures is the determination of the electron energy distribution. Electrons suffer many collisions and their energy distribution can be found only through a solution of the appropriate energy balance and transport equations and be based on knowledge of various elastic and inelastic electron scattering cross sections. Finally, swarm experiments provide accurate data on the magnitude of the total electron attachment rate constant.

As it will be demonstrated in the next chapters, swarm and beam techniques can complement each other to a great extent concerning the type of information they can provide. This is particularly true when the electron-molecule interaction leads to dissociative attachment and thus both techniques probe the same rapidly dissociating negative ion state. In this case the attachment rate constants measured by the swarm method are found to be pressure independent and they can be related directly to those of the dissociating NISs as probed by the beam technique. In a number of such cases the so-called swarm-beam combination (see Section III) is effectively utilized in a quantitative way to yield the magnitude and the energy dependence of the absolute electron attachment cross section.

# II. TIME-OF-FLIGHT MASS SPECTROMETER

## A. Apparatus

The TOF mass spectrometer used in this study was constructed at Oak Ridge National Laboratory and is similar to the Bendix Model 14-206. The principles of operation of this type of mass spectrometer have been described by Wiley and McLaren (1955). The particular mass spectrometer has been used and discussed extensively in earlier studies (Compton et al., 1966; Collins et al., 1970; Naff, 1971; Hadjiantoniou et al., 1973; and Johnson, 1977). The major improvement made in the apparatus during this work was its automation by the introduction of a PDP-11 computer. The discussion here primarily deals with the computer enhancement capability of the experiment, but a brief description of the mass spectrometer itself is included as well.

A schematic diagram of the entire apparatus is shown in Figure II-1. The TOF mass spectrometer can be described as having three parts: (1) the ion source consisting of the electron source ("electron gun") and the collision chamber where the ions are formed, (2) the flight tube which is the field-free region where ions are separated by their times of flight, (3) the detection system which is an electron multiplier with pulse shaping and pulse selecting electronics. The computer is employed to control the electron gun and to measure the pulse rate of a particular ion signal from the electron detection system.

In the ion source electrons are produced by a heated tungsten filament containing 3% Rhenium and pulsed into the collision chamber through the focusing electrodes (number 1 through 5 in Figure II-1) of

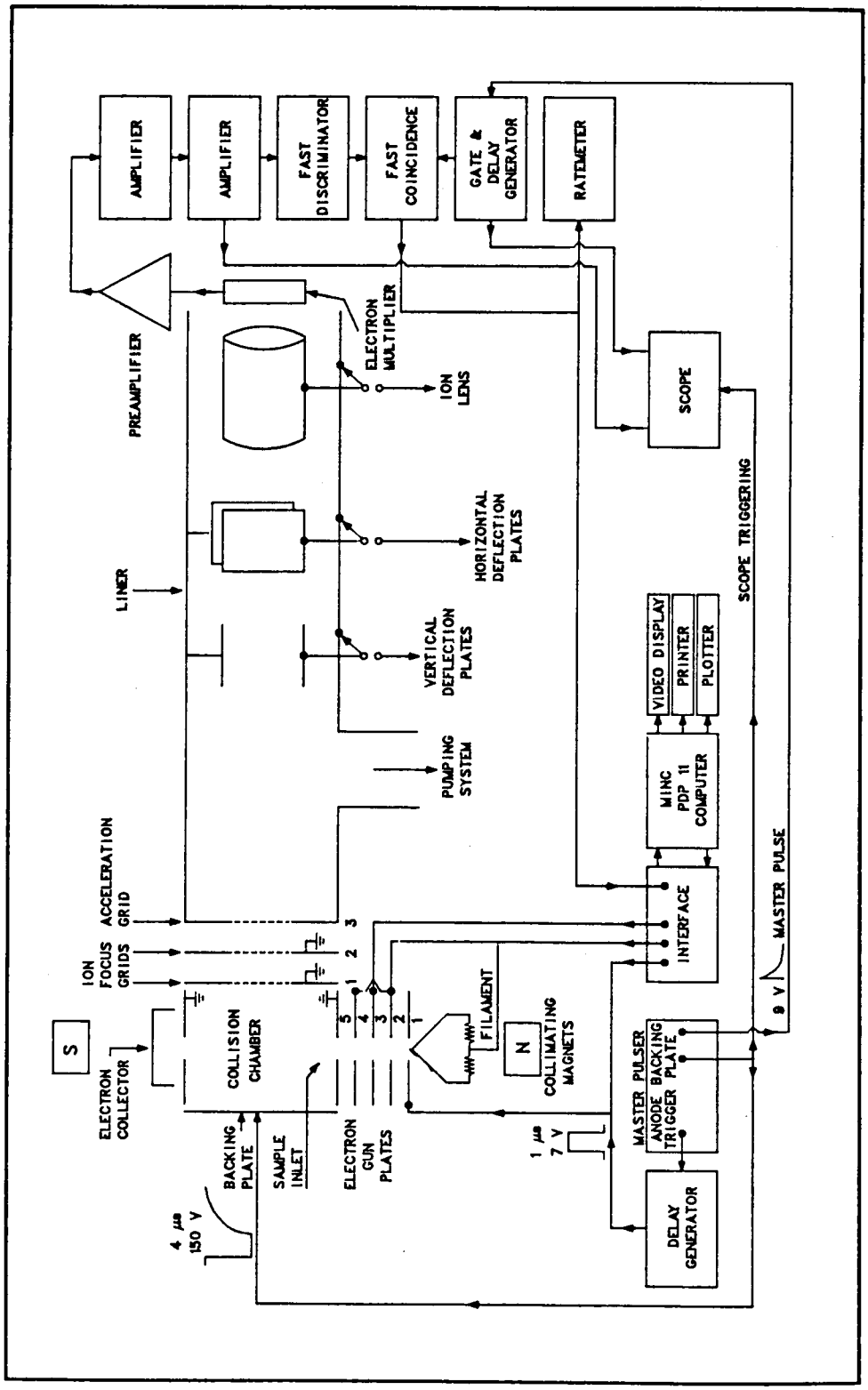


Figure II-1. Schematic diagram of the time-of-flight mass spectrometer.

the electron gun. The electron pulsing is controlled by the first of these electrodes called the anode. The anode is normally negatively biased to turn back all electrons released by the filament. Every 100 μs a positive pulse of 7 V magnitude and 1 μs duration is applied to the anode to allow electrons to pass through into the collision chamber. At 0.5 μs after the anode pulse, a large negative pulse of 100-200 V magnitude and 4 μs duration is applied to the backing plate to push the negative ions formed by the electron pulse into the flight tube. As is shown in Figure II-1 the backing plate pulse has a very sharp leading edge. A small negative bias has to be continuously applied to the backing plate to compensate for the small positive overshoot of the pulse.

The shape of the energy distribution of the electron beam which enters the collision chamber is controlled by the potentials applied on the electrodes of the electron gun as shown in Figure II-2. The electron beam is collimated by the slits of the electrodes, and its alignment is further improved by a magnetic field B which is perpendicular to the electrodes [Figure II-2(a)]. Figure II-2(b) shows the potentials in the gun, and Figure II-2(c) shows the resulting electron energy distribution. The anode is shown with the positive pulse applied to allow all electrons leaving the filament to pass through. The second and fourth electrodes are kept at the same potential as the filament and serve as an einzel lens to improve focusing. The third electrode, called the retarding electrode, blocks the passage of different portions of the electron distribution as it is shown. The fifth electrode is kept at ground potential.

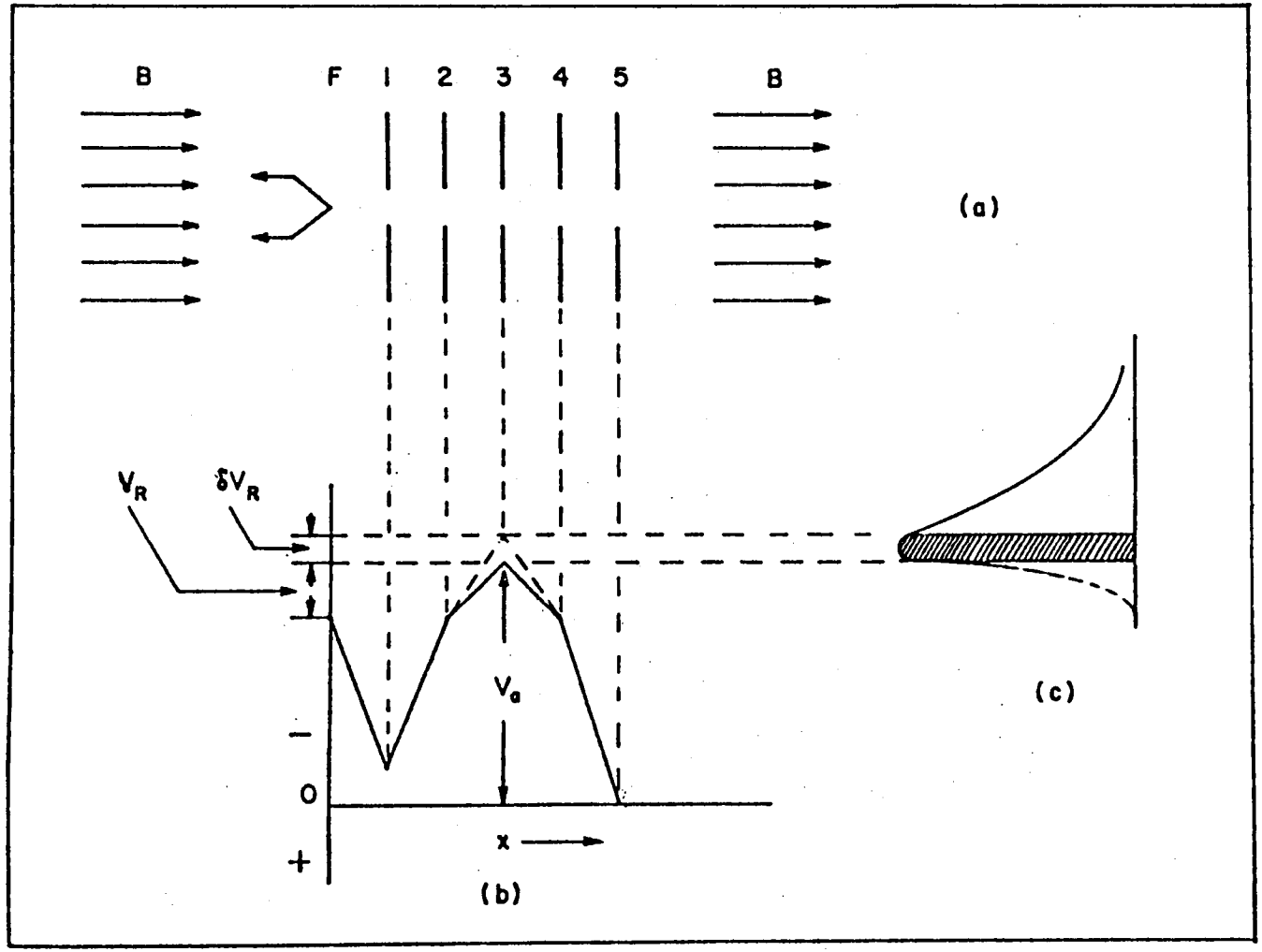


Figure II-2. Schematic diagram of the retarding potential difference technique. (a) Electron source; (b) potential energy of an electron; (c) electron energy distribution (see text).

The energy distribution of the electrons as they leave the filament is essentially Maxwellian. The full width at half maximum (FWHM) of the distribution is about 1 eV and is characteristic of the filament temperature. The profile of the distribution is given by the curve in Figure II-2(c), both solid and broken portions. The electron source in Figure II-2 can operate in two modes: (1) in the retarding potential difference (RPD) mode, first described by Fox et al. (1955), and (2) in the ordinary or non-RPD mode. In the ordinary mode the retarding electrode is negatively biased with respect to the filament by an amount $V_R$ [Figure II-2(b)] to block the low-energy electrons. This results in an energy distribution with a sharp lower cutoff [solid portion of curve in Figure II-2(c)] having a FWHM of $\sim$0.5 eV. In the RPD technique, the retarding potential, $V_R$, can be varied slightly under computer control to obtain a quasi-monoenergetic electron beam. If $V_R$ is changed by a small amount $\delta V_R$, then the electron energy distribution which enters the collision chamber will change by the amount shown in the shaded area in Figure II-2(c). By subtracting the ion currents before and after $\delta V_R$ is applied, the signal due to the electrons in a narrow energy range of width $\delta V_R$ is obtained. The value of $\delta V_R$ is normally set to 0.1 volt and would ideally produce an electron distribution with a FWHM of 0.1 eV. The actual width of the electron energy distribution, however, depends on the experimental conditions and generally falls between 0.10 and 0.15 eV for a $\delta V_R$ setting of 0.1 eV. It should be pointed out that the electron energy distribution obtained by the RPD method is a virtual one as it comes from the

difference of two real energy distributions. This makes the beam not readily useful for certain measurements (like measurements of auto-detachment lifetimes) which are too sensitive to noise. Furthermore, the RPD technique is restricted for measurements of rather strong negative ion signals. The quality of its operation and other problems which are encountered have been discussed by many authors (Fox et al., 1955; Burns, 1964; Simpson, 1961; Marmet, 1964, and Shulz, 1960), whereas a theoretical description of its operation is given by Gordon et al. (1969).

The energy of the electrons when they reach the collision chamber is determined by $V_a$ [(Figure II-2(b)], the potential difference between the retarding electrode (scanned by the computer) and the collision chamber (ground potential). $V_a$ is measured directly, and it provides an accurate measure of relative energy shifts of the quasi-monoenergetic electron distribution. Due to stray contact potentials, $V_a$ does not accurately measure the absolute energy of the electron beam. The energy scale can be calibrated by using a negative ion with a large cross section which peaks at a known electron energy. The difference between the known peak and the observed peak is the amount by which the energy scale must be shifted.

The flight tube (shown in Figure II-1) is a field-free region maintained at a high positive potential (which can be adjusted from 1.0 to 4.5 KV in steps of 0.5 KV) relative to the collision chamber. Negative ions are accelerated to a high kinetic energy as they drift from the position of their formation to the entrance of the flight tube

(acceleration grid 3 in Figure II-1), and then travel the length of it at constant velocity. The first two ion focus grids are kept at ground potential to prevent penetration of the field into the collision chamber. The deflection plates along the path of flight can be used to deflect all ions when measuring lifetimes of metastable negative ions, and are normally kept at the same potential as the flight tube liner. The negative ions can be slowed down by the application of a negative voltage to the ion lens but it too is normally kept at the same potential as the flight tube liner.

The detection system is composed of the electron multiplier and associated pulse shaping and pulse selecting electronics, a block diagram of which is shown in Figure II-1. The electron multiplier is a magnetic-type multiplier (Bendix model M306) which assumes equal detection efficiency for both an ion or a neutral species resulting from electron detachment during the time of flight. When the ion or neutral species is detected by the electron multiplier, a pulse is produced which is fed into a high impedance unity gain preamplifier (Keithley model 111) and then to two timing filter amplifiers (ORTEC model 454). The amplified pulse then goes to an oscilloscope and is also fed into a fast discriminator (ORTEC model 417). The discriminator produces a standard square output pulse for every incoming pulse above a certain amplitude. The minimum level is set below the amplitude of any true mass pulse, so the discriminator will discriminate only against noise. The pulses from the discriminator are fed into a fast coincidence unit (ORTEC model 414A) along with a pulse from a gate and delay generator

(ORTEC model 416A) triggered by the master pulse. The amount of delay is variable and is set equal to the time of flight of the mass of interest. The coincidence unit then will produce a pulse only if the mass signal is received within a selected resolving time of the gate pulse. The oscilloscope is triggered by the backing plate pulse and provides a continuous display of the mass spectrum as a function of time of flight. It also is used to set the gate pulses on the desired mass. The output of the coincidence unit represents the signal corresponding to a specific mass, and this signal is counted and recorded. One output of the coincidence goes to a ratemeter (ORTEC model 441) which provides a continuous reading of the count rate. Another output of the coincidence goes to the interface panel. The interface unit was designed and fabricated to be adaptable to computer control. Located within the interface panel and under computer control are modular D.C. power supplies used to provide the various voltages to the electrodes of the electron gun, and two digital counters for concurrent counting of pulses from two different selected masses. A software program employing FORTRAN SUBROUTINES and run by the computer is used to operate the mass spectrometer. For a selected mass, the program is used to scan the electron energy across the negative ion resonance and to display on the video terminal the negative ion intensity as a function of electron energy. The acquired signal is then stored on the floppy disk of the computer for future recall and manipulation.

B. Experimental and Analytical Procedures

The TOF mass spectrometric study of each molecule of the present work included the following stages: (1) mass identification of "all" the negative ions formed from the molecule under electron impact, (2) measurement of the intensity of each observed negative ion as a function of electron energy, and (3) measurement of the autodetachment lifetimes, $\tau_a$, of those anions which were found to be metastable within the time of flight of the anion.

Prior to any measurements on any of the molecules under investigation the calibration gas $SF_6$ was admitted into the collision chamber. The presence of $SF_6$ in the system served a multiple purpose. Since the electron attachment cross section for $SF_6$ is very strong and narrow peaking at ∿0.0 eV (Hickam and Fox, 1955; Christophorou et al., 1971a; Chutjian, 1981), the shape of the $SF_6^-$* resonance was used to monitor the electron energy distribution. To establish the operating conditions of the instrument the procedure described below was followed. First the filament current was set at ∿2 A to give a current at the electron collector (Figure II-1) of ∿1-3 x $10^{-7}$ and ∿1-3 x $10^{-9}$ A without and with electron pulsing, respectively. Then the $SF_6^-$* resonance as a function of electron energy was observed on the computer video terminal, and the magnetic field alignment, the filament current and backing plate bias were varied until a strong (∿4000 counts per second at the peak, at a pressure ∿1 x $10^{-6}$ Torr) and narrow (FWHM = ∿0.5 eV) resonance was obtained. If the above conditions could not be fulfilled, this was considered as an indication that the instrument was

misfunctioning and the cause of the trouble had to be found and removed.

1. Mass identification. After establishing satisfactory operation of the system, the molecule under study was introduced into the collision chamber. When first trying to identify the masses of the negative ions produced from the molecule, the operating pressure was increased to $\sim 1 \times 10^{-4}$ Torr, which is well above the normal operating pressure of $< 3 \times 10^{-5}$ Torr. This ensured that weak ions were detected and identified. In this way we were able to detect anions whose intensity was as low as one part in one thousand of the intensity of the strongest negative ion from the same molecule. The basic parameter determining the mass separation in the TOFMS is the time of flight, t, of the ion, given by

$$t = L\sqrt{M/(2E)} \quad , \qquad \text{(II-1)}$$

where L is the distance that the ion travels, M is the mass of the ion and E is the kinetic energy the ion receives on entering the flight tube. A discussion on the mass resolution of the TOFMS and relevant references can be found in Johnson (1977). Instead of using Equation (II-1) for mass identification, which would require precise knowledge of L and E, a known mass signal was used for mass calibration. For two ions of different mass which are present in the spectrometer at the same time, Equation (II-1) can be used to write

$$M_x = M(t_x/t)^2 \quad , \qquad \text{(II-2)}$$

where the subscript x refers to the unknown mass. The time of flight can be measured with an accuracy of a few tenths of a percent by using the delayed sweep of the oscilloscope. The strong signal of $SF_6^-*/SF_6$ was used as a calibration mass. The resulting mass determinations were accurate to at least ±0.3 amu for all ions in this study.

2. Negative ion intensity as a function of electron energy. Once the various negative ions were identified, their relative peak intensities and their relative cross sections as a function of $\varepsilon$ were measured. During these measurements care was taken that the operating pressure was kept in a range in which: (1) The intensity of each observed negative ion varied linearly with pressure. This ensured that the negative ion being studied was the result of a primary rather than of a secondary reaction. It can be stated that this condition was fulfilled when the pressure was $\leq$ 3-4 x $10^{-5}$ Torr or even higher in some cases. (2) The peak counts per second (c/s) for very strong ions did not exceed 4000 c/s. This number was found to be a safe limit below which no saturation of the signal occurred, e.g., the measured signal was not underestimated. Justification for this number comes from the following. Ions or neutrals species which might arrive at the detection system in times closer than 1 μs cannot be distinguished, and only the first one will be counted. This is due to the fact that the fast discriminator in the detection system has a recovery time of 1 μs and therefore cannot properly be triggered on the second of two pulses which are closer than 1 μs. In this study no two ions of the same or different type had a time-of-flight difference <1 μs. This definitely was the

case for any two ions of different type, even if they were produced within the same electron pulse, since their difference in mass implied a difference in the time of flight >1 μs. For two ions of the same type we have to recall that electrons are pulsed into the collision chamber for 1 μs 10,000 times a second. So even if it is assumed that only one (and no more) ion is formed per pulse, then the maximum count rate expected for this ion would be 10,000 c/s which was never reached, since the count rate was kept <4000 c/s. For the proper counting of "all" species, ions and neutrals and those having both strong and weak currents, the settings of the amplifiers, discriminator and gate pulse had to be chosen carefully so that single particle equal efficiency counting is taking place.

As it has been mentioned in the previous section, the energy, $\varepsilon$, of the electron beam from the electron gun, is varied by changing the quantity $V_a$, the potential difference between the retarding electrode and ground. A software program run by the computer was used to scan repeatedly the electron energy. The gate was set on a particular mass signal and $\varepsilon$ was repeatedly scanned and the counts at every energy point were accumulated until a smooth curve giving the ion current as a function of $\varepsilon$ was observed on the computer video terminal. The raw experimental data for each negative ion obtained in this way represented the shape of its cross section broadened by the electron beam energy distribution. The data had first to be energy calibrated, as it was explained in Section IIA. Resonances often used for energy scale calibration are $SF_5^-/SF_6$, $Cl^-/HCl$, and $O^-/N_2O$. The $SF_5^-/SF_6$ resonance which

peaks at 0.37 eV (Christophorou et al., 1971a) was used in this work. The positions of the peaks in the cross sections of all observed negative ions were reproducible with a scatter of ±0.05 eV. Considering the overall uncertainty, however, the accuracy of the values given for peak position is ±0.1 eV. To eliminate the effect of the broad electron energy distribution on the measured relative cross sections of the negative ions observed, an unfolding technique similar to that of Allen and Grimm (1979) was employed.

The measured ion current of each observed ion as a function of electron energy, $I(\varepsilon)$, is related to the "true" ion current, $I(\varepsilon')$, through

$$I(\varepsilon) = \int_0^\infty F(\varepsilon,\varepsilon')\ I(\varepsilon')\ d\varepsilon' \ , \qquad \text{(II-3)}$$

where $F(\varepsilon,\varepsilon')$ is the experimental smearing function (i.e., the profile of the electron pulse). We assumed that $F(\varepsilon,\varepsilon')$ is represented by the reverse of the cross section function, $\sigma_a(\varepsilon)$, for $SF_6^{-*}$ taken under identical experimental conditions as for $I(\varepsilon)$. Smoothing was performed by replacing each point $I(\varepsilon_i)$ by the weighted average $[I(\varepsilon_{i-1}) + 2I(\varepsilon_i) + I(\varepsilon_{i+1})]/4$ prior to unfolding. For some ions a comparison was made between the unfolded functions obtained from $I(\varepsilon)$ without RPD and the functions $I(\varepsilon)$ measured with RPD which showed good agreement between the two functions with respect to the appearance onset, FWHM, and energy dependence (see Figure II-3).

The energy scale calibration and the determination of the electron energy distribution both rely on the operating conditions of the ion

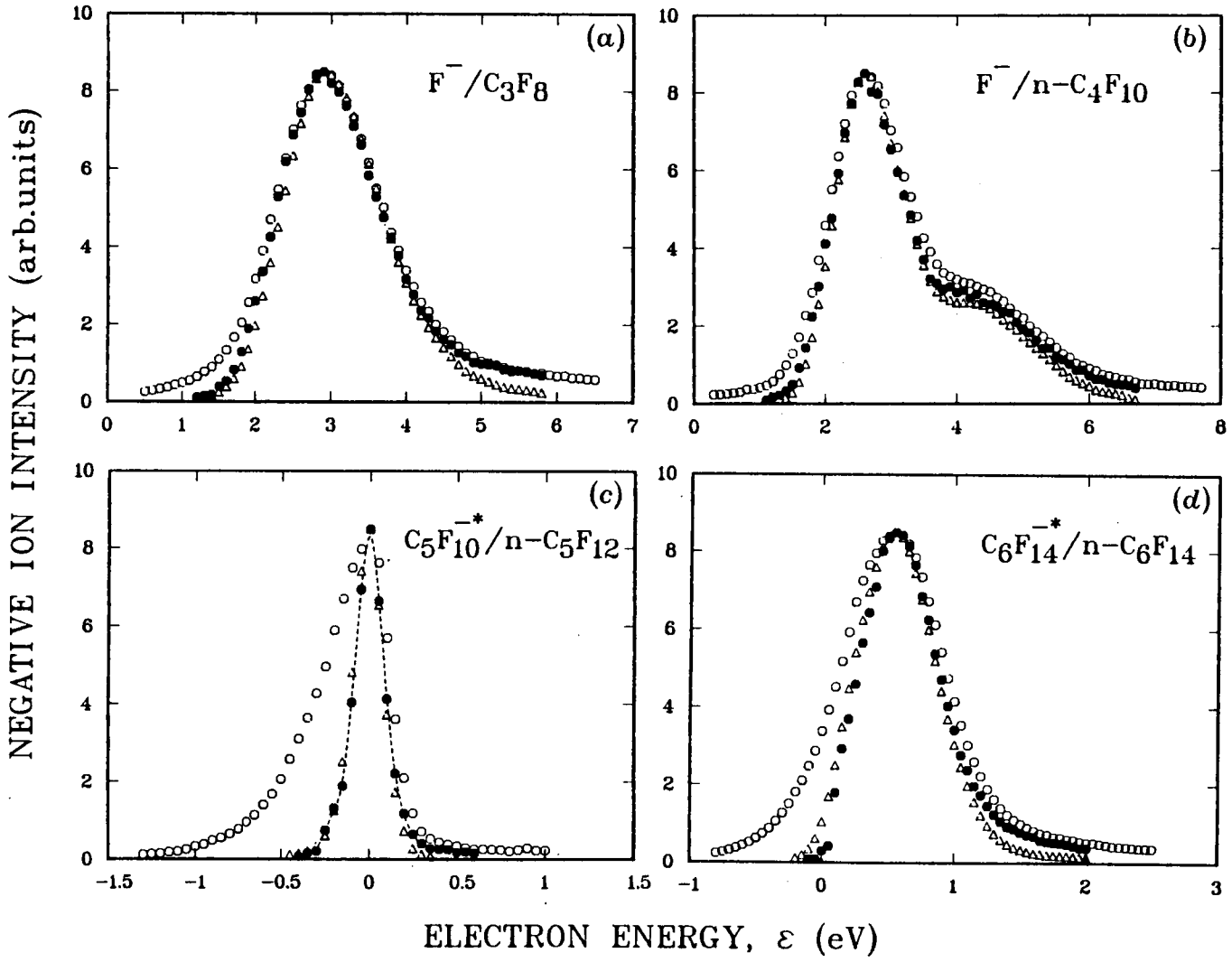


Figure II-3. Comparison of negative ion currents as a function of electron energy obtained without the RPD[(o) nonunfolded, (Δ) unfolded] and with the RPD (●) for selected ions. (a) $F^-/C_3F_8$, (b) $F^-/n\text{-}C_4F_{10}$, (c) $C_5F_{10}^{-*}/n\text{-}C_5F_{12}$, (d) $C_6F_{14}^{-*}/n\text{-}C_6F_{14}$.

source. Factors such as magnetic field alignment, filament current, backing plate bias, effect of the sample on the gun conditions, may cause the energy scale to shift or the beam distribution to change. During the course of this study a continuous monitoring of these two parameters with time was made. For almost all but a few cases no noticeable changes were observed within the time necessary to complete an entire set of measurements.

3. Autodetachment lifetimes of negative ions. If a metastable negative ion has an autodetachment time, $\tau_a$, which is greater than or of the order of its time of flight, then the TOFMS can be employed for measurements of $\tau_a$. Let us assume that at time t=0 a total number of negative ions $N^T$ are entering the flight tube all with the same kinetic energy. As these ions travel along the flight tube, some undergo autodetachment becoming neutrals, but still continuing to travel with the same velocity they had at the time of autodetachment (which is that at t=0) and both neutrals and negative ions reach the detector and are detected with equal efficiency. The signal will then give a measure of $N^T$. If, however, a potential is applied on the horizontal deflection plates (Figure II-1, p. 21), the survived ions will be swept away from the beam and only the neutrals, $N^0$, are detected. The negative ion signal $N^-$ will be given by $N^T - N^0$. If we now assume that the $\tau_a$ obeys an exponential decay law, viz.,

$$N^- = N^T e^{-t/\tau_a} \qquad \text{(II-4)}$$

$\tau_a$ can be determined from a measurement of $N^-/N^T$ and t. Usually $N^-/N^T$

is measured for a number of values of t, the latter being varied by changing the flight tube acceleration voltage. Then from Equation (II-4) it is obvious that $\tau_a$ will be given by the inverse slope of the plot of $-\ell n(N^-/N^T)$ versus t. Determining $\tau_a$ in this way is referred to as the "slope method." At times the negative ion signal may be too weak to allow such plots, and in those cases, $\tau_a$ is determined by averaging many values of $\tau_a$ calculated directly from individual measurements of $N^-/N^T$. For negative ions whose signal was strong to permit lifetime measurements as a function of electron energy, the $\tau_a$ was found to vary with $\varepsilon$. The variation of $\tau_a$ with $\varepsilon$ in connection with the spread of the electron energy, is a complex subject discussed in previous work (e.g., Christophorou, 1978; Johnson, 1977). Throughout the lifetime measurements of this study the operation of the instrument was monitored by measuring the $\tau_a$ of the strong parent ion of $SF_6^-*/SF_6$. The lifetime measurements can be affected by the electron gun conditions and these and a number of other possible sources of error have to be considered in the measurements; they have been discussed in detail by various authors (e.g., Collins et al., 1970; Naff, 1971; Hadjiantoniou et al., 1973).

## C. Materials

The compounds used for the present study were obtained as follows: The gases $CF_4$ and $C_3F_8$ were obtained from Union Carbide Corporation, LINDE Division, with a stated minimum purity of 99.7% and 99%, respectively, $C_2F_6$ and $CClF_3$, from Matheson Gas Products, with a stated minimum purity of 99.6% and 99%, respectively, n-$C_4F_{10}$ and n-$C_5F_{12}$ from

Columbia Organic Chemicals Company, Inc., with a stated minimum purity of 95%, n-$C_6F_{14}$ from Pierce Chemical Company with a stated minimum purity >95% and i-$C_4F_{10}$, $CF_3OCF_3$, $CF_3OCF_2H$ and $CF_2HOCF_2H$ from PCR Research Chemicals, Inc., with a quoted minimum purity of 95-99%. Gas chromatography and positive ion mass spectrometric analysis have indicated that the purity of these compounds was much higher than the quoted minimum value. The compounds i-$C_5F_{12}$, neo-$C_5F_{12}$, c-$C_5F_{10}$, $CF_3OCH_3$ and $CF_3SCH_3$ were synthesized by Dr. J. Adcock of the Chemistry Department of The University of Tennessee. For $CF_3SCF_3$ two samples were used, one purchased from Armagedon Chemical Company and the other prepared by Dr. J. Adcock. The compounds n-$C_5F_{12}$ and n-$C_6F_{14}$, which are liquids at room temperature, were deoxygenated prior to use by the freeze-pump-thaw method. All the other samples, which are gases at room temperature, were used without further purification. In general, the negative ion spectra were "clean" with all masses identifiable with specific fragments of the molecules investigated. It was found difficult, however, to obtain the fluorosulphide compounds studied completely free of traces of Cl-containing impurities.

## III. THE HIGH TEMPERATURE SWARM APPARATUS

### A. The Electron Swarm Method

The electron swarm method has been used extensively over the last twenty-five years. A detail description of the method can be found in earlier works (e.g., Bortner and Hurst, 1958; Christophorou, 1971; Christodoulides and Christophorou, 1970; McCorkle and Christophorou, 1972; Rademacher, 1974). In this section only a brief description of

the basic principles of the technique will be given. This will help the reader to realize more easily the various modifications made on the swarm apparatus during this work to extend the measurements to high temperatures (up to 900 K).

In the electron swarm method (first described by Bortner and Hurst, 1958) a swarm of electrons is produced in a given plane by a well-collimated $\alpha$-particle source (Figure II-4). Under the influence of an externally applied uniform electric field, E, the electrons drift to a positive collector plate (anode) where they are collected. The total number densities, N, employed are such that the electrons attain an equilibrium energy distribution, $f(\varepsilon, E/N)$, very quickly, e.g., from the very beginning of their drift space. The distribution function is broad and is determined from the nature of the gas, the temperature and the density-reduced electric field E/N (Volts $cm^2$). To overcome the problem of the lack of accurate knowledge of $f(\varepsilon, E/N)$ for every gas studied, swarm experiments on electron attachment are performed in binary mixtures. The electron attaching gas is mixed in minute amounts (usually less than one part in one million) with an abundant nonelectron attaching gas, called "buffer" or "carrier" gas, for which $f(\varepsilon,E/N)$ is known over a wide range of E/N values. In such cases it is important (especially when the buffer gas is a rare gas) to keep the partial pressure of the attaching gas as low as possible so that its presence does not affect the $f(\varepsilon, E/N)$ or the electron transport properties of the buffer gas. The gases nitrogen ($N_2$) and argon (Ar) are most commonly used as buffer gases. By changing E/N and buffer gas one can scan easily the mean energy range from thermal to 5 eV.

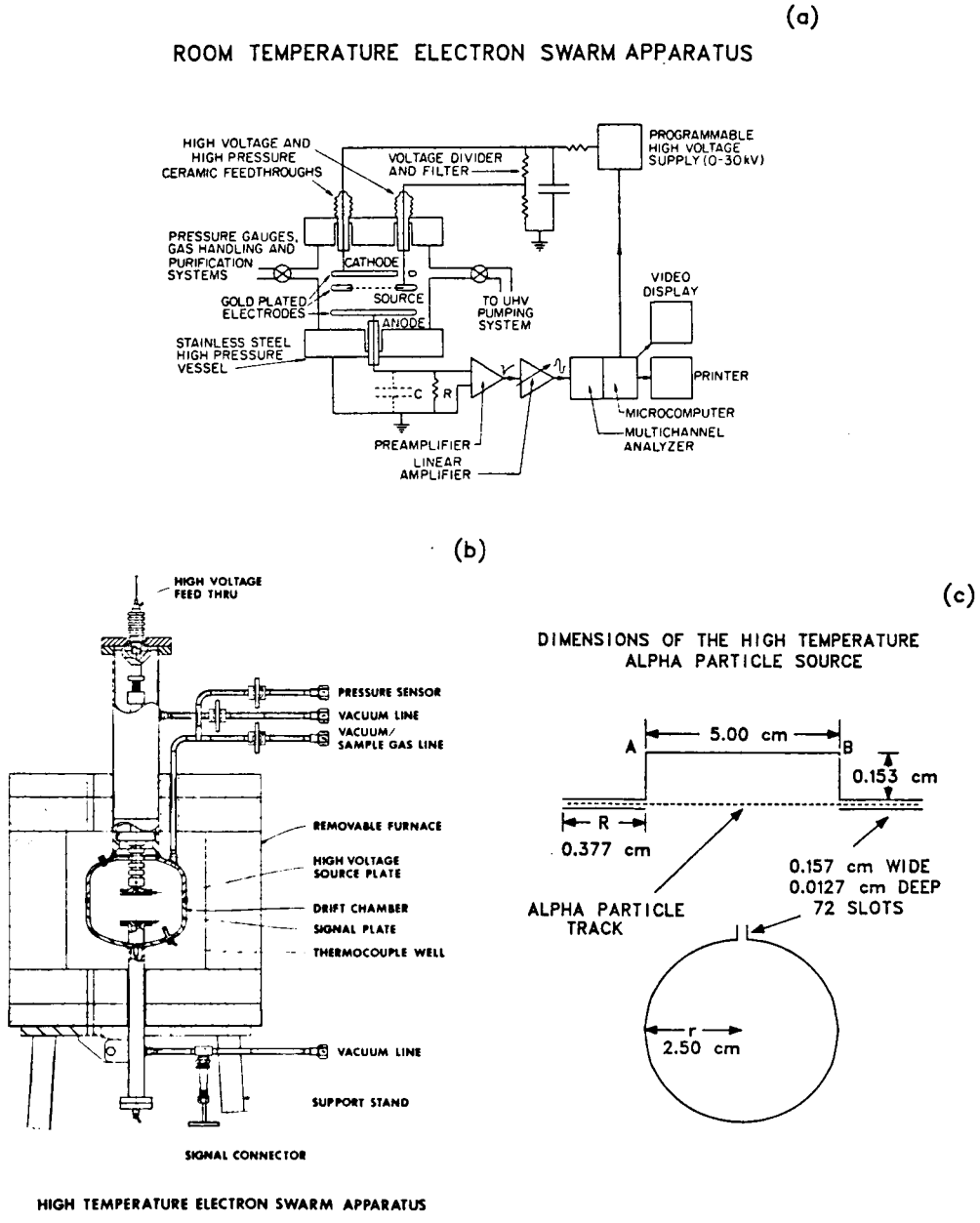


Figure II-4. Comparison of the room temperature [in (a)] and the high temperature [in (b) and (c)] electron swarm apparatuses.

The swarm studies monitor the rate of removal of electrons in the swarm as a function of E/N. Let n(x) be the number of electrons at a distance x from the source plane and let dn(x) be the number of electrons removed from the swarm by the attaching gas as the swarm drifts a distance dx. We then have

$$dn(x) = -\eta n(x)dx \ , \qquad \text{(II-5)}$$

where $\eta$ is the probability of electron attachment per cm traveled in the field direction. Using dx = wdt, where w is the drift velocity of the swarm, and integrating Equation (II-5) we obtain the solution

$$n(t) = n_0 \exp[-(\eta/N_a)N_a wt] \ , \qquad \text{(II-6)}$$

where $\eta/N_a$ is defined as the attachment coefficient with the units of $cm^2$, $N_a$ is the partial attaching gas number density, and $n_0$ is the initial number of electrons produced by each $\alpha$-particle.

The change in voltage at the anode due to the drift of the swarm in the gap is

$$\frac{dV(t)}{dt} = -\frac{n(t)ew}{Cd} \qquad 0 \leq t \leq \tau_1 \ , \qquad \text{(II-7)}$$

where e is the electronic charge, d is the drift distance between the source electrode and the anode, and C is the effective capacitance to ground at the anode, and includes contributions from the capacitance between the electrodes, the input of the preamplifier and connecting cables (C ≈ 50 pf). Equation (II-7) describes the voltage induced on the anode by motion of the electrons provided that the time constant

of the anode circuit, $\tau_A = RC$, is large compared to the transit time of the electron swarm, $\tau_1 = d/w$ ($\tau_A \gtrsim 10^{-3}$ s and $\tau_1 \gtrsim 10^{-6}$ s in these experiments). Substituting Equation ((II-6) into Equation (II-7) and integrating between t = 0 and t = t the variation of the collector potential is found to be

$$V(t) = - \frac{n_0 e}{Cd(n/N_a)N_a} [1 - \exp\{-(n/N_a) \frac{N_a dt}{\tau_1}\}] \quad 0 \leq t \leq \tau_1 . \quad \text{(II-8)}$$

The voltage given by Equation (II-8) is then fed through a charge sensitive preamplifier to a linear pulse amplifier that has a response to a step function given by

$$V'(t) = \frac{t}{\tau_0} \exp[- \frac{t}{\tau_0}] , \quad \text{(II-9)}$$

where $\tau_0$ is the integrating and differentiating time constant of the amplifier ($\tau_0$ = 15 μs in this study). The output of the amplifier for times $\tau > \tau_1$ is given by

$$V(\tau) = \int_0^{\tau_1} \frac{dV(t)}{dt} V'(\tau - t)\, dt , \quad \text{(II-10)}$$

which on integration gives (Bortner and Hurst, 1958)

$$V(\tau) = \frac{A \exp[- \tau/\tau_0]}{(\tau_1 - \tau_0 f)} [(\exp(U\tau_1) - 1)\tau - \exp(U\tau_1)(\tau_1 - 1/U) - \frac{1}{U}] , \quad \text{(II-11)}$$

where $A = n_0 e/C$, $f = (n/N_a)N_a d$ and $U = (\tau_1 - \tau_0 f)/\tau_0\tau_1$ .

The maximum of $V(\tau)$, $V(\tau')$, at the time $\tau'$ can be found in an analytical form by first finding $\tau'$ through solution of

$$\frac{dV(\tau')}{d\tau} = 0 \ , \qquad \text{(II-12)}$$

and then substituting $\tau'$ in Equation (II-11). In practice, the determination of the attachment coefficient $\eta/N_a$ from $V(\tau')$ is done as follows: The voltage $V(\tau)$ is fed into a multichannel analyzer (MCA) operating in the pulse height analysis mode. For a fixed E/N and temperature the channel corresponding to the maximum of $V(\tau)$ is found, first for the pure carrier gas and then for the binary mixture of the attaching-carrier gas. The ratio of these two channels is the experimentally determined parameter needed to calculate $\eta/N_a (=f/N_a d)$. The product of $\eta/N_a$ and the electron drift velocity, w, at each E/N gives the absolute attachment rate constant, $k_a$ (in units of $cm^3\ s^{-1}$). Knowledge of $f(\varepsilon,E/N)$ allows one to transfer $k_a(E/N)$ into the more meaningful quantity $k_a(\langle\varepsilon\rangle)$, where $\langle\varepsilon\rangle$ is the mean electron energy determined at each E/N from the known buffer gas $f(\varepsilon, E/N)$.

## B. Apparatus and Experimental Procedures

1. Modification of the chamber and the $\alpha$-particle source. The apparatus of the present study was designed and built with the capability of performing measurements of electron attachment rate constants over the temperature range 300-1200 K. Although the basic principles for the operation of the apparatus are the same as those employed in the past (Section IIIA), we found it necessary to introduce a few modifications in the construction of the chamber of the present high-temperature swarm apparatus (HTSA). In Figure II-4 are shown for comparison the chambers and the source arrangements of the

room temperature swarm apparatus (RTSA) and the HTSA. Two basic differences between the two apparatuses are noticed from this figure.

The first difference concerns the chamber as a whole. The HTSA chamber is a one body chamber, with a shape different from that of the RTSA, the main difference being the two long necks of the former. With this construction of the new chamber it is calculated that even when the temperature at the collision region is 1200 K, the temperature at the end flanges will not exceed 400 K. In this way the system can be heated up and cooled down without the fear of creating a leak. The new geometry of the HTSA chamber might have eliminated the leak problem, but it imposed a limitation on the maximum permissible operating temperature for the following reason. The swarm experiment has its optimum performance when the electron swarm is formed as close to the center of the source plate as possible. For this to happen the source plate diameter and the total number density have to be chosen in such a way that the $\alpha$-particle stops near the center of the plate, since it is known that an $\alpha$-particle drifting in a gas produces the maximum number of ion pairs at the end of its track. However, due to the construction of the chamber, the radius of the source plate (as well as that of the collector) cannot be made greater than 2.5 cm. For an $\alpha$-particle of 5.16 MeV energy (produced from a $Pu^{239}$ source) to have this range, the operating pressure has to be $\sim$2000 Torr at room temperature. Given that the chamber can be safely operated at pressures up to 6000 Torr at the maximum operating temperature, this means that the higher permissible temperature should not exceed $\sim$900 K. The

chamber, of course, can be heated at the maximum temperature of 1200 K, provided that the pressure at this temperature is $\leq$ 3000 Torr.

Besides the maximum temperature limitation problem, a second problem was found to be related to the shape of the HTSA chamber. The measured attachment rate constants were observed to show a significant time dependence. If, however, the two gases (attaching and buffer) were first premixed in a compact-shaped cylinder and then introduced into the collision chamber, the measured rates were found to be time independent. The extensive use of insulating material, associated also with the shape of the chamber, created obstacles for the overcome of which considerable time was invested. It was found that the insulators were losing their insulating properties becoming conductors as the temperature was raised. The original insulators made out of lava material were replaced by new macor (ceramic material) insulators which permitted measurements up to 600 K. To go above this temperature new $Al_2O_3$ insulators are needed, which at the time this work was done were not possible to obtain.

The second difference between the HTSA and the RTSA concerns the source-electrodes arrangement. In the HTSA, the cathode (high-voltage electrode) is identical with the source plate. This arrangement is advantageous over the RTSA arrangement. It makes unnecessary the use of a second high voltage feedthrough [Figure II-4(a)] which would be needed to provide the proper voltage to the source plate in case this was separate from the cathode. Furthermore, separated source and cathode plates would mean more difficulties in mounting

these two plates and additional uncertainties in determining various separation distances. Figure II-4(c) gives the dimensions of the HTSA α-source. The radioactive material was electroplated on a thin ribbon of platinum, which was mounted in a groove, cut at a distance R from the inside edge of the annulus. To avoid back scattering of the α-particles from the plane AB [Figure II-4(c)], the distance R was chosen to be 0.377 cm. This distance is much higher compared to the values (0.0355 cm < R < 0.0965 cm) used for the RTSA sources. With these dimensions, however, the intensity of the signal obtained with the present source was found to be lower by a factor of ten compared to that obtained with the room temperature sources. This not only made the statistics of the measurements poorer but also required longer times for the measurements to be performed. It is felt that this was the most serious deficiency of the present apparatus as compared with the RTSA. As it is seen from Figure II-4(c), increase in the number of slots was not possible. Also the source was already used at its maximum activity, whereas a decrease in the distance R was not permissible. Thus no remedy was found possible for the low count rate.

2. The entire apparatus. A schematic diagram of the entire apparatus is shown in Figure II-5. The apparatus may be described as consisting of three parts: the drift chamber, the gas manifold, and the carrier gas purification system. The chamber and the manifold were pumped by a turbo-molecular pump (Pfeiffer TSU 111 type), whereas the gas purification system was pumped by a diffusion pump (Varian HS-2). Background pressures of $\sim 10^{-8}$ Torr were obtained

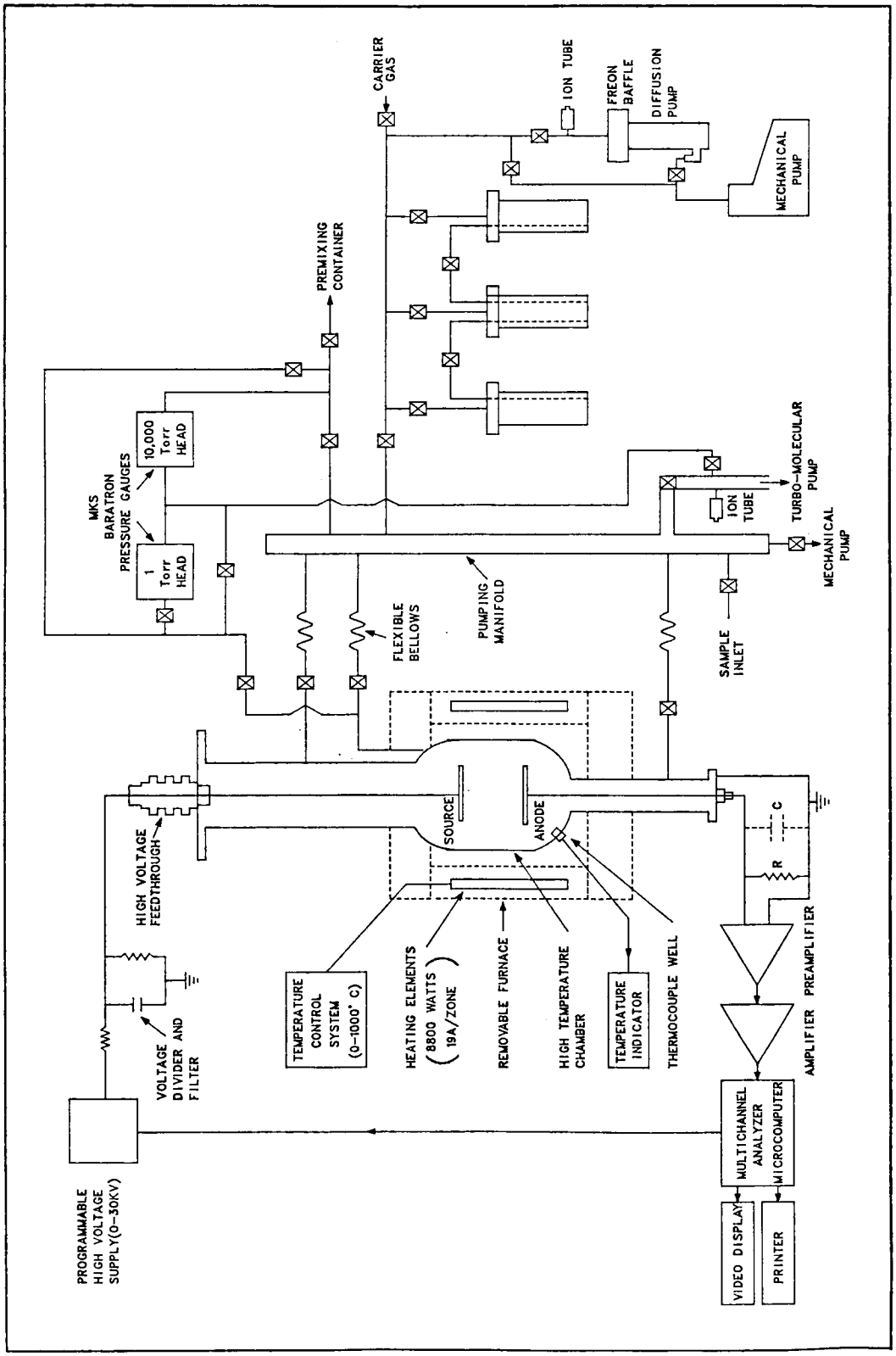


Figure II-5. Schematic diagram of the high temperature electron swarm apparatus.

between measurements, with an outgassing rate <0.1 μ/hr. The total and partial attaching gas pressures were measured, respectively, with a 10,000 (±0.1) Torr and a 1.00000 (±0.00001) Torr MKS Baratron bakable heads (170 Series). The electronics of the system are similar to those of the room temperature system shown in Figure II-4(a) (p. 38). The drift voltages were provided by Bertan programmable power supplies (model 205A-10N and 205A-30N for voltages up to 10 and 30 KV, respectively), and measured using a precision voltage divider and a Keithley (model 176) digital multimeter. The induced anode voltages produced by the electron swarm were detected and amplified by a pre-amplifier (Tennelec No. TC 161D) and a linear amplifier (Tennelec No. TC222) and passed into a microprocessor based 2048 chennel MCA (Nucleus model 2048) where the distribution of the resultant peak voltages pulse height were stored. The pulse height histogram was analyzed by the microprocessor to find the most probable pulse height, which was then used to obtain $\eta/N_a$, and then $k_a$, using a simple numerical iteration procedure. The microprocessor then reset the programmable voltage supply and hence E/N, and a new histogram was obtained and the whole procedure was repeated.

3. Temperature system. As it has been already pointed out the capability of measuring electron attachment rates of various molecules over a relatively large range of temperatures was built into the apparatus. A specially designed furnace (series 3210, split type) and control system (series 230), both built by the Applied Test System, Inc., were used for this purpose. The walls of the cylindrical-shaped

furnace, of 2.5" thickness at the side and 3" at the top and bottom, were made of low "K" factor vacuum cast ceramic fiber insulation that provides minimum heat loss, high temperature capability and rigid structure. Extra insulation plates were fitted at the top and bottom of the furnace to minimize heat loss, while a stainless steel shell was covering the side walls of the furnace. Two zones—upper and lower—of 8800 Watts heating elements each, were embedded into the inside of the insulation walls of the furnace. The two zones were heated independently by the passage of 19 AMP/zone current provided by the temperature controllers to which they were connected. Two thermocouples, the one being used to measure the temperature of the upper zone and the other to measure the temperature of the lower zone were also connected to the temperature controllers (one for each zone). The desirable temperature at which the swarm chamber had to be heated was set on the setpoint of the two controllers (0-1000°C range, 1°C resolution). Six chromel-alumel type KX thermocouples were placed into an equal number of wells extended inside the chamber so that to measure the temperature as close to the collision region (space between the $\alpha$-particle source and the collector) as possible. Two of the thermocouples (one measuring the temperature at the upper and the other at the lower part of the chamber) were connected to a Honeywell multipoint chart recorder. The other four thermocouples were connected to a digital temperature indicator (Instrulab 5000 series). It was observed that because of heat losses there was a gradient of temperatures between the inside walls of the furnace and the outside walls of the chamber. This required that the temperature

settings on the setpoint controllers had to be higher than (depending on) the actual temperature of the chamber as read by the temperature indicator. By the use of the furnace and the accessory equipment described above, the desirable temperature of the chamber could easily be set with an uncertainty of ±1°C. The determination of the actual temperature, however, was not better than ±2.2°C, since this was the limit error specified for the thermocouples used.

4. Experimental procedures and errors. The whole experimental procedure applied in the present experiment was very briefly as follows: The chamber was first brought to the desired temperature, after it had been baked for ∿48 hours at a higher temperature so that the outgassing rate was low. At a fixed temperature the pure gas was first admitted into the chamber, and using the procedure as described in Section IIIA.2 a series of the channel numbers corresponding to the most probable pulse height ("peak channel number") as a function of E/N was obtained. A mixture of the attaching gas (one part in $10^5$ to $10^8$ of the total gas pressure) with the buffer gas, which had been prepared in the premixing cylinder, was then admitted into the chamber and a new series of peak channel numbers as a function of E/N was obtained. The ratio of the peak channel numbers at every E/N were used to determine the $\eta/N_a$ at the corresponding E/N. The partial pressure of the attaching gas was extremely small, and thus it was permissible to assume that the influence of the attaching gas on the electron energy distribution function was negligible. To observe and to remove any possible such influence, the measurements as a function of the partial attaching gas pressure were performed, and the pressure

independent attaching rates could be obtained from an extrapolation of the rates to zero partial attaching gas pressures. Similar sets of measurements were performed at all temperatures studied. Before every measurement the buffer gas (quoted purity 99.9995%) was further purified by fractional distillations in the liquid nitrogen traps of the carrier gas purification system. The attaching gases were deoxygenated with repeated freeze-pump-thaw cycles.

The possible sources of errors and their uncertainties are summarized in Table II-1. The total uncertainty in the determination of $k_a$ is estimated to be 6-8%.

C. Analytical Methods

The electron attachment rate constants, $k_a$, measured directly in the swarm experiment, can be used to obtain the absolute electron attachment cross sections, $\sigma_a(\varepsilon)$ for each of the attaching molecules. The quantities $k_a(E/N)$ and $\sigma_a(\varepsilon)$ are related through

$$k_a(E/N) = \left(\frac{2}{m}\right)^{1/2} \int_0^\infty \varepsilon^{1/2}\, \sigma_a(\varepsilon) f(\varepsilon, E/N) d\varepsilon \ , \qquad \text{(II-13)}$$

where $\varepsilon$ is the electron energy, m is the electron mass and $f(\varepsilon,E/N)$ is the electron energy distribution function at each value of E/N. For the present study, as it has been pointed out in Section IIIB.4, the $f(\varepsilon, E/N)$ used are assumed to be those of the pure buffer gas and the addition of vanishingly small quantities of the attaching gas does not perturb $f(\varepsilon, E/N)$. For this study the $f(\varepsilon, E/N)$ for $N_2$ and Ar were obtained from a numerical solution of the Boltzmann transport equation

Table II-1. Sources of errors and their estimated uncertainties in the electron attachment swarm apparatus

| Source | Error |
|---|---|
| Drift distance | ±1.0% |
| Chamber temperature | ±0.5% |
| Total gas pressure | ±0.5% |
| Electric field voltage | ±0.5% |
| Partial attaching gas pressure | ±2.0% |
| Electron swarm transit time | ±0.5% |
| Statistical uncertainty in determining the average electron signal pulse height | ±1-2% |
| Approximations in the analysis of the pulse heights to obtain the electron attachment rate constant | Expected to be small when the electron swarm transit time > the time constant of the linear amplifier (15 μs) |
| Non-ideal response characteristics of the linear amplifier | Same conditions apply as above |

developed by Luft (1975). A recent comprehensive discussion on the derivation of the distribution functions is found in Hunter and Christophorou (1983), whereas older treatments on this subject can be found in, e.g., Christophorou, 1971, and McCorkle and Christophorou, 1972.

The utilization of Equation II-13 to determine $\sigma_a(\varepsilon)$ can be employed in two ways: through the swarm unfolding technique and through the swarm-beam technique.

1. Swarm unfolding technique. In the swarm unfolding technique, first derived by Christophorou et al. (1971b) $\sigma_a(\varepsilon)$ is determined solely from the swarm determined $k_a(E/N)$ and from a knowledge of $f(\varepsilon, E/N)$. To perform the unfolding procedure, the monoenergetic attachment rate constant $k_m(\varepsilon)$ is first defined as

$$k_m(\varepsilon) = \sigma_a(\varepsilon)\left(\frac{2}{m}\right)^{1/2} \varepsilon^{1/2} \quad . \tag{II-14}$$

Thus the measured rate constant at the mean energy $\langle\varepsilon\rangle_j$ (i.e., at the jth value of E/N) is expressed as

$$k_a(\langle\varepsilon\rangle_j) = \int_0^\infty k_m(\varepsilon) f(\varepsilon, \langle\varepsilon\rangle_j) d\varepsilon \quad . \tag{II-15}$$

To start the iteration procedure, $k_m(\varepsilon)$ is initially approximated by the $k_a(\langle\varepsilon\rangle)$ or by another function [the final values of $\sigma_a(\varepsilon)$ are independent of the initial choice of $k_m(\varepsilon)$—see Christophorou et al., 1971b], with the constraint that $k_m(\varepsilon) = 0$ above the maximum energy accessible by the distribution function at the highest E/N value. These

values of $k_m(\varepsilon)$ are then substituted into Equation (II-15) and a new series of values of $k_a(\langle\varepsilon\rangle_j)$ are calculated for every $\langle\varepsilon\rangle_j$ (e.g., for every E/N) value used.

If we define the weighting factors $W(\langle\varepsilon\rangle_j)$ to be the ratios of the experimental rate constants $k_{exp}(\langle\varepsilon\rangle_j)$ and the calculated rate constants $k_{cal}(\langle\varepsilon\rangle_j)$, a new function $k_m(\varepsilon)$ can be determined through

$$k_{m_{new}}(\varepsilon) = k_{m_{old}}(\varepsilon) \frac{\sum_j W(\langle\varepsilon\rangle_j)^n f(\varepsilon,\langle\varepsilon\rangle_j) W'(\langle\varepsilon\rangle_j)}{\sum_j f(\varepsilon,\langle\varepsilon\rangle_j) W'(\langle\varepsilon\rangle_j)} , \qquad \text{(II-16)}$$

where n is an accelerator factor >1 which can be used to speed up the convergence rate and $W'(\langle\varepsilon\rangle_j)$ is an "importance factor" which may be used to attach a different significance to each of the $k_{exp}(\langle\varepsilon\rangle_j)$ values depending on the estimated accuracy.

The new value of $k_m(\varepsilon)$ is substituted in Equation (II-15) and the whole procedure is repeated several times until the residuals are minimized, i.e.

$$\sum_j [k_{exp}(\langle\varepsilon\rangle_j) - k_{cal}(\langle\varepsilon\rangle_j)]^2 \rightarrow \text{minimum} . \qquad \text{(II-17)}$$

The weighting factors, then, approach the value one and the mono-energetic rates $k_m(\varepsilon)$ do not change with successive iterations.

The use of the unfolding procedure as described above requires a considerable degree of experience and discernment, otherwise it can lead to misfacts and false results. For example, continuation of the iterating procedure beyond a certain number of iterations, statistical

uncertainties in the experimental data and the nature of the data itself (see Chapter VI) may lead to spurious effects on the unfolded function. See a further discussion on this subject in Hunter and Christophorou (1983).

2. Swarm-beam method. The swarm-beam method (Christophorou, 1971) provides a second way to determine $\sigma_a(\varepsilon)$ from Equation (II-13) by combining the negative ion currents $I(\varepsilon)$ obtained by the beam technique and the $k_a(<\varepsilon>)$ measured by the swarm technique. There are, however, some limitations but also some advantages discussed in Chapter V, where this method has been employed.

Briefly in this method, $\sigma_a(\varepsilon)$ is represented by

$$\sigma_{ai}(\varepsilon) = K_i T_i I(\varepsilon) \qquad \text{(II-18)}$$

where $\sigma_{ai}(\varepsilon)$ is the ith trial attachment cross section function obtained when $I(\varepsilon)$ is transferred from arbitrary to absolute units by the factor $K_i$ and is translated by $T_i$ along the energy axis. The constants $K_i$ and $T_i$ are determined by a double least square procedure through

$$\frac{d}{dT_i}\left[\sum_j\left[\left(\frac{2}{m}\right)^{1/2} K_i \int_0^\infty \varepsilon^{1/2} T_i I(\varepsilon) f(\varepsilon,<\varepsilon>_j)d\varepsilon - k_a(<\varepsilon>_j)\right]^2\right] = 0 \; . \qquad \text{(II-19)}$$

# CHAPTER III

## ELECTRON ATTACHMENT TO THE PERFLUOROALKANES n-$C_NF_{2N+2}$ (N = 1-6)

### I. INTRODUCTION

In this chapter are presented and discussed the results of a study on the negative ions produced by direct electron impact on the perfluoroalkanes (PFAs): tetrafluoromethane ($CF_4$), hexafluoroethane ($C_2F_6$), perfluoropropane ($C_3F_8$), n-perfluorobutane (n-$C_4F_{10}$), n-perfluoropentane (n-$C_5F_{12}$), and n-perfluorohexane (n-$C_6F_{14}$). Negative ion formation by slow electron ($\sim$0-10 eV) impact with these molecules is of intrinsic, as well as of practical, interest. The study of these molecules provides information on the effect of the size of the molecule on its electron attaching properties. Additionally, an increased number of uses have been found in recent years for these PFAs in various applications. Their high dielectric strength (due to their ability to attach slow electrons) (James et al., 1980; Wootton et al., 1980) makes them potentially useful as gaseous insulators, especially in combination with other gases (Christophorou et al., 1982c). Also the magnitude and energy dependence of the electron attachment rate constants for some of these molecules are such as to make them good for applications in fast gas mixtures for neutron counters (Christophorou et al., 1979; Kopp et al., 1982), diffuse discharge switches (see e.g., Christophorou et al., 1982d), plasma etching (Coburn and Winters, 1979), etc.

# II. RESULTS

## A. Negative Ion Formation from Molecules of the Form $n\text{-}C_NF_{2N+2}$ (N = 1-6)

1. $CF_4$. Two complementary fragment ions, $CF_3^-$ and $F^-$, were observed for $CF_4$. Their relative cross sections as a function of $\varepsilon$ are shown in Figure III-1(a). Each curve represents the average of at least four sets of data. Each set of data has been deconvoluted [Section IIB-(2), Chapter II], and the average of the corresponding unfolded functions are shown in Figure III-1(b). The relative peak intensities, energy of the maximum ion intensity, FWHM, and appearance onsets for the two anions are listed in Table III-1, where a comparison with literature data is made (see Section IV for discussion).

2. $C_2F_6$. The nonunfolded and the unfolded relative cross sections for the three anions ($C_2F_5^-$, $CF_3^-$, and $F^-$) observed for $C_2F_6$ are shown, respectively, in Figures III-2(a) and III-2(b). The pertinent physical quantities are listed in Table III-1 and are compared with literature data. The $C_2F_5^-$ resonance peaks at 4.8 eV; it is much weaker in intensity and narrower in FWHM compared with the $F^-$ and $CF_3^-$ resonances which both peak at $\sim$4 eV. Note that these NISs at $\sim$4 eV are $\sim$3 eV lower than those observed at $\sim$7 eV in $CF_4$.

3. $C_3F_8$. Five fragment negative ions were observed for $C_3F_8$: $C_3F_7^-$, $C_2F_5^-$, $C_2F_3^-$, $CF_3^-$ and $F^-$. Their relative cross sections as a function of $\varepsilon$ are shown in Figure III-3(a) with the corresponding unfolded cross section functions shown in Figure III-3(b). The peak

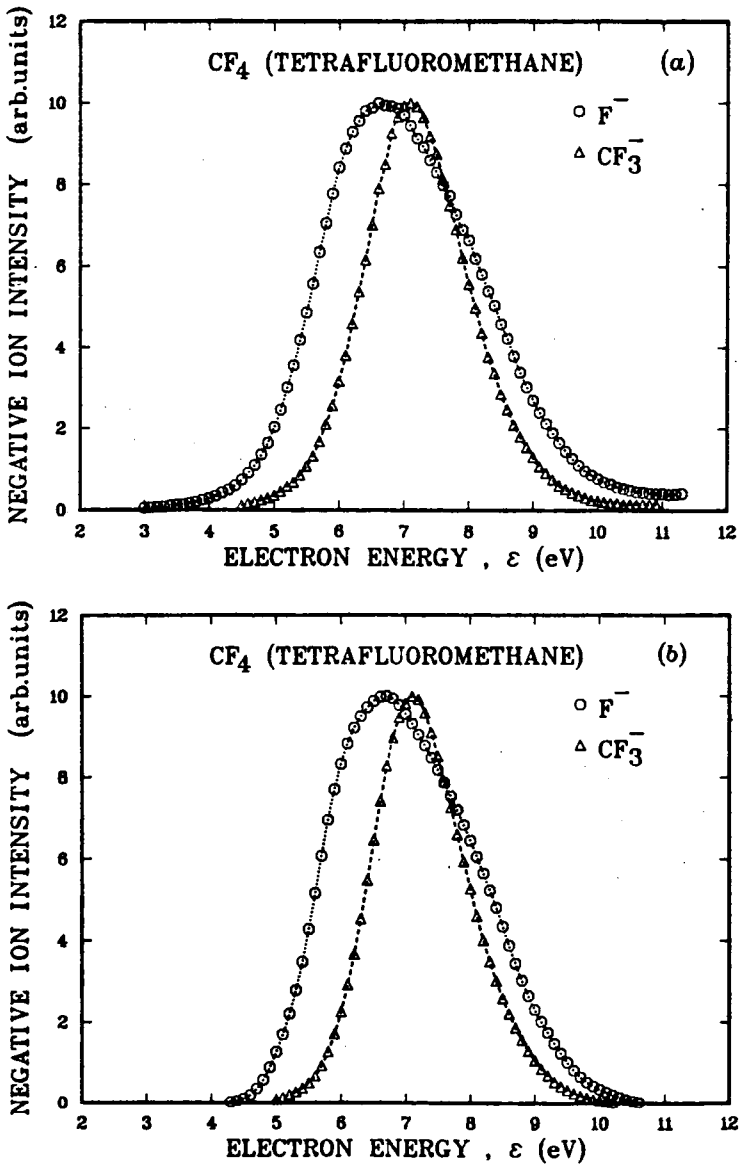


Figure III-1. Negative ion intensity as a function of ε for $CF_4$. (a) Nonunfolded data; (b) unfolded data.

Table III-1. Negative ions due to low-energy electron impact on $CF_4$ and $C_2F_6$

| Molecule | Negative ion | Relative peak intensity | Energy of maximum ion intensity (eV)[b] | FWHM[a] (eV)[c] | Appearance onset (eV)[c] |
|---|---|---|---|---|---|
| $CF_4$ | $CF_3^-$ | 1000,(660),[d](570)[e] | 7.1±0.05,(6.9)[d] | 1.7,(1.9)[e] | 5.1±0.1,(5.4)[d,e] |
| | $F^-$ | 1000,(1000)[d,e] | 6.7±0.05,(6.15)[d] | 2.75,(2.5)[e] | 4.5±0.1,(4.65),[d](4.7)[e] |
| | | | (∼7.5)[d] | | (∼6.2)[d] |
| $C_2F_6$ | $C_2F_5^-$ | <1,(10)[d] | 4.8±0.1 | 0.75 | 3.5±0.1 |
| | $CF_3^-$ | 316,(210),[d](240)[f] | 4±0.05,(4.4),[d](3.75)[f] | 1.7 | 2.4±0.1,(2.2),[d](2.8)[f] |
| | $F^-$ | 1000,(1000)[d,f] | 3.9±0.05,(4.3),[d](3.75)[f] | 2.2 | 2±0.1,(2.1),[d](2.2)[f] |

[a]Full width at half maximum of the respective negative ion intensity as a function of electron energy.

[b]Energy scale calibration determined using for the $SF_5^-/SF_6$ resonance the value of 0.37 eV. The ± refers to the standard deviation from the average.

[c]Values listed are from the unfolded data.

[d]P. W. Harland and J. L. Franklin, J. Chem. Phys. 61, 1621 (1974).

[e]K. A. G. MacNeil and J. C. J. Thynne, Int. J. Mass Spectrom. Ion Phys. 3, 455 (1970).

[f]M. M. Bibby and G. Carter, Trans. Faraday Soc. 59, 2455 (1963).

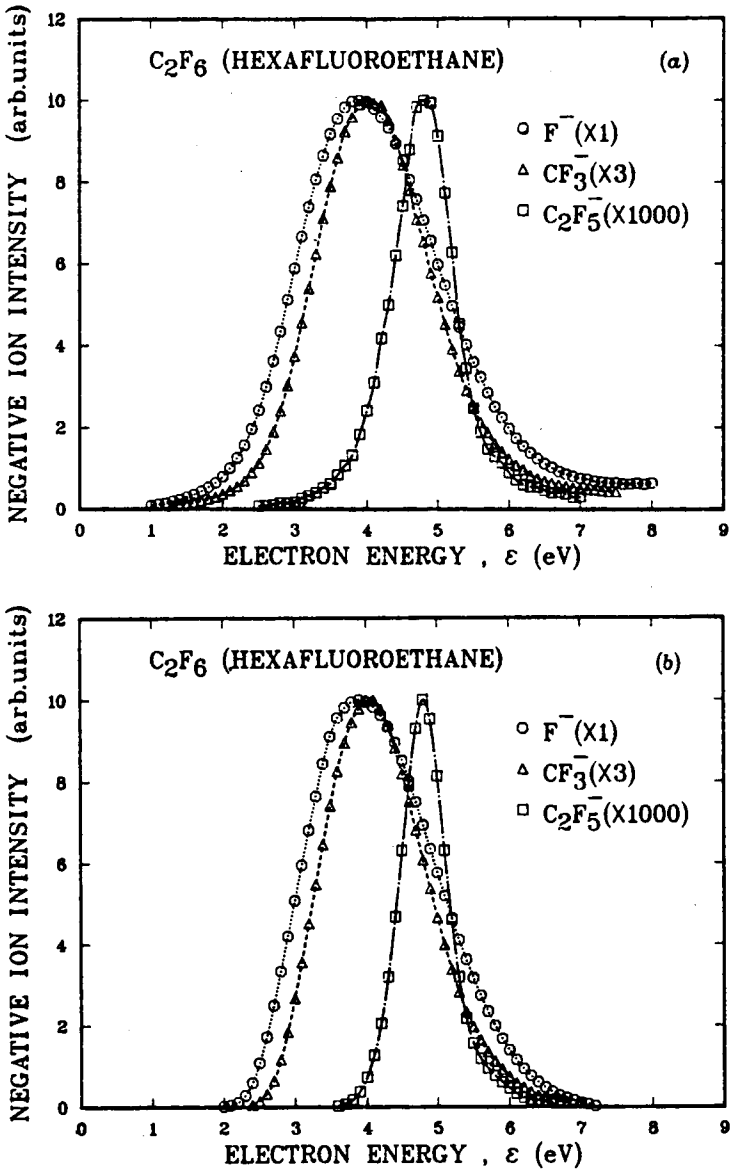


Figure III-2. Negative ion intensity as a function of ε for $C_2F_6$. (a) Nonunfolded data; (b) unfolded data (note the multiplication factors).

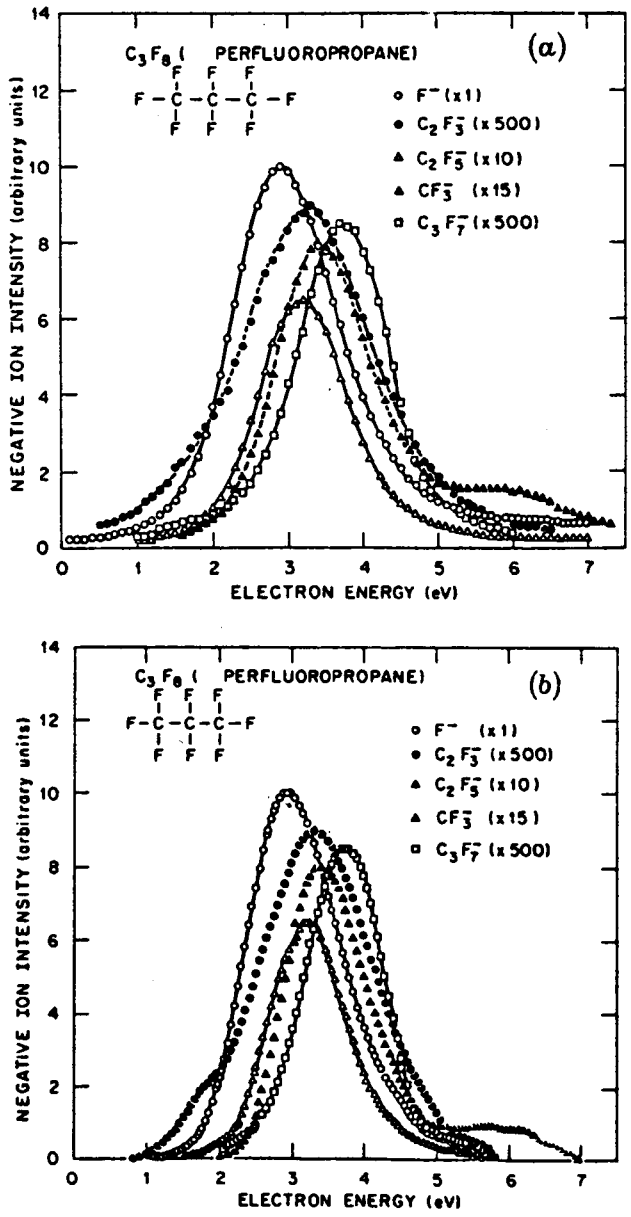


Figure III-3. Negative ion intensity as a function of $\varepsilon$ for $C_3F_8$. (a) Nonunfolded data; (b) unfolded data (note the multiplication factors).

intensities, resonance maxima, FWHM, and onsets for each negative ion are summarized in Table III-2 and are compared with literature data. The complementary ions $CF_3^-$ and $C_2F_5^-$ and the ion $C_2F_3^-$ have their resonance maxima at 3.3 ± 0.2 eV. The peak position of the predominant ion $F^-$ and its weak complementary ion $C_3F_7^-$ are shifted to lower and higher energies, respectively, relative to the position of a possible common NIS at 3.3 ± 0.2 eV. There is also evidence for a second NIS at >5.5 eV.

4. n-$C_4F_{10}$. The n-$C_4F_{10}$ molecule is the first member of the perfluoroalkane series for which we observed a parent negative ion. The energy dependences of the weak parent anion signal and the observed five fragment anions ($C_4F_9^-$, $C_3F_7^-$, $C_2F_5^-$, $CF_3^-$, and $F^-$) are shown in Figure III-4(a). The corresponding unfolded cross section functions are shown in Figure III-b(b). In Table III-3 are summarized pertinent quantities which are compared with literature data. With the exception of $C_4F_9^-$, the results from the present work agree well with those of Harland and Thynne (1973). The appearance onsets for $C_3F_7^-$, $C_2F_5^-$, and $CF_3^-$ as determined by Reese et al. (1956) and Greenhaus (1965) are considerably higher than those of the present work. Differences have also been observed in the relative abundances of the various negative ions as they have been determined by different authors (see Table III-3).

The parent ion $C_4F_{10}^{-*}$ has its peak intensity at ∿0.6 eV, well below the energy of 3.0 ± 0.2 eV, where the dissociative attachment resonances exhibit their maxima. There is a grouping of the fragment anion maxima at ∿3 eV which may indicate common short-lived ($<<10^{-6}$ s) NIS(s) as the

Table III-2. Negative ions due to low-energy electron impact on $C_3F_8$

| Negative ion | Relative peak intensity | Energy of maximum ion intensity (eV)[b] | FWHM[a] (eV)[c] | Appearance onset (eV)[c] |
|---|---|---|---|---|
| $C_3F_7^-$ | 1.7,(0.4)[d] | 3.75,(3.9)[d] | 1.2,(1.1)[d] | 2.5±0.2,(2.9),[d](2.4)[e] |
| $C_2F_5^-$ | 66,(23),[d](73),[f](63)[g] | 3.2,(3.4),[d](3.2)[f] | 1.25,(1)[d] | 2.1±0.2,(2.4),[d](1.7),[e](2.1),[f](2)[g] |
| $C_2F_3^-$ | 1.8 | 3.3 | 1.85 | 1.1±0.1 |
| $CF_3^-$ | 54,(20),[d](63),[f](39)[g] | 3.4,(3.6),[d](3.4)[f] | 1.35,(1.2)[d] | 2.4±0.2,(2.5),[d](2),[e](2,2),[f](2.1)[g] |
| | 2 | >5.5(unresolved structure),(5.7)[d] | (0.9)[d] | >5,(5.2)[d] |
| $F^-$ | 1000,(1000)[d,f,g] | 2.9,(3.1),[d](3)[f] | 1.5,(1.2)[d] | 1.7±0.2,(1.8),[d](1.35),[e](1.8),[f](1.6)[g] |

[a]Full width at half maximum of the respective negative ion intensity as a function of electron energy.

[b]Energy scale calibration determined using for the $SF_5^-/SF_6$ resonance the value of 0.37 eV. A standard deviation of ±0.05 eV from the average should be considered for each value.

[c]Values listed are from the unfolded data.

[d]P. W. Harland and J. C. J. Thynne, Int. J. Mass Spectrom. Ion Phys. 9, 253 (1972).

[e]C. Lifshitz and R. Grajower, Int. J. Mass Spectrom. Ion Phys. 3, 211 (1969).

[f]M. M. Bibby and G. Carter, Trans. Faraday Soc. 59, 2455 (1963).

[g]H. L. Greenhaus, Negative Ion Formation by Electron Impact in Some Perfluoroalkanes (University Microfilms, Ann Arbor, Michigan, 1965).

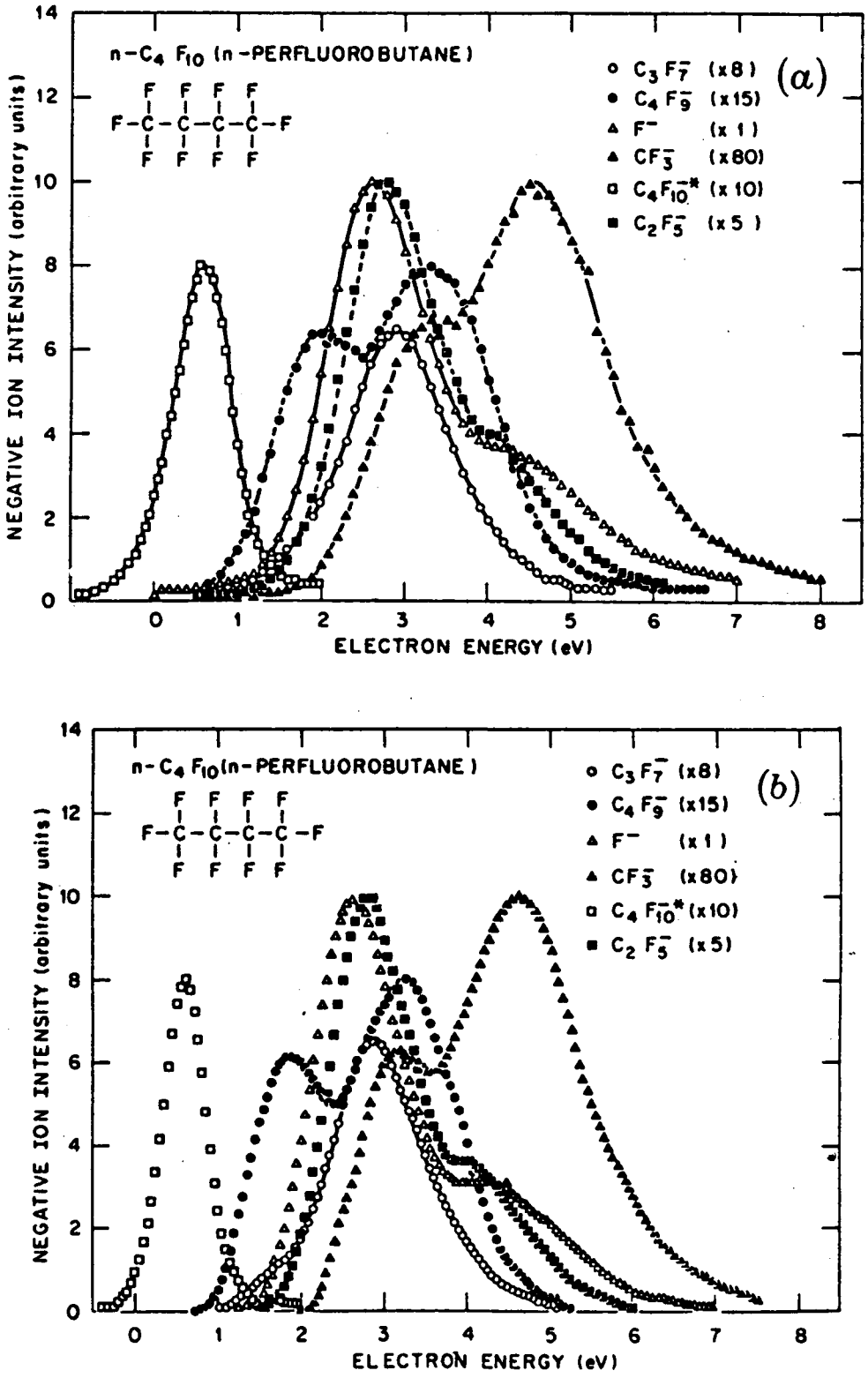


Figure III-4. Negative ion intensity as a function of $\varepsilon$ for n-$C_4F_{10}$. (a) Nonunfolded data; (b) unfolded data (note the multiplication factors).

Table III-3. Negative ions due to low-energy electron impact on n-$C_4F_{10}$

| Negative ion[b] | Relative peak intensity | Energy of maximum ion intensity (eV)[c] | FWHM[a] (eV)[d] | Appearance onset (eV)[d] |
|---|---|---|---|---|
| $C_4F_{10}^{-*}$ | 80,(<1),[e](8)[f] | 0.6±0.05 | 0.57 | ∿0,(0.0),[e](0.3±0.3)[f] |
| $C_4F_9^-$ | 46,(1),[e](2),[f](57)[g] | 1.85±0.1[h] | | 1±0.1,(2.2),[e](2.2),[f](2.1)[g] |
| | 53,(2),[f](57)[g] | 3.25±0.05,[h](∿2.7)[e] | | <2.0±0.3,(4.1)[g] |
| $C_3F_7^-$ | 80,(13),[e](28),[f](57)[g] | 2.85±0.05,(2.9)[e] | 1.25,(0.8)[e] | 1.2±0.3,(2.1),[e](3.6),[f](2.8)[g] |
| $C_2F_5^-$ | 200,(103),[e](137),[f](171)[g] | 2.8±0.05,(3)[e] | 1.2,(0.9)[e] | 1.8±0.15,(2.1),[e](2.6),[f](2.8)[g] |
| | 72,(29)[e] | 4±0.1,(4.4)[e] | (0.9)[e] | <4,(3.8)[e] |
| $CF_3^-$ | 8,(2),[e](10),[f](9)[g] | 3.2±0.1,(3.2)[e] | | 2.2±0.1,(2.3),[e](4),[f](3.3)[g] |
| | 13,(4),[e](12)[f] | 4.6±0.05,(4.6)[e] | 1.9,(1.2)[e] | >3.2±0.3,(3.8)[e] |
| $F^-$ | 1000,(1000)[e,f,g] | 2.65±0.05,(2.9)[e] | (0.9)[e] | 1.6±0.1,(2),[e](1.6),[f](1.2)[g] |
| | 300,(240)[e] | 4.2±0.1,(4.4)[e] | 1.35,(0.9)[e] | <4,(3.8)[e] |

[a]Full width at half maximum of the respective negative ion intensity as a function of electron energy.

[b]An asterisk (*) indicates that the ion is long lived with respect to autodetachment.

[c]Energy scale calibration determined using for the $SF_5^-/SF_6$ resonance the value of 0.37 eV. The ± refers to the standard deviation from the average.

[d]Values listed are from the unfolded data.

[e]P. W. Harland and J. C. J. Thynne, Int. J. Mass Spectrom. Ion Phys. 11, 445 (1973).

[f]H. L. Greenhaus, Negative Ion Formation by Electron Impact in Some Perfluoroalkanes (University Microfilms, Ann Arbor, Michigan, 1965).

[g]R. M. Reese, V. H. Dibeler, and F. L. Mohler, J. Res. Nat. Bur. Stand. 57, 367 (1956).

[h]Possibly due to ions from i-$C_4F_{10}$ (see text).

precursor(s) of these ions at this energy. A similar suggestion can be made for the secondary maxima in the $I(\varepsilon)$ functions of $F^-$, $CF_3^-$, and $C_2F_5^-$ at 4.2 ± 0.3 eV. The peak of the $C_4F_9^-$ cross section at ∿1.8 eV is probably due to the presence of an i-$C_4F_{10}$ impurity, as can be seen from the results for the i-$C_4F_{10}$ fragmentation under electron impact and also on the basis of energetic considerations (see Section III).

5. n-$C_5F_{12}$. The parent, $C_5F_{12}^{-*}$, and eight fragment, $C_5F_{11}^-$, $C_5F_{10}^{-*}$, $C_4F_9^-$, $C_4F_8^-$, $C_3F_7^-$, $C_2F_5^-$, $C_2F_3^-$, $F^-$, ions have been observed when slow electrons collided with n-$C_5F_{12}$. The parent anion is the most intense. The relative cross sections are shown in Figures III-5(a) and III-5(b), and the relative peak intensities, resonance maxima, FWHM, and onsets are summarized in Table III-4. Four NISs can be identified for n-$C_5F_{12}$: a low-lying one at ∿0.6 eV leading mostly to parent anions, a second NIS at ∿1.6 eV leading mostly to dissociative attachment fragments, and a third and fourth NIS, respectively, at ∿2.5 and ∿3.5 eV each leading to dissociative attachment fragments. The observation of dissociative attachment at ∿0.0 eV, if real, implies that parent negative ions are produced at a higher energy than are fragment anions (see discussion in Section III).

6. n-$C_6F_{14}$. The behavior of n-$C_6F_{14}$ under low-energy electron impact is similar to that of n-$C_5F_{12}$. The parent ion $C_6F_{14}^{-*}$ is the predominant ion with its peak at 0.55 eV. The observed fragment anions are: $C_6F_{13}^-$, $C_6F_{12}^-$, $C_5F_{11}^-$, $C_5F_{10}^-$, $C_5F_9^-$, $C_4F_9^-$, $C_4F_7^-$, $C_3F_7^-$, and $F^-$. The average yields of all the ions detected as a function of electron energy are given in Figures III-6(a) and III-6(b), and the pertinent quantities

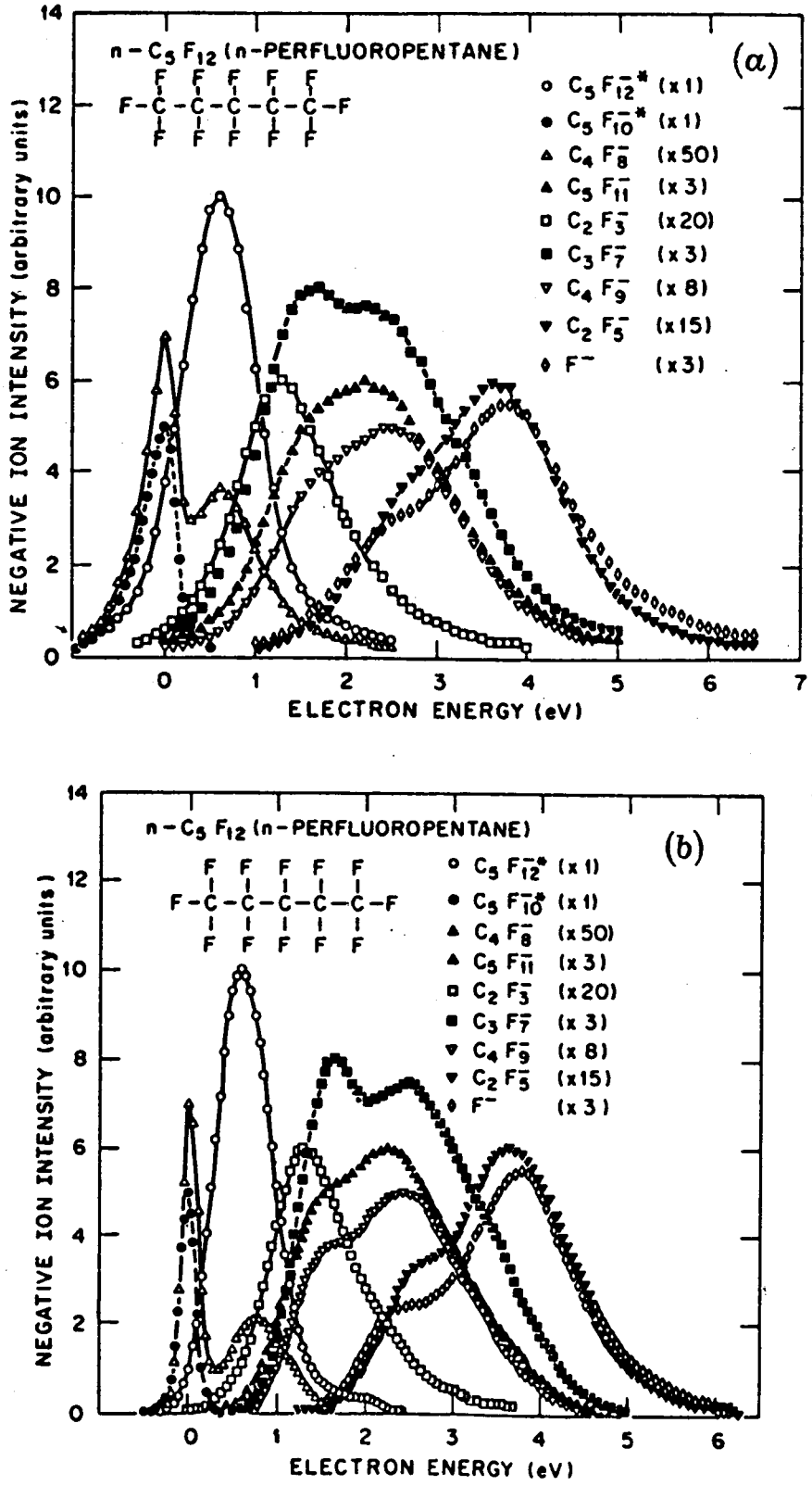


Figure III-5. Negative ion intensity as a function of ε for n-$C_5F_{12}$. (a) Nonunfolded data; (b) unfolded data (note the multiplication factors).

Table III-4. Negative ions due to low-energy electron impact on n-$C_5F_{12}$

| Negative ion[b] | Relative peak intensity | Energy of maximum ion intensity (eV)[c] | FWHM[a] (eV)[d] | Appearance onset (eV)[d] |
|---|---|---|---|---|
| $C_5F_{12}^{-*}$ | 1000 | 0.6±0.05 | 0.75 | ∿0 |
| $C_5F_{11}^-$ | 170 | 1.65∿0.1 | 2.05[e] | 0.65∿0.1 |
| | 200 | 2.25±0.05 | | <1.65 |
| $C_5F_{10}^{-*}$ | 500 | ∿0 | 0.2 | |
| $C_4F_9^-$ | 51 | 1.7±0.1 | 2.0[e] | 0.8±0.15 |
| | 66 | 2.45±0.05 | | <2 |
| $C_4F_8^-$ | 15 | ∿0 | 0.22 | |
| | 5 | 0.75∿0.1 | 0.75 | 0.2∿0.05 |
| $C_3F_7^-$ | 300 | 1.65∿0.1 | 2.3[e] | 0.9∿0.15 |
| | 280 | 2.4±0.2 | | <2±0.5 |
| $C_2F_5^-$ | 22 | 2.7±0.1 | | 1.7±0.1 |
| | 40 | 3.65±0.05 | 1.5 | >2.7 |
| $C_2F_3^-$ | 33 | 1.3±0.05 | 1.1 | 0.5±0.2 |
| $F^-$ | 80 | 2.5±0.1 | 1.65 | 0.65±0.1 |
| | 180 | 3.8±0.05 | | >2.5 |

[a]Full width at half maximum of the respective negative ion intensity as a function of electron energy.

[b]An asterisk (*) indicates that the ion is long lived with respect to autodetachment.

[c]Energy scale calibration determined using for the $SF_5^-/SF_6$ resonance the value of 0.37 eV. The ± refers to the standard deviation from the average.

[d]Values listed are from the unfolded data.

[e]Includes both peaks.

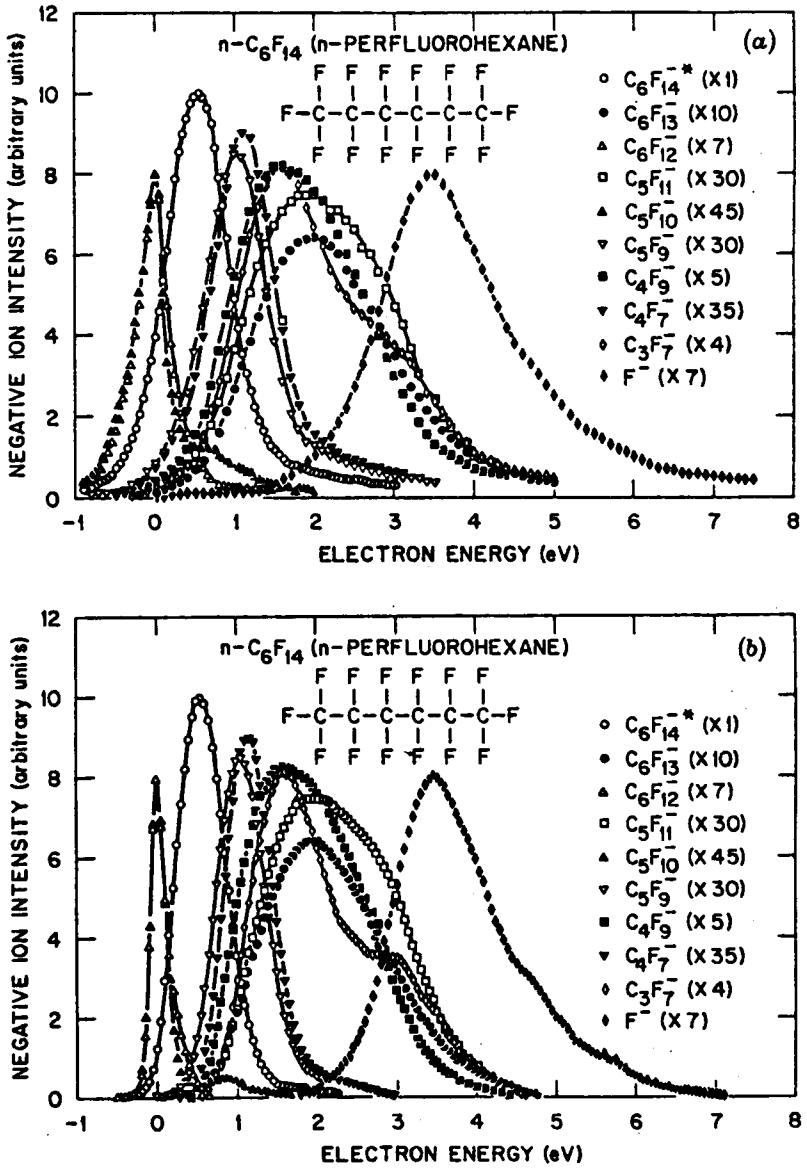


Figure III-6. Negative ion intensity as a function of $\varepsilon$ for n-$C_6F_{14}$. (a) Nonunfolded data; (b) unfolded data (note the multiplication factors).

are summarized in Table III-5. In addition to the NIS at 0.55 eV leading to formation of the parent negative ion, two additional NISs leading to dissociative attachment can be identified at 1.8 and ∿3.4 eV. These NISs may be compared with those of n-$C_5F_{12}$ at 2.5 and ∿3.7 eV. The formation of $C_6F_{12}^-$ and $C_5F_{10}^-$ at 0.0 eV and of $C_5F_9^-$ and $C_4F_7^-$ at ∿1.1 eV involves the breakage of more than one bond and possibly also atomic rearrangement of the anion itself (see discussion in Section III).

B. The Autodetachment Lifetimes of the Long-Lived Parent and Fragment Negative Ions of the n-$C_NF_{2N+2}$ (N = 4-6) Molecules

The parent anions of n-$C_4F_{10}$, n-$C_5F_{12}$, and n-$C_6F_{14}$ were found to be long lived with $\tau_a > 10^{-6}$ s. The $\tau_a$ of the parent anions of n-$C_5F_{12}$ and n-$C_6F_{14}$ were found to decrease with increasing $\varepsilon$ (Figures III-7 and III-8) as did the $\tau_a$ of the long-lived fragment ion $C_5F_{10}^{-*}$/n-$C_5F_{12}$ (Figure III-9). The n-$C_4F_{10}^{-*}$ ion was too weak to allow for similar measurements to be made; its $\tau_a$ was estimated to be 21 ± 4 μs. The lifetime data presented in Figures III-7(a) to III-9(a) are the averages of five sets of data taken at five different times; each set of data was obtained by repeated scanning of the electron energy across the negative ion resonance (at different accelerating voltages) and by averaging at each point the corresponding value of $\tau_a$. In Figures III-7(b) to III-9(b) the $\tau_a$ values determined at a number of energies by the slope method are shown. In Table III-6 are listed the values of $\tau_a$ at the peak of the respective negative ion resonances.

The variation of $\tau_a$ with $\varepsilon$ and the increase of $\tau_a$ with increasing number of vibrational degrees of freedom of the molecule observed in

Table III-5. Negative ions due to low-energy electron impact on n-$C_6F_{14}$

| Negative ion[b] | Relative peak intensity | Energy of maximum ion intensity (eV)[c] | FWHM[a] (eV)[d] | Appearance onset (eV)[d] |
|---|---|---|---|---|
| $C_6F_{14}^{-*}$ | 1000 | 0.55 | 0.7 | ∿0 |
| $C_6F_{13}^-$ | 64 | 2±0.02 | 1.85 | 0.65±0.1 |
| $C_6F_{12}^-$ | 120 | ∿0 | 0.24 | |
| $C_5F_{11}^-$ | 25 | 2±0.05 | 2 | 0.7±0.1 |
| $C_5F_{10}^-$ | 18 | ∿0 | 0.24 | |
| | 1 | 0.85±0.05 | | 0.5±0.1 |
| $C_5F_9^-$ | 28 | 1.05±0.05 | 0.7 | 0.4±0.15 |
| $C_4F_9^-$ | 165 | 1.65±0.05 | 1.8 | 0.6±0.1 |
| $C_4F_7^-$ | 25 | 1.15±0.05 | 0.7 | 0.55±0.15 |
| $C_3F_7^-$ | 210 | 1.6±0.02 | 1.3 | 0.75±0.1 |
| | 88 | 3 | | >2.5 |
| $F^-$ | 114 | 3.45±0.05 | 1.5 | 1.8±0.1 |
| | | 4.5(shoulders) | | |
| | | 5.8(shoulders) | | |

[a]Full width at half maximum of the respective negative ion intensity as a function of electron energy.

[b]An asterisk (*) indicates that the ion is long lived with respect to autodetachment.

[c]Energy scale calibration determined using for the $SF_5^-/SF_6$ resonance the value of 0.37 eV. The ± refers to the standard deviation from the average.

[d]Values listed are from the unfolded data.

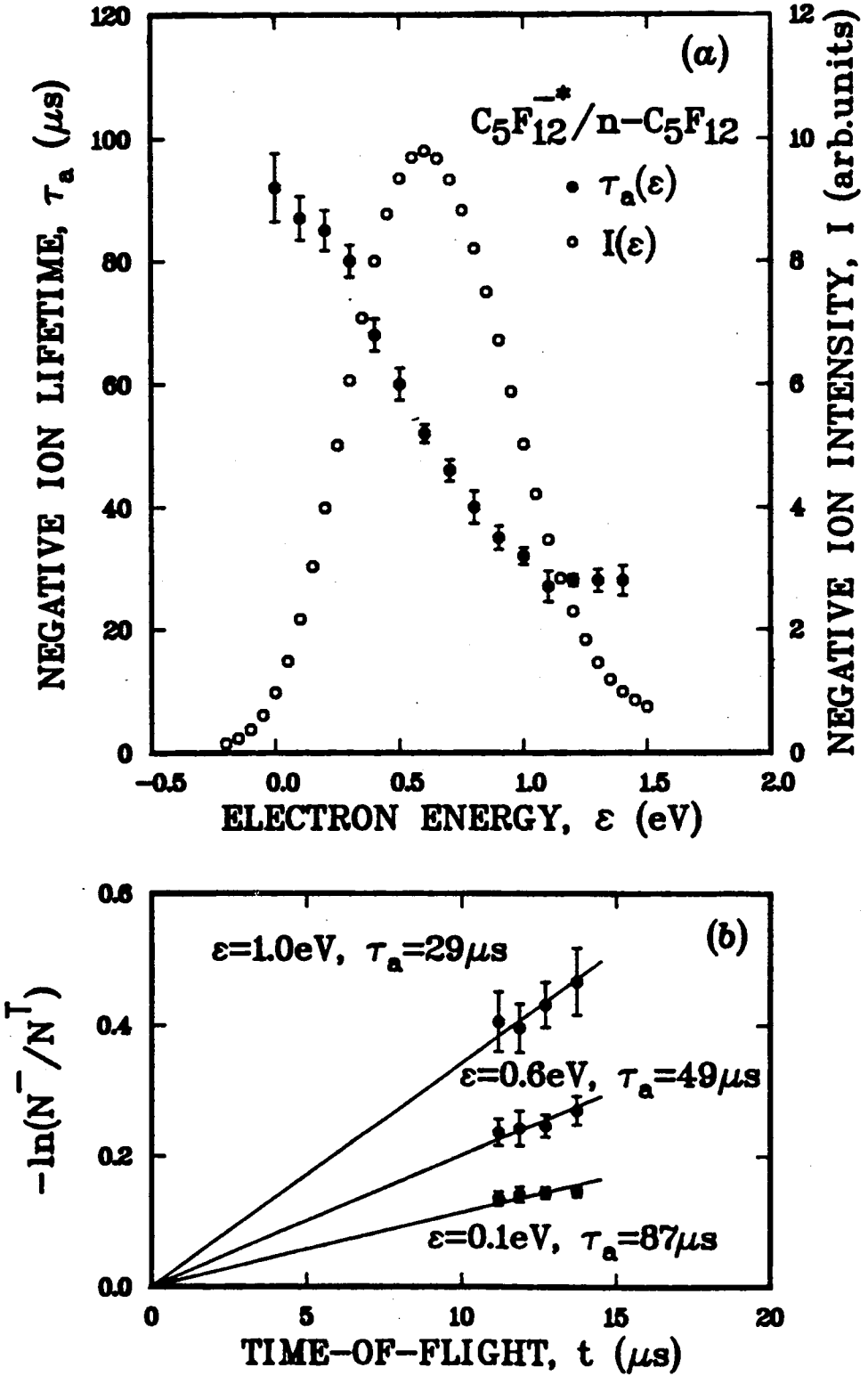


Figure III-7. (a) Negative ion lifetime and negative ion intensity (unfolded results) for $C_5F_{12}^{-*}/n\text{-}C_5F_{12}$ as a function of electron energy. (b) Determination of $\tau_a$ for $C_5F_{12}^{-*}/n\text{-}C_5F_{12}$ at 0.1, 0.6, and 1 eV by the slope method.

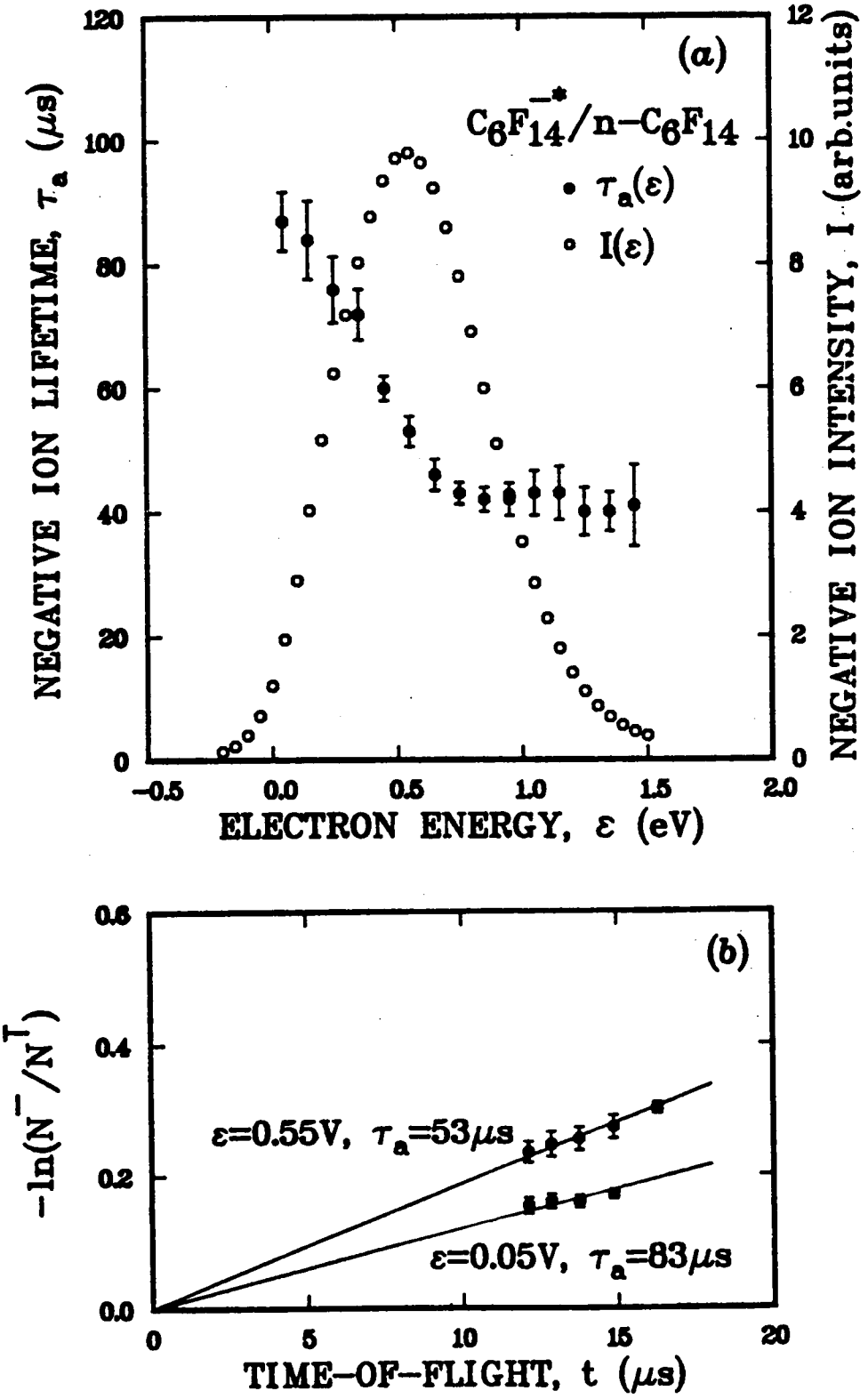


Figure III-8. (a) Negative ion lifetime and negative ion intensity (unfolded results) for $C_6F_{14}^{-*}/n-C_6F_{14}$ as a function of electron energy. (b) Determination of $\tau_a$ for $C_6F_{14}^{-*}/n-C_6F_{14}$ at 0.05 and 0.55 eV by the slope method.

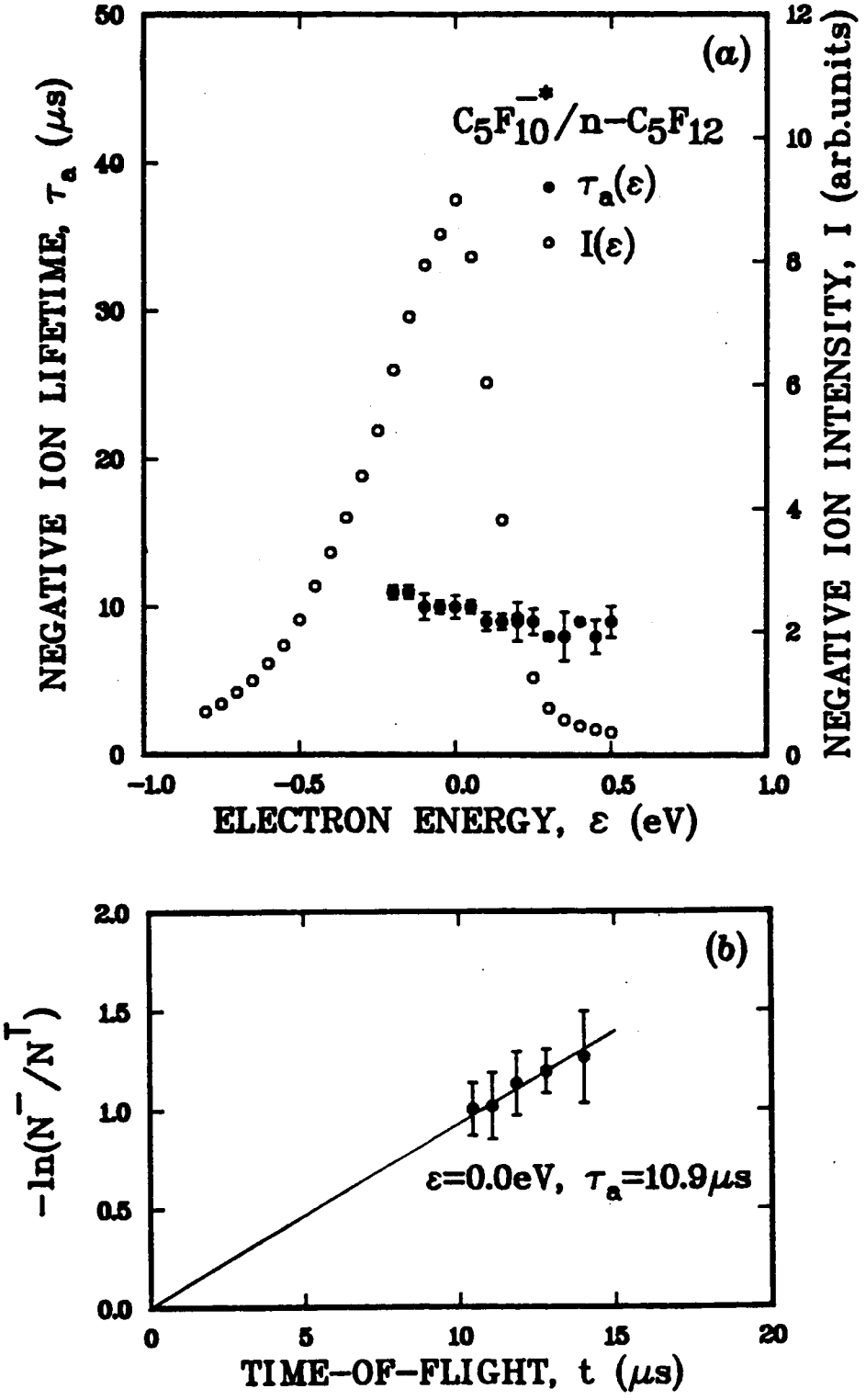


Figure III-9. (a) Negative ion lifetime and negative ion intensity (nonunfolded results) for $C_5F_{10}^{-*}/n\text{-}C_5F_{12}$ as a function of electron energy. (b) Determination of $\tau_a$ for $C_5F_{10}^{-*}/n\text{-}C_5F_{12}$ at ~0.0 eV by the slope method.

Table III-6. Lifetimes of long-lived negative ions observed in collisions of slow electrons with n-$C_NF_{2N+2}$ (N = 4-6)

| Long-lived negative ion | Parent molecule | |
|---|---|---|
| $C_4F_{10}^{-*}$ | n-$C_4F_{10}$ | 21±4,[a](12.7)[b] |
| $C_5F_{10}^{-*}$ | n-$C_5F_{12}$ | 10.9±0.7[c] |
| $C_5F_{12}^{-*}$ | n-$C_5F_{12}$ | 49±2,[c](34.3)[b] |
| $C_6F_{14}^{-*}$ | n-$C_6F_{14}$ | 53±2,[c](43.9)[b] |

[a]Determined from an average of over 150 separate measurements.

[b]J. C. J. Thynne, Dynamic Mass Spectrometry, edited by D. Price (Herden and Son, Ltd., London, 1972), Vol. 3, p. 67.

[c]Lifetime decreases with increasing electron energy. The values listed in the table are the lifetimes at the resonance peak determined by the slope method (see text).

the present study are consistent with previous studies (see Section IIB.(3) in Chapter II).

## III. DISSOCIATIVE ATTACHMENT ENERGETICS AND THERMOCHEMICAL DATA

For a reaction of the form

$$e + RX \rightarrow R^- + X \ , \qquad \text{(III-1)}$$

the heat of reaction, $\Delta H_r$, is related to the heats of formation $\Delta H_f(R)$, $\Delta H_f(X)$, $\Delta H_f(RX)$ of R, X, and RX, respectively, and the electron affinity, EA(R), of R by

$$\Delta H_r = \Delta H_f(R) - EA(R) + \Delta H_f(X) - \Delta H_f(RX) \ . \qquad \text{(III-2)}$$

Also, $\Delta H_r$ is related to the appearance onset, $AO(R^-)$, of $R^-$ by

$$AO(R^-) = \Delta H_r + E^* \ , \qquad \text{(III-3)}$$

where $E^*$ is the excess energy of the reaction comprised of the internal energy of excitation and the total translational energy of the fragments. We made use of Equations (III-2) and (III-3), or of Eq. (III-3) and the energy balance equation

$$AO(R^-) = D(R\text{-}X) - EA(R) + E^* \ . \qquad \text{(III-4)}$$

[D(R-X) is the bond dissociation energy of RX], and the thermochemical data in Table III-7 in an effort to identify possible fragmentation mechanisms of the NISs leading to the production of the observed fragment anions and also to deduce electron affinities of radicals, heats

Table III-7. Thermochemical data used in Chapter III

| Quantity | Values (in eV) and references | Quantity | Values (in eV) and references |
|---|---|---|---|
| $\Delta H_f(F)$ | 0.82[a] | $\Delta H_f(n\text{-}C_4F_{10})$ | -21.9[c] |
| $\Delta H_f(CF_2)$ | -1.72[b] | $\Delta H_f(C_5F_{11})$ | -21.48[c] |
| $\Delta H_f(CF_3)$ | -4.94[a] | $\Delta H_f(n\text{-}C_5F_{12})$ | -26.0[c] |
| $\Delta H_f(CF_2{=}CF)$ | -1.99[c] | $\Delta H_f(C_6F_{13})$ | -25.58[c] |
| $\Delta H_f(CF_4)$ | -9.58[a] | $\Delta H_f(n\text{-}C_6F_{14})$ | -30.1[c] |
| $\Delta H_f(C_2F_4)$ | -6.74[a] | EA(F) | 3.45[e] |
| $\Delta H_f(C_2F_5)$ | -9.19[c] | $EA(CF_3)$ | 2.1[f] |
| $\Delta H_f(C_2F_6)$ | -13.7[c] | $EA(CF_3\text{-}C)$ | 2.8,3.1[g] |
| $\Delta H_f(C_3F_5)$ | -7.9[d] | $EA(CF_2{=}CF)$ | 2.1±0.2[g] |
| $\Delta H_f(C_3F_6)$ | -11.22[c] | $EA(C_2F_5)$ | 2.1[f] |
| $\Delta H_f(n\text{-}C_3F_7)$ | -13.29[c] | $EA(C_4F_7/2\text{-}C_4F_8)$ | ∿3.5[g] |
| $\Delta H_f(i\text{-}C_3F_7)$ | -13.87[c] | $EA(2\text{-}C_4F_8)$ | >0.6,<0.9[h] |
| $\Delta H_f(C_3F_8)$ | -17.82[c] | $EA(C_5F_9/C_4F_6(CF_3)_2)$ | 3.1±0.3[g] |
| $\Delta H_f(2\text{-}C_4F_8)$ | -16.6[b] | $D(F\text{-}C_NF_{2N+1}),N=2,3...$ | 5.35[c] |
| $\Delta H_f(c\text{-}C_4F_8$ | -15.7[b] | D(F-F) | 1.64[i] |
| $\Delta H_f(C_4F_9)$ | -17.38[c] | D(C-C) | 3.7 ± 0.2[j] |

[a] J. L. Franklin, J. G. Dillard, H. M. Rosenstock, J. T. Herron, K. Draxl, and F. H. Field, NSRDS-NBS 26 (1969).

[b] S. W. Benson and H. E. O'Neal, NSRDS-NBS 21 (1970).

[c] W. M. Bryant, J. Polym. Sci. 56, 277 (1962).

[d] I. Sauers, L. G. Christophorou, and J. G. Carter, J. Chem. Phys. 71, 3016 (1979).

[e] R. S. Berry and C. W. Reimann, J. Chem. Phys. 38, 1540 (1963).

[f] H. M. Rosenstock, K. Draxl, B. W. Steiner, and J. T. Jerron, J. Phys. Chem. Ref. Data 6, Suppl. No. 1 (1977).

[g] J. C. J. Thynne, Dynamic Mass Spectrometry, edited by D. Price (Herden and Son, Ltd., London, 1972), Vol. 3, p. 67.

[h] P. R. Hammond, J. Chem. Phys. 55, 3468 (1971).

[i] B. Darwent, NSRDS-NBS 31 (1970).

[j] Obtained using for the reaction $C_NF_{2N+2} \rightarrow C_{N-x}F_{2N+2-y} + C_xF_y$ the energy balance equation $D(C\text{-}C) = \Delta H_r = \Delta H_f(C_{N-x}F_{2N+2-y}) + \Delta H_f(C_xF_y) - \Delta H_f(C_NF_{2N+2})$ with the thermochemical data of this table.

of formation of fragment anions, and dissociation energies for various C-C and C-F bonds.

The appearance onsets of the observed fragment anions and the proposed reactions leading to their formation along with the respective $\Delta H_r$ are listed in Tables III-8 to III-10. In the same tables are listed values of E* estimated from Equation (III-3) for these reactions and are compared with literature data whenever available. It should be noted that when E* is not known, only limiting values are determined for the thermochemical data listed in Tables III-8 to III-10. In general, the data we obtained (Tables III-8 to III-10) show satisfactory consistency except for a few cases discussed later in this section.

The relative cross sections of a number of fragment anions exhibit (Figures III-3 to III-6 (pp. 59, 62, 65, and 67); Tables III-2 to III-5 (pp. 61, 63, 66, and 69)) two (or more) maxima. We interpret (see Tables III-8 to III-10) these maxima as originating from separate NISs with different asymptotic limits depending on the kind of products which we assumed to be in their electronic ground states (except for the reaction $e + CF_4 \rightarrow F^- + CF_3^*$, where $CF_3^*$ can be electronically excited). When multiple-fragment reactions are involved in the production of a particular anion, energetic considerations were used to identify the most likely reaction(s). Further discussion on the multiple- versus two-fragment reactions is given in the next section. We were unable to identify specific reactions for $C_3F_7^-/n\text{-}C_5F_{12}$, $C_4F_9^-/n\text{-}C_5F_{12}$, and $C_5F_{11}^-/n\text{-}C_5F_{12}$ peaking at, respectively, 2.4, 2.45, and 2.25 eV.

It was pointed out in Section IIA.(4) that the cross section maximum for $C_4F_9^-$ from $n\text{-}C_4F_{10}$ at 1.85 eV may be due to an $i\text{-}C_4F_{10}$

Table III-8. Possible dissociative attachment processes leading to the formation of $F^-$ from n-$C_NF_{2N+2}$, N = 1-6, and thermochemical data deduced

| AO (eV) | Reaction | $\Delta H_r$[a] (eV) | Thermochemical data deduced (eV) |
|---|---|---|---|
| 4.5±0.1 | $e + CF_4 \rightarrow F^- F CF_3$ | 2.0 | $E^*$[b] = 2.5(3.26) |
| 2.0±0.1 | $e + C_2F_6 \rightarrow F^- + C_2F_5$ | 1.9 | $D(F\text{-}C_2F_5) \leq 5.45\pm0.1$ (5.35)[c] |
| 1.7±0.2 | $e + C_3F_8 \rightarrow F^- + C_3F_7$ | 1.9 | $D(F\text{-}C_3F_7) \leq 5.15\pm0.2$(5.35) |
| 1.6±0.1 | $e + n\text{-}C_4F_{10} \rightarrow F^- + C_4F_9$ | 1.9 | $D(F\text{-}C_4F_9) \leq 5.05\pm0.1$(5.35) |
| <4 | $F^- + 2\text{-}C_4F_8 + F$ | 3.5[d] | |
| | $F^- + C_3F_6 + CF_3$ | 3.1 | |
| | $F^- + C_2F_5 + C_2F_4$ | 3.35 | |
| 1.65±0.1 | $e + n\text{-}C_5F_{12} \rightarrow F^- + C_5F_{11}$ | 1.9 | $D(F\text{-}C_5F_{11}) \leq 5.1\pm0.1$(5.35) |
| >2.5 | $F^- + F + C_5F_{10}$ | 3.4[e] | |
| | $F^- + C_3F_7 + C_2F_4$ | 3.35 | |
| | $F^- + C_3F_6 + C_2F_5$ | 2.95 | |
| 1.8±0.1 | $e + n\text{-}C_6F_{14} \rightarrow F^- + C_6F_{13}$ | 1.9 | $D(F\text{-}C_6F_{13}) \leq 5.25\pm0.1$(5.35) |
| ~4.5(shoulder | $F^- + F + C_6F_{12}$ | 3.4[e] | |
| | $F^- + C_4F_9 + C_2F_4$ | 3.35 | |
| | $F^- + C_3F_7 + C_3F_6$ | 3.0 | |
| ~5.8(shoulder) | $F^- + C_3F_6 + C_2F_4 + CF_3$ | 4.6 | |
| | $F^- + C_3F_6 + C_2F_5 + CF_2$ | 5.35 | |

[a] Heat of reaction determined by using Equation (III-2) and the data of Table III-7.

[b] Excess energy determined from Equation (III-3). Numbers in parentheses are results of P. N. Harland and J. L. Franklin, J. Chem. Phys. 61, 1621 (1974).

[c] Bond dissociation energies determined from Equation (III-4) using $E^* \geq 0$ eV. The numbers in parentheses are the values of J. L. Bryant, J. Polym. Sci. 56, 277 (1962).

[d] If the structure of $C_4F_8$ is cyclic (c-$C_4F_8$), then $\Delta H_r$ = 4.4 eV.

[e] See Footnote c of Table III-10 for $\Delta H_f$ of $C_5F_{10}$ and $C_6F_{12}$.

Table III-9. Possible dissociative attachment processes leading to the formation of $C_NF_{2N+1}^-$ from n-$C_NF_{2N+2}$, N = 1-6, and thermochemical data deduced

| Ion | AO (eV) | Reaction | $\Delta H_r$[a] (eV) | Thermochemical data deduced (eV) |
|---|---|---|---|---|
| $CF_3^-$ | 5.1±0.1 | $e + CF_4 \rightarrow CF_3^- + F$ | 3.35 | $E^*$[b] = 1.75±0.1(2.0) |
| | 2.4±0.1 | $e + C_2F_6 \rightarrow CF_3^- + CF_3$ | 1.7 | $E^* = 0.7±0.1(0.66)$ |
| | 2.4±0.2 | $e + C_3F_8 \rightarrow CF_3^- + C_2F_5$ | 1.6 | $E^* = 0.8±0.2(0.85)$ |
| | >5 | $\rightarrow CF_3^- + CF_3 + CF_2$ | 4.1 | |
| | | $\rightarrow CF_3^- + C_2F_4 + F$ | 4.85 | |
| | 2.2±0.1 | $e + n\text{-}C_4F_{10} \rightarrow CF_3^- + C_3F_7$ | 1.6 | $E^* = 0.6±0.1$ |
| | >3.2±0.3 | $\rightarrow CF_3^- + C_2F_4 + CF_3$ | 3.2 | |
| $C_2F_5^-$ | 3.5±0.1 | $e + C_2F_6 \rightarrow C_2F_5^- + F$ | 3.25 | $D(F\text{-}C_2F_5)$[c] $\leq$ 5.6±0.1 |
| | 2.1±0.2 | $e + C_3F_8 \rightarrow C_2F_5^- + CF_3$ | 1.6 | $E^* = 0.5$ |
| | 1.8±0.15 | $e + n\text{-}C_4F_{10} \rightarrow C_2F_5^- + C_2F_5$ | 1.4 | $E^* = 0.4±0.15$ |
| | <4 | $\rightarrow C_2F_5^- + CF_3 + CF_2$ | 3.95 | |
| | 1.7±0.1 | $e + n\text{-}C_5F_{12} \rightarrow C_2F_5^- + C_3F_7$ | 1.4 | $D(F_5C_2\text{-}C_3F_7) \leq 3.8±0.1$ |
| | >2.7 | $\rightarrow C_2F_5^- + C_2F_4 + CF_3$ | 3.0 | |
| $C_3F_7^-$ | 2.5±0.2 | $e + C_3F_8 \rightarrow C_3F_7^- + F$ | (2.7±0.4) | $EA(C_3F_7) \geq 2.65±0.4$[d] |
| | 1.2±0.3 | $e + n\text{-}C_4F_{10} \rightarrow C_3F_7^- + CF_3$ | (1.2±0.4) | $EA(C_3F_7) \geq 2.5±0.4$[d] |
| | 0.9±0.15 | $e + n\text{-}C_5F_{12} \rightarrow C_3F_7^- + C_2F_5$ | (0.9±0.15) | $EA(C_3F_7) \geq 2.6±0.15$,[e] $2.9±0.25$[d] |
| | 0.75±0.1 | $e + n\text{-}C_6F_{14} \rightarrow C_3F_7^- + C_3F_7$ | (0.75±0.1) | $EA(C_3F_7) \geq 2.75±0.1$[e] |
| | >2.5 | $\rightarrow C_3F_7^- + C_2F_4 + CF_3$ | (2.4±0.1) | |
| $C_4F_9^-$ | 1.0±0.1 | $e + n\text{-}C_4F_{10} \rightarrow C_4F_9^- + F$ | (1.3±0.2) | $EA(C_4F_9) \geq 4.05±0.2$[d,f] |
| | <2.0±0.3 | $\rightarrow C_4F_9^- + F$ | (2.3±0.4) | $EA(C_4F_9) \geq 3.05±0.4$[d] |
| | 0.8±0.15 | $e + n\text{-}C_5F_{12} \rightarrow C_4F_9^- + CF_3$ | (0.8±0.15) | $EA(C_4F_9) \geq 2.9±0.15$[e] |
| | 0.6±0.1 | $e + n\text{-}C_6F_{14} \rightarrow C_4F_9^- + C_2F_5$ | (0.6±0.1) | $EA(C_4F_9) \geq 2.9±0.1$[e] |
| $C_5F_{11}^-$ | 0.65±0.1 | $e + n\text{-}C_5F_{12} \rightarrow C_5F_{11}^- + F$ | (0.9±0.2) | $EA(C_5F_{11}) \geq 4.45±0.2$[d] |
| | 0.7±0.1 | $e + n\text{-}C_6F_{14} \rightarrow C_5F_{11}^- + CF_3$ | | $EA(C_5F_{11}) \leq 3$[e] or $EA(C_5F_{11}) = 4.5$, $E^* = 1.5$ |
| $C_6F_{13}^-$ | 0.65±0.1 | $e + n\text{-}C_6F_{14} \rightarrow C_6F_{13}^- + F$ | (0.75±0.2) | $EA(C_6F_{13}) \geq 4.6±0.2$[d] |

[a] Heat of reaction determined by using Equation (III-2) and the data of Table III-7. Values in parentheses were obtained by using the EA values listed in the last column of this table.

[b] Excess energy determined from Equation (III-3). Numbers in parentheses are results of P. W. Harland and J. L. Franklin, J. Chem. Phys. 61, 1621 (1974).

[c] Bond dissociation energy determined from Equation (III-4) using $E^* \geq 0$ eV.

[d] Electron affinity determined from Equation (III-4) using the dissociation energy deduced from the complementary anion production. It was assumed that $E^* \geq 0$.

[e] Electron affinity determined from Equations (III-2) and (III-3) with $E^* \geq 0$ and the data in Table III-7.

[f] See discussion in text.

Table III-10. Possible dissociative attachment processes leading to the formation of anions of the form $C_NF_{2N}^-$ and $C_NF_{2N-1}^-$ and thermochemical data deduced

| Anion | | Reaction | | $\Delta H_r$[a] (eV) | Thermochemical data deduced (eV) |
|---|---|---|---|---|---|
| $C_4F_8^-$ | 0.0 | $e + n\text{-}C_5F_{12} \xrightarrow{1} C_4F_8^- + CF_4$ | | $16.42+\Delta H_f(C_4F_8^-)$ | $EA(C_4F_8) \simeq 0.7$[b] |
| | | $\xrightarrow{2} C_4F_8^- + CF_3 + F$ | | $21.9+\Delta H_f(C_4F_8^-)$ | $EA(C_4F_8) \simeq 6.2$[b] |
| $C_5F_{10}^-$ | 0.0 | $e + n\text{-}C_5F_{12} \xrightarrow{3} C_5F_{10}^{-*} + F_2$ | | $26.0+\Delta H_f(C_5F_{10}^{-*})$ | $EA(C_5F_{10}) \simeq 5.2$[c] |
| | | $\xrightarrow{4} C_5F_{10}^{-*} + F + F$ | | $27.65+\Delta H_f(C_5F_{10}^{-*})$ | $EA(C_5F_{10}) \simeq 6.8$[c] |
| | 0.0 | $e + n\text{-}C_6F_{14} \xrightarrow{5} C_5F_{10}^- + CF_4$ | | $20.5+\Delta H_f(C_5F_{10}^-)$ | $EA(C_5F_{10}) \simeq 0$[c] |
| | | $\xrightarrow{6} C_5F_{10}^- + CF_3 + F$ | | $26.0+\Delta H_f(C_5F_{10}^-)$ | $EA(C_5F_{10}) \simeq 5.2$[c] |
| $C_6F_{12}^-$ | 0.0 | $e + n\text{-}C_6F_{14} \xrightarrow{7} C_6F_{12}^- + F_2$ | | $30.1+\Delta H_f(C_6F_{12}^-)$ | $EA(C_6F_{12}) \simeq 5.2$[c] |
| | | $\xrightarrow{8} C_6F_{12}^- + F + F$ | | $31.75+\Delta H_f(C_6F_{12})$ | $EA(C_6F_{12}) \simeq 6.8$[c] |
| $C_2F_3^-$ | 1.1±0.1 | $e + C_3F_8 \rightarrow C_2F_3^- + CF_4 + F$ | | $9.05+\Delta H_f(C_2F_3^-) \simeq 5$[d] | |
| | 0.5±0.2 | $e + n\text{-}C_5F_{12} \rightarrow C_2F_3^- + C_2F_5 + CF_4$ | | $7.25+\Delta H_f(C_2F_3^-) \simeq 3$[d] | |
| $C_4F_7^-$ | 0.55±0.15 | $e + n\text{-}C_6F_{14} \rightarrow C_4F_7^- + CF_4 + CF_3$ | | $15.6+\Delta H_f(C_4F_7^-)$ | $EA(C_4F_7) \simeq 3.0\pm0.45$[e] $(\sim 3.5)$[f] |
| $C_5F_9^-$ | 0.4±0.15 | $\rightarrow C_5F_9^- + CF_4 + F$ | | $21.35+\Delta H_f(C_5F_9^-)$ | $EA(C_5F_9) \simeq 4.6\pm0.45$[e] $(3.1)$[f] |

[a] Heat of reaction determined by using Equation (III-2) and the data of Table III-7.

[b] Using $\Delta H_f(C_4F_8^-) = \Delta H_f(C_4F_8) - EA(C_4F_8)$ and the $\Delta H_f(C_4F_8)$ for the cyclic structure, c-$C_4F_8$ (Table III-7).

[c] The EA values were determined from Equation (III-2). The $\Delta H_f$ values, -20.8±0.2 and -24.9 0.2 eV, for $C_5F_{10}$ and $C_6F_{12}$, respectively, were calculated using $C_5F_{10} \rightarrow C_3F_5 + C_2F_5$ and $C_6F_{12} \rightarrow C_3F_5 + C_3F_7$, respectively, with $\Delta H_r$ = D(C-C) = 3.7±0.2 eV and the $\Delta H_f$ for $C_3F_5$, $C_2F_5$, and $C_3F_7$ from Table III-7.

[d] By assuming the structure $CF_2$=CF for $C_2F_3$ and using $\Delta H_f(C_2F_3^-) = \Delta H_f(C_2F_3) - EA(C_2F_3)$ and the data in Table III-7.

[e] The EA values were determined from Equation (III-2). The $\Delta H_f$ values, -12.1±0.3 and -16.3±0.3 eV, for $C_4F_7$ and $C_5F_9$, respectively, were calculated using $C_4F_8 \rightarrow C_4F_7 + F$ and $C_5F_{10} \rightarrow C_5F_9 + F$, respectively, with $\Delta H_r$ = D(C-F) = 5.3±0.3 eV and the $\Delta H_f$ for 2-$C_4F_8$ and F from Table III-7 and $C_5F_{10}$ from footnote c of this table.

[f] Literature values (from Table III-7).

impurity. Support for this contention comes from two sources: (i) the cross section for $C_4F_9^-$ from i-$C_4F_{10}$ has a rather strong maximum at this energy and (ii) if we use the first AO of $C_4F_9^-$ from n-$C_4F_{10}$ to calculate via Equation (III-4) the EA of $C_4F_9$, we obtain a value for the EA of $C_4F_9$ which is more than 1 eV larger than that deduced from similar data from either n-$C_5F_{12}$ or n-$C_6F_{14}$. If, however, the AO for the second $C_4F_9^-$/n-$C_4F_{10}$ maximum is used, the EA ($C_4F_9$) value obtained is more consistent with the EA ($C_4F_9$) obtained from the $C_4F_9^-$/n-$C_5F_{12}$ and $C_4F_9^-$/n-$C_6F_{14}$ measurements (see Table III-9).

The formation of $C_4F_8^-$ and $C_5F_{10}^{-*}$ from n-$C_5F_{12}$ and $C_5F_{10}^-$ and $C_6F_{12}^-$ from n-$C_6F_{14}$ at ∿0.0 eV (i.e., well below the peak of the corresponding parent anion at 0.6 eV) is rather puzzling. (Notice also a second maximum in the relative cross section of $C_4F_8^-$/n-$C_5F_{12}$ and $C_5F_{10}^-$/n-$C_6F_{14}$ at ∿0.7 and ∿0.85 eV, respectively.) Reaction 1 in Table III-10 gives EA ($C_4F_8$) = 0.7 eV, whereas reaction 2 gives (Table III-10) EA ($C_4F_8$) = 6.2 eV. Similarly, reactions 3, 6, and 7 (Table III-10) gives consistent but rather large values (>5 eV) for the EA of $C_5F_{10}$ and $C_6F_{12}$ radicals. Such large values for the EA of the species $C_4F_8$, $C_5F_{10}$, and $C_6F_{12}$ are rather unlikely, and these fragment anions may be due to traces of impurities. A study of c-$C_5F_{10}$ (Chapter IV) showed that $C_5F_{10}^{-*}$ is a very strong anion at 0.0 eV and has the same $\tau_a$ as the $C_5F_{10}^{-*}$ from n-$C_5F_{12}$.

It is difficult to understand the production of $C_2F_3^-$ from $C_3F_8$ and n-$C_5F_{12}$, appearing at energies 1.1 and 0.5 eV, respectively. If we assume for $C_2F_3$ the structure $CF_2 = CF$, the heats of the reactions leading to the formation of $C_2F_3^-$ are 5 and 3 eV, respectively. If, on

the other hand, we assume the structure to be $CF_3$-C, the heats of the reactions are even higher. In both cases the appearance onsets are well below the heats of the reactions.

## IV. DISCUSSION AND CONCLUSIONS

### A. Types and Relative Intensities of Parent and Fragment Negative Ions as a Function of Molecular Size. Calculation of Separation Times and Autodetachment Lifetimes

1. Parent anions. From the results presented in Section II, it is evident that low-energy electrons attach to PFAs dissociatively and/or nondissociatively. Which mode of attachment will predominate depends on the size of the molecule. For the lower PFAs ($CF_4$, $C_2F_6$, and $C_3F_8$) only fragment negative ions have been observed. The $F^-$ ion was found to be the most abundant anion. For n-$C_4F_{10}$ a weak parent negative ion was detected, but for this molecule, too, $F^-$ still remains the most abundant anion. For the larger members of the series we studied (i.e., n-$C_5F_{12}$ and n-$C_6F_{14}$) the parent negative ion is formed and is more intense than any of the fragment negative ions. Interestingly, for all three molecules the parent anion cross section peaks at ∿0.6 eV. This contrasts with earlier findings (Sauers et al., 1979) on the unsaturated and cyclic perfluorocarbons for which the parent anion cross section was found to peak at ∿0.0 eV. As in the case of the unsaturated and cyclic perfluorocarbons, the parent anions of n-$C_4F_{10}$, n-$C_5F_{12}$, and n-$C_6F_{14}$ were found to be long lived with autodetachment lifetimes of the order of $10^{-5}$ s. Actually, the lifetimes of n-$C_5F_{12}^{-*}$ and n-$C_6F_{14}^{-*}$—49 and 53 μs at 0.6 eV, respectively—increase with increasing molecular size and decrease with increasing electron energy

from 90 and 90 μs at 0.0 eV to 30 and 40 μs at 1.1 eV, respectively). It seems also that the larger the number of vibrational degrees of freedom of the molecule, the smaller the rate of decline of the lifetime with increasing $\varepsilon$.

The results of a swarm study (see Hunter and Christophorou, 1983) and Part C of this section) showed that the electron attachment cross sections, $\sigma_a$, for the PFAs studied increase with increasing size of the molecule. However, not only the size of the molecule but also its shape and the deformation of the transient anion (and thus the effectiveness of dissipation of the excess energy) affect both the magnitude of the attachment cross section for the formation of parent negative ions and their $\tau_a$. Thus, whereas parent negative ion formation in i-$C_4F_{10}$ is stronger than in n-$C_4F_{10}$, it becomes weaker for neo-$C_5F_{12}$ (see Chapter IV for results on i-$C_4F_{10}$ and neo-$C_5F_{12}$) compared with n-$C_5F_{12}$.

The EA of perfluorocarbon radicals (Section III; Tables III-8 to III-10) increases with increasing size of the radicals. An analogous statement can be made for the perfluoroalkane molecules themselves. This would imply that the equilibrium distance for the parent negative ion increases when the molecule becomes larger since the vertical attachment energy is the same (0.6 eV) for n-$C_4F_{10}$, n-$C_5F_{12}$, and n-$C_6F_{14}$.

2. Fragment anions; separation times and autodetachment lifetimes; potential energy curves. The present work has shown that in slow-electron-PFA molecule collisions in addition to the parent negative ions and $F^-$, other fragment negative ions are produced of the form

$C_NF^-_{2N+1}$, $C_NF^-_{2N}$, and $C_NF^-_{2N-1}$ with N = 1-6. The ions $F^-$ and $C_NF^-_{2N+1}$ involve single bond (C-C or C-F) breakage, whereas the anions of the form $C_NF^-_{2N}$ and $C_NF^-_{2N-1}$ require the cleavage of more than one bond. It should be stressed here that even the ions $F^-$ and $C_NF^-_{2N+1}$ whose formation is assigned to two-fragment processes may be formed also in multiple-fragment reactions (see part B in this section).

Although for a polyatomic molecule $C_NF_{2N+2}$, both the molecular neutral state and the negative ion state are described by potential energy surfaces rather than by two dimensional potential curves as in the case of diatomic molecules, the formation of complementary ions ($e + RX \rightarrow X^- + R$; $R^- + X$) may be viewed as dissociation along the R-X coordinate of the energy surface following the electron capture and be approximated by a "diatomic-like" molecule process.

Adopting a diatomic-like picture, the separation time, $\tau_s$ (which we define as the time it takes for the fragments $X^-$ and R to move from $r_0$ to $r_c$ along the coordinate r(R-X), where $r_0$ is the internuclear distance at equilibrium of the neutral molecule, and $r_c$ is the point of intersection of the potential energy curves for the initial neutral state $V_0(r)$ and the final negative ion state $V_-(r)$), is given by

$$\tau_s = \left(\frac{\mu}{2}\right)^{1/2} \int_{r_0}^{r_c} \frac{dr}{[V_-(r_0) - V_-(r)]^{1/2}} , \qquad \text{(III-5)}$$

where $\mu$ is the reduced mass of R and X.

For $V_0(r)$ we chose a Morse function

$$V_0(r - r_0) = D_e\{1 - \exp[-\beta(r - r_0)]\}^2 , \qquad \text{(III-6)}$$

where $D_e = D + hc\omega/2$ (D is the dissociation energy of R-X, h is Planck's constant, and c is the speed of light) and

$$\beta = 0.1218\omega\ (\mu/D_e)^{1/2}\ , \qquad \text{(III-7)}$$

where $\beta$ is in $10^8$ $cm^{-1}$, if the wave number $\omega$ (determined from the average frequency of vibration of the normal modes of the R-X bond) is in $cm^{-1}$, $\mu$ in atomic mass units, and $D_e$ in $cm^{-1}$.

For the negative ion potential energy curve we assumed a purely repulsive function of the form

$$V_-(r) = D_e - EA(X) + Be^{-Cr}\ . \qquad \text{(III-8)}$$

The constants B and C were determined by imposing the condition that $V_-(r_0) = \varepsilon_0 + hc\omega/2$ ($\varepsilon_0$ is the peak energy of the negative ion resonance), and that the slope of the curve at $r_0$ is equal to the ratio of the FWHM of the negative ion resonance to the FWHM of the Gaussian curve describing the probability distribution for the ground vibrational state of the molecule.

In Figure III-10 are shown the $V_0(r)$ and $V_-(r)$ curves for $CF_4$ and $C_2F_6$. In the same figure are shown also the probability density distributions

$$\psi_0^2 = (\alpha/\pi)^{1/2} \exp\ [-\alpha(r - r_0)^2]\ , \qquad \text{(III-9)}$$

($\alpha = 2.965\ 10^{-2}\ \mu\omega$ in $10^{16}$ $cm^{-2}$) for the v = 0 level for these molecules. The curves were calculated using the data listed in Table III-11.

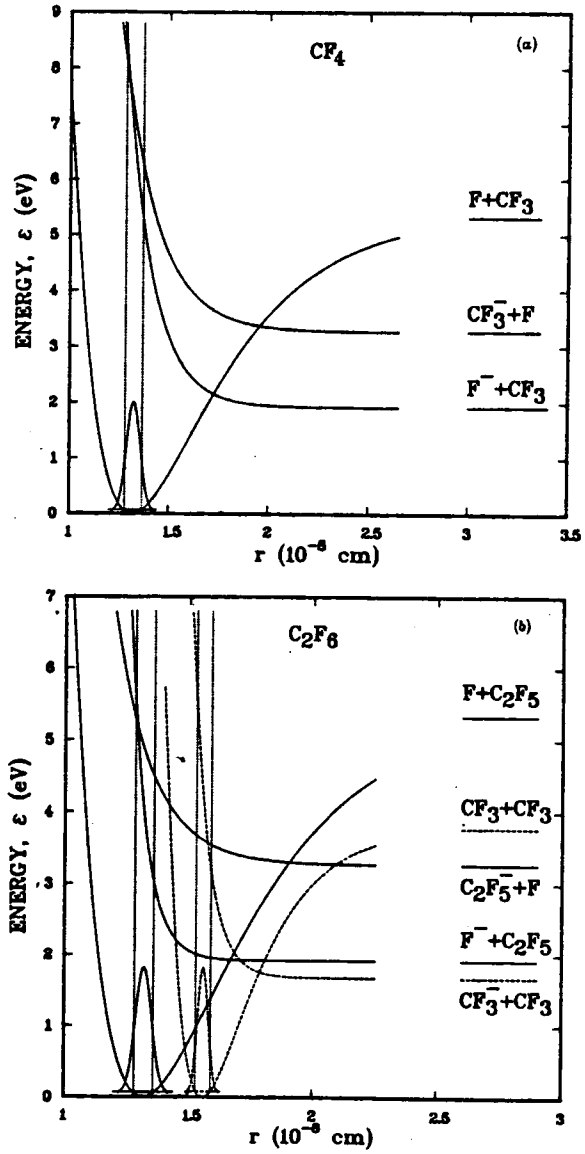


Figure III-10. Potential energy diagrams for (a) $CF_4$ and $CF_4^-$*, (b) $C_2F_6$ and $C_2F_6^-$*. The ——— curve is along the r(C-F) coordinate and the ----- curve is along the r(C-C) coordinate. The curves for the neutral states were obtained using the Morse function, and the curves for the negative ion states using the experimental data as described in the text [Section VA.(2)].

Table III-11. Values of $\mu$, $\omega$, $D_e$, $r_0$, $\beta$, $\alpha$, $\sigma_{da}(\epsilon_{max})$, $r_c$, $\tau_s$, and $\bar{\tau}_a$ [a]

| Process | $\mu$ | $\omega$ [b] ($cm^{-1}$) | $D_e$ [c] (eV) | $r_0$ [d] ($10^{-8}$ cm) | $\beta$ ($10^8$ $cm^{-1}$) | $\alpha$ ($10^{16}$ $cm^{-2}$) | $\sigma_{da}(\epsilon_{max})$ [e] ($10^{-18}$ $cm^2$) | $r_c$ ($10^{-8}$ cm) | $\tau_s$ ($10^{-15}$ s) | $\bar{\tau}_a$ ($10^{-15}$ s) |
|---|---|---|---|---|---|---|---|---|---|---|
| $e + CF_4 \rightarrow F^- + CF_3$ | 14.90 | 1095.0 | 5.368 | 1.32 | 2.474 | 483.7 | 0.79 | 1.725 | 7.4 | 1.30 |
| $e + CF_4 \rightarrow CF_3^- + F$ | 14.90 | 1095.0 | 5.368 | 1.32 | 2.474 | 483.7 | 0.79 | 1.955 | 12.29 | 2.19 |
| $e + C_2F_6 \rightarrow F^- + C_2F_5$ | 16.38 | 1106.0 | 5.369 | 1.32 | 2.620 | 537.1 | 9.89 | 1.669 | 8.99 | 2.87 |
| $e + C_2F_6 \rightarrow C_2F_5^- + F$ | 16.38 | 1106.0 | 5.369 | 1.32 | 2.620 | 537.1 | 3.30 | 1.906 | 18.3 | 1.55 |
| $e + C_2F_6 \rightarrow CF_3^- + CF_3$ | 34.50 | 1228.0 | 3.776 | 1.56 | 5.034 | 1256.1 | 0.00989 | 1.787 | 8.68 | 1.74 |

[a] See text for explanation of symbols.

[b] T. Shimanouchi, Tables of Molecular Vibrational Frequencies, NSRDS-NBS 39, Vol. I (1972).

[c] Bond dissociation energy (average value from Tables III-8 to III-10) plus zero-point energy. Use the conversion 1 eV = 8065.75 $cm^{-1}$ in using $D_e$ in Equation (III-7) of the text.

[d] JANAF Thermochemical Tables, edited by D. R. Stull (Dow Chemical Company, Midland, Michigan, 1969).

[e] Determined by making use of the swarm data (Hunter and Christophorou, 1983) in combination with the present data (see text).

The mean autodetachment lifetime $\bar{\tau}_a$ was calculated from Equation (III-10) which relates $\tau_s/\bar{\tau}_a$ to the measured dissociative electron attachment cross section for a diatomic (or diatomic-like molecule (see Section IIC.(2) in Chapter I)

$$\sigma_{da}(\varepsilon)_{v=0} = \frac{4\pi^{3/2}\bar{g}}{(2m/\hbar^2)\varepsilon}\frac{\Gamma_{\bar{a}}}{\Gamma_d}\exp\left[\frac{\Gamma_a^2 - 4(\bar{\varepsilon}_0 - \varepsilon)^2}{\Gamma_d^2}\right]\exp\{-\tau_s/\bar{\tau}_a\}\ . \tag{III-10}$$

In Equation (III-10) m is the electron mass, $\varepsilon$ is the incident electron energy, $\bar{g}$ is a statistical factor, $\Gamma_d$ is the experimentally determined dissociative attachment width, $\Gamma_{\bar{a}}$ is the partial autoionization width, $\Gamma_a$ is the total autoionization width, $\bar{\varepsilon}_0 = \varepsilon_0 + hc\omega/2$. We took $\bar{g} = 1$, $\Gamma_{\bar{a}} = \Gamma_a$ [this is true if there is no excited state of the neutral molecule below the negative ion state, which is the case for all the molecules in the present study (Robin, 1974)], $\bar{\varepsilon}_0 = \varepsilon_{max}$ (experimentally determined peak energy), $\bar{\tau}_a = \hbar/\Gamma_a$. To obtain the $\sigma_{da}$ values for the various anions, we made use of the swarm data (Hunter and Christophorou, 1983) in combination with the present data. For example for $\sigma_{F^-}/CF_4$, we assumed that the peak value for the total attachment cross section, $(\sigma_a)_T$, obtained from the swarm study is equal to the sum of the peak values of the cross section for $F^-$ and $CF_3^-$. If we use the fact that $\sigma_{F^-}$ and $\sigma_{CF_3^-}$ at their respective peaks are equal (Table III-1, p. 57), then $\sigma_{F^-} = (\sigma_a)_T/2$. The $\tau_s$ and $\bar{\tau}_a$ determined as described above [Equations (III-5) and (III-10)] and by using the data shown in Table III-11 are listed in the last two columns of Table III-11.

The following general observation is made for the present study: In a two-fragment dissociative attachment process the negative ion with

the lower asymptotic limit (corresponding to the fragment with the larger EA) peaks at lower energy than its complementary anion and, with the exception of $F^-$ from $CF_4$ and n-$C_6F_{14}$, is more intense (see Tables III-1 to III-5 (pp. 57, 61, 63, 66, 69) and III-8 to III-10 (pp. 77-79). This may be attributed to the fact that $\tau_s$ is shorter for the anion peaking at lower energy (Table III-11) and also due to the fact that $\sigma_{da}$ is inversely proportional to $\varepsilon$ [Equation (III-10)]. In light of this argument the following observations concerning the relative cross sections of fragment anions can be understood: (i) As the size of the molecule increases, the abundance of the small negative ion fragments produced in a direct two-fragment dissociation process decreases. Thus, $CF_3^-$ from n-$C_5F_{12}$ and $CF_3^-$, $C_2F_5^-$ from n-$C_6F_{14}$ have not been detected. (ii) The intensity of $F^-$ relative to that of the complementary $(M-F)^-$ changes drastically from one molecule to another. For example, the ratios of the relative peak cross section values, $I_{F^-}/I_{(M-F)^-}$, for $C_2F_6$, $C_3F_8$, n-$C_4F_{10}$, and n-$C_5F_{12}$ are, respectively, 1000:1, 500:1, 1000:53, and 80:200 showing a decline with increasing (M-F) fragment size. The $F^-$ and $(M-F)^-$ from $CF_4$ and n-$C_6F_{14}$ do not follow this trend (see Discussion below). (iii) for PFAs ($C_2F_6$, n-$C_4F_{10}$, and n-$C_6F_{14}$) with an even number of carbon atoms, the second most intense negative ion fragment is that which results from a symmetric breaking of the parent molecule (Tables III-1, III-3, and III-5).

A comment should be made on the relative intensities of $F^-$ and $(M-F)^-$ for the molecules $CF_4$ and n-$C_6F_{14}$. According to the general observation made at the beginning of the previous paragraph, we would

expect for $CF_4$ (as for the case of $C_2F_6$, $C_3F_8$, and n-$C_4F_{10}$) the $F^-$ to be more intense than $(M-F)^-$, and for n-$C_6F_{14}$ (as for the case of n-$C_5F_{12}$) the $(M-F)^-$ to be more intense than $F^-$. Of all molecules studied, $CF_4$ is the only molecule for which the fragment ions $F^-$ and $CF_3^-$ are formed with considerable translational energy (Tables III-8 and III-9, pp. 77 and 78). This results in smaller $\tau_s$ for both anions (Table III-11); this alone, however, does not explain the equal peak intensities for $F^-$ and $CF_3^-$. It can be seen from Figure III-2 (p. 58) that the $F^-$ resonance is too broad (FWHM = 2.75 eV) and asymmetric (broader to the high-energy side) with an indication of a hump of $\sim$8 eV. It seems reasonable to assume that below $\sim$6 eV the energetic $F^-$ ions are produced primarily through the reaction $e + CF_4 \rightarrow F^- + CF_3$, and in this energy region $F^-$ is indeed more intense than $CF_3^-$ as is expected on the basis of the data of the other PFAs. For energies >6 eV, however, $F^-$ can be produced with less kinetic energy via $e + CF_4 \rightarrow F^- + F + CF_2$ with a resultant reduction in its intensity. For $\varepsilon > 8$ eV the reaction $e + CF_4 \rightarrow F^- + CF_3^*$ [the first excited electronic state of $CF_3$ is at 5.9 eV (Hastie and Margrave, 1969)] becomes energetically possible. Concerning the $F^-$/n-$C_6F_{14}$, we proposed in Table III-8 that its formation at the onset 1.8 eV is due to a two-fragment reaction. From Figure III-11, however, it seems that the formation of $F^-$ at the peak energy 3.45 eV may be due to a multiple- rather than a two-fragment reaction. In this regard it should be noticed that whereas in n-$C_4F_{10}$ the $F^-$ is produced predominately via a two-fragment reaction, in n-$C_5F_{12}$ the $F^-$ ion is formed more efficiently via a multiple-fragment reaction.

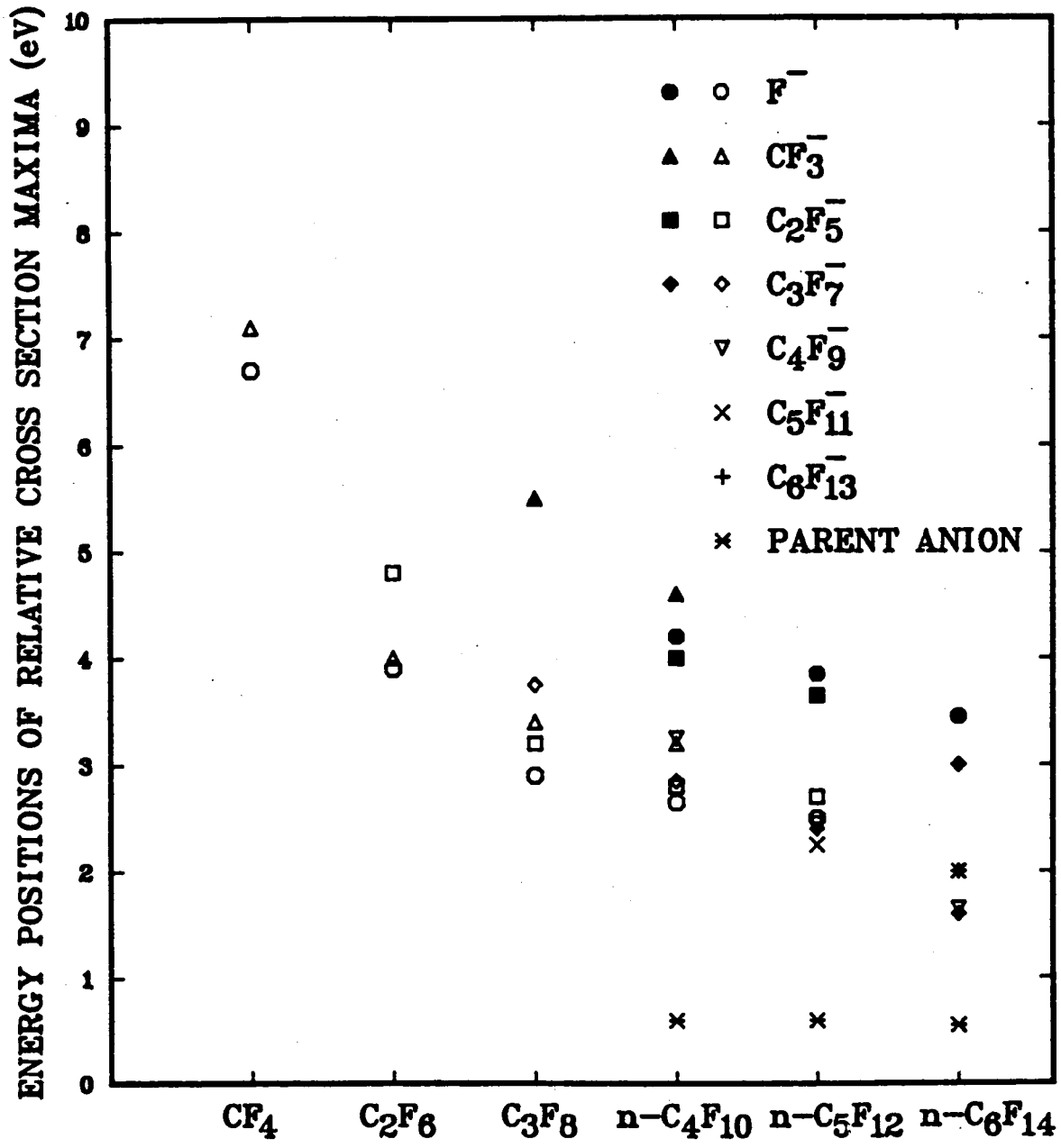


Figure III-11. Energy positions of relative cross section maxima versus molecular size.

B. Numbers and Positions of NISs

For each molecule we studied, the resonance peaks for the various anions group in certain energy regions. This would indicate the existence of negative ion states, precursors of the multiple anions. Figure III-11 summarizes the energy positions of the relative cross section maxima for parent anions and anions of the form $n\text{-}C_NF_{2N+1}^-$ (N = 0-6) observed from the normal PFAs. Three types of resonances are evident from Figure III-11. Firstly, there are the resonances leading to the parent ion formation at 0.6 eV independently of the molecular size. Secondly, there are the resonances (open symbols) which lead to direct fragmentation of the NIS (Tables III-8 to III-10, pp. 77-79). Thirdly, there are those resonances (solid symbols) which lead to multiple fragmentation of the NIS (Tables III-8 to III-10). The dissociation accompanied with multiple radical formation is at higher energies; it may have various asymptotic limits and, because of many possible combinations, many peaks for a particular small fragment anion. Also, it may involve electron-excited Feshbach resonances. It is also clear from Figure III-11 that the NISs leading to dissociation processes occur at lower energies as the size of the molecule increases. This reflects the fact that the negative ion states are lowered with increasing size of the molecule. It may also reflect the fact that the dissociation leads to bigger rather than smaller negative ion fragments. It has already been pointed out in Section IV.A that the larger the size of the fragment, the greater its EA. This would result in a lowering of the asymptotic limit and the peak energy for the production of the negative ion.

C. Comparison with Electron Swarm Data

Although data obtained using the electron beam technique may not always be straightforwardly compared with data obtaind using the electron swarm technique, they can complement each other in many respects. Short-lived negative ion states ($<10^{-6}$ s) which in a TOFMS experiment cannot be observed (unless they lead to dissociative attachment fragments) can be stabilized by collisions in a swarm experiment where high pressures are employed. A swarm study of the PFAs by Hunter and Christophorou (1983) has shown that electron attachment to $CF_4$ and $C_2F_6$ is independent of gas pressure. This is consistent with the presence of only dissociative attachment for these molecules and negative EA. A strong pressure dependence of the attachment rate constant, $k_a$, was observed for $C_3F_8$ indicating that although in the beam study only fragment ions were observed, the EA of this molecule is slightly positive allowing short-lived ($<10^{-10}$ s) $C_3F_8^{-*}$ to be stabilized under high-pressure conditions. For n-$C_4F_{10}$, the $k_a$ were less dependent on pressure, and the pressure dependence was virtually absent for n-$C_5F_{12}$ and n-$C_6F_{14}$, a finding consistent with the present study where besides the fragment anions the parent anions formed are long lived. Also consistent with the present study are the swarm data on the increase in $k_a$ and the shifting of the $k_a(\langle\varepsilon\rangle)$ function toward lower energy with increasing molecular size. Finally, the unfolded total (i.e., for all negative ions formed, parent and fragments) cross section for electron attachment agrees satisfactorily with the present results (Hunter and Christophorou, 1983). The agreement is especially good for $CF_4$ and $C_2F_6$ for which the

same rapidly dissociative NISs are probed [see Hunter and Christophorou (1983) for further discussion].

# CHAPTER IV

# ELECTRON ATTACHMENT TO i-$C_4F_{10}$, i-$C_5F_{12}$, neo-$C_5F_{12}$ AND c-$C_5F_{10}$

## I. INTRODUCTION

Electron attachment to the perfluorocarbon molecules has received increased interest over the last few years. In the previous chapter the results of a study on the normal perfluoroalkanes n-$C_NF_{2N+2}$ (N = 1-6) were presented. The purpose of that study was to investigate the effect of molecular size on the electron attachment properties of a series of similar molecules.

In this chapter an investigation is made of another aspect of the attachment of low-energy electrons to polyatomic fluorocarbon molecules using the TOF mass spectrometric technique, namely the possible effect(s) of the geometrical structure of a molecule on its electron attaching properties. The molecules perfluoro-iso-butane (i-$C_4F_{10}$), perfluoro-iso-pentane (i-$C_5F_{12}$), perfluoro-neo-pentane (neo-$C_5F_{12}$) and perfluoro-cyclo-pentane (c-$C_5F_{10}$) were chosen for this purpose. The names and chemical structures of these molecules are shown in Figure IV-1.

## II. RESULTS

### A. Negative Ion Formation

1. i-$C_4F_{10}$. The parent $C_4F_{10}^{-*}$ and four fragment $C_4F_9^-$, $C_3F_7^-$, $CF_3^-$, and $F^-$ negative ions were observed in low-energy electron impact with i-$C_4F_{10}$. The relative abundances of all anions as a function of electron

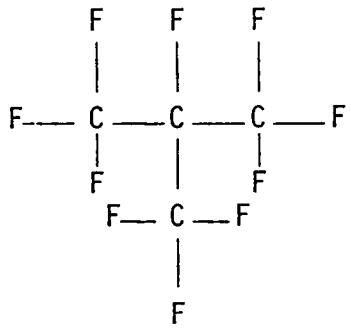

Perfluoro-iso-butane

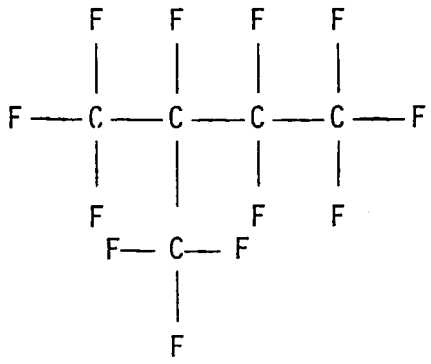

Perfluoro-iso-pentane

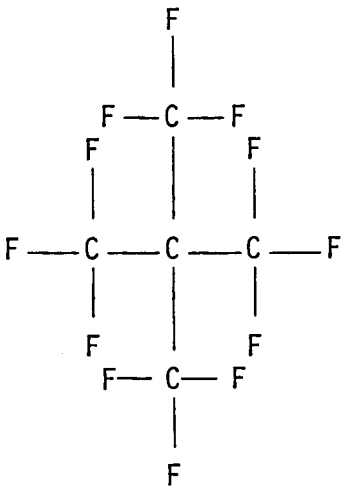

Perfluoro-neo-pentane

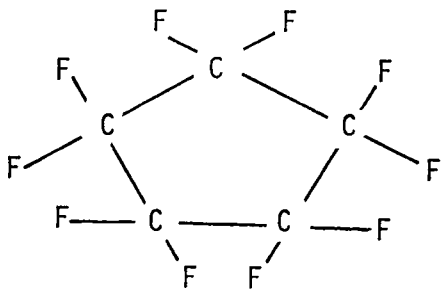

Perfluoro-cyclo-pentane

Figure IV-1. Chemical structure of the perfluorocarbons studied in this chapter.

energy are shown in Figure IV-2(a) and the corresponding unfolded functions in Figure IV-2(b). The pertinent data on relative peak intensities, resonance maxima, full widths at half maximum (FWHM), and appearance onsets are summarized in Table IV-1, along with those for n-$C_4F_{10}$ for comparison. The i-$C_4F_{10}$ molecule behaves differently under electron impact from its isomer n-$C_4F_{10}$. The most striking difference is that in contrast to n-$C_4F_{10}$, for i-$C_4F_{10}$ the parent ion i-$C_4F_{10}^{-*}$ is the most intense ion. Also, the $C_2F_5^-$ ion was not observed for i-$C_4F_{10}$ which is reasonable since its formation would require the severing of two C-C bonds and the intramolecular transfer of a fluorine atom to a $CF_3$-CF radical. For i-$C_4F_{10}$ the fragment ions $C_4F_9^-$ and $C_3F_7^-$ are stronger compared to those from n-$C_4F_{10}$, their peak intensity being, respectively, ∿75 and ∿55% that of the predominant ion i-$C_4F_{10}^{-*}$.

The data in Figure IV-2(b) indicate that there are three NISs below 5 eV for the i-$C_4F_{10}$: a low-lying one at 0.6 eV leading mostly to parent anions, a second one at ∿1.8 eV leading mostly to fragment anions, and a third NIS in the range 3.2 to 4 eV leading exclusively to fragment anions. The 1.8 eV NIS lies ∿1 eV lower compared with n-$C_4F_{10}$.

2. i-$C_5F_{12}$. The nonunfolded and unfolded relative cross sections for the strong parent anion $C_5F_{12}^{-*}$ and the four fragment anions $C_5F_{11}^-$, $C_4F_9^-$, $C_3F_7^-$, and $F^-$ observed for i-$C_5F_{12}$ are shown, respectively, in Figures IV-3(a) and IV-3(b). The pertinent physical quantities are summarized in Table IV-2, where a comparison is made with the relevant quantities for n-$C_5F_{12}$. The relative peak intensities, energy of maximum ion intensity, FWHM and appearance onsets for $C_5F_{12}^{-*}$, $C_5F_{11}^-$,

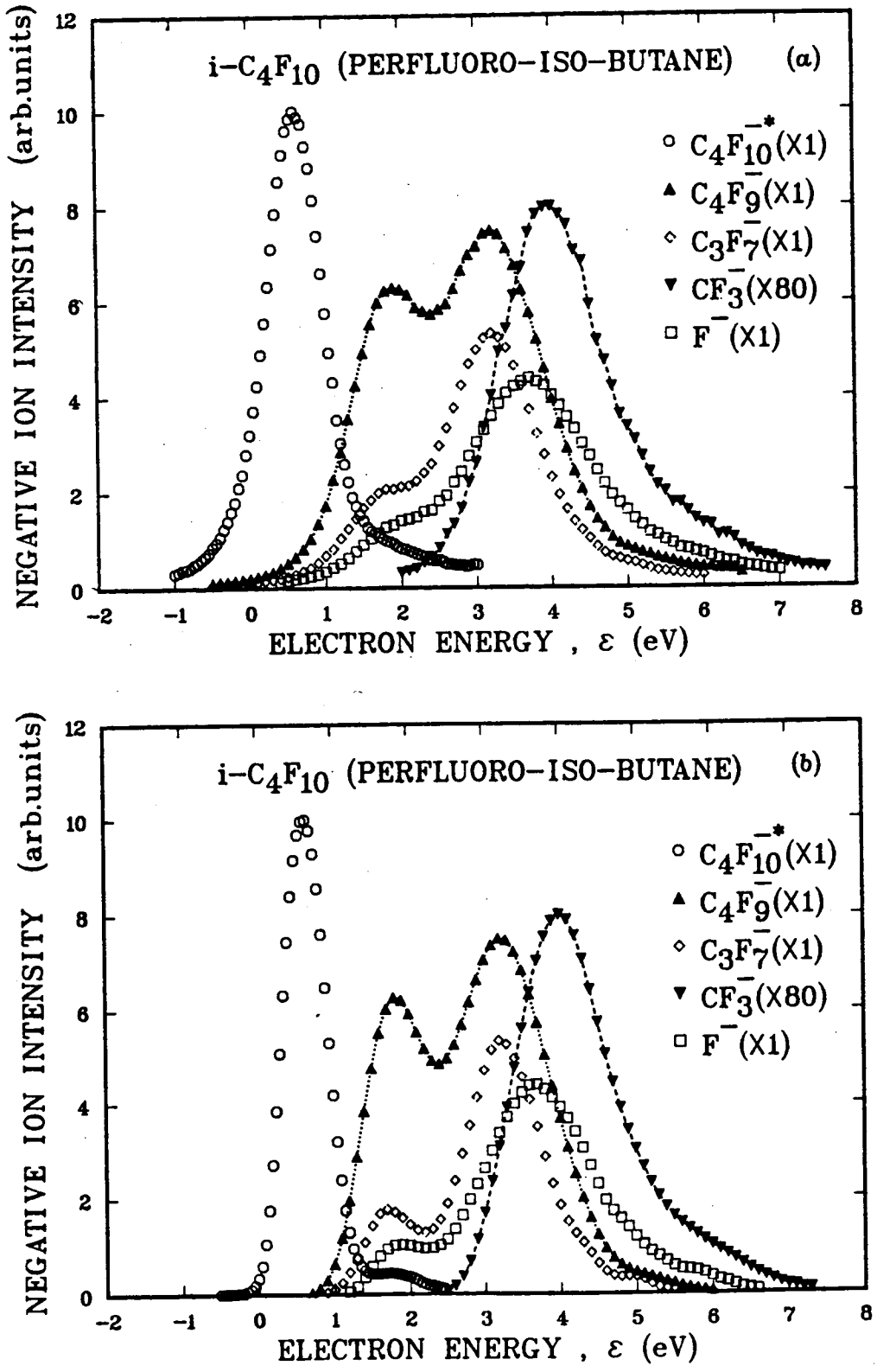


Figure IV-2. Negative ion intensity as a function of ε for i-$C_4F_{10}$. (a) Nonunfolded data; (b) unfolded data (note the multiplication factors).

Table IV-1. Negative ions due to low-energy electron impact on $i\text{-}C_4F_{10}$

| Negative ion[b] | Relative peak intensity | Energy of maximum ion intensity (eV)[c] | FWHM[a] (eV)[d] | Appearance onset (eV)[d] |
|---|---|---|---|---|
| $C_4F_{10}^{-*}$ | 1000(80)[e] | 0.6±0.05(0.6)[e] | 0.65(0.57)[d] | ∿0 (∿0)[e] |
| $C_4F_9^-$ | 630(46) | 1.85±0.1(1.85) | 2.6[f] | 0.9±0.1(1.0) |
| | 750(53) | 3.2±0.05(3.25) | | 2.0±0.3(<2) |
| $C_3F_7^-$ | 177 | 1.7±0.1 | | 0.9±0.1 |
| | 535 (80) | 3.2±0.05(2.85) | 1.2(1.25) | 2.2±0.2(1.2) |
| $CF_3^-$ | (8) 10(13) | (3.2) 4±0.05(4.6) | 1.5(1.9) | (2.2) 2.5±0.1(>3.2) |
| $F^-$ | 103(1000) | 1.85±0.1(2.65) | (1.35) | 1.2±0.1(1.6) |
| | 440(300) | 3.7±0.05(4.2) | 1.6 | 2.1±0.2(<4) |

[a]Full width at half maximum of the respective negative ion intensity as a function of electron energy.

[b]An asterisk (*) indicates that the ion is long lived with respect to autodetachment.

[c]Energy scale calibration determined using for the $SF_5^-/SF_6$ resonance the value of 0.37 eV. The ± refers to the standard deviation from the average.

[d]Values listed are from the unfolded data.

[e]Numbers in parentheses refer to $n\text{-}C_4F_{10}$ (Chapter III). Information on the anion $C_2F_5^-$ observed for $n\text{-}C_4F_{10}$ but not for $i\text{-}C_4F_{10}$ is not shown in this table.

[f]Includes both peaks.

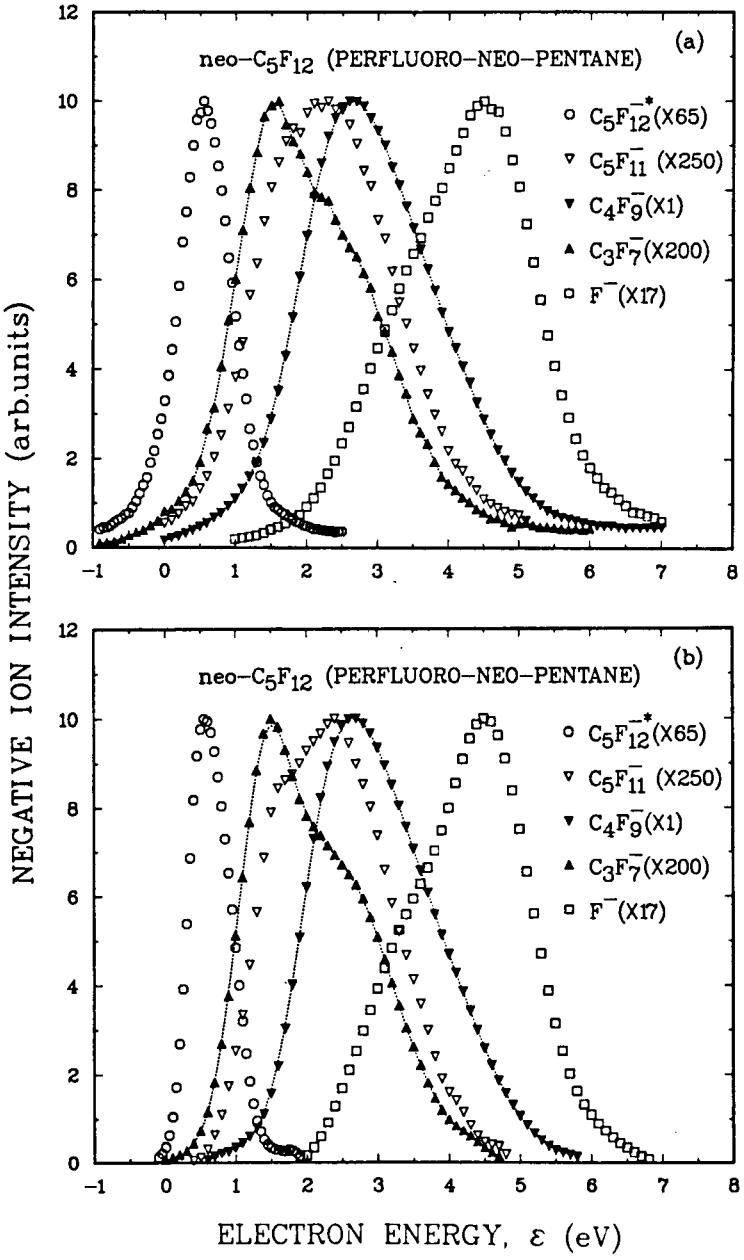


Figure IV-3. Negative ion intensity as a function of ε for i-$C_5F_{12}$. (a) Nonunfolded data; (b) unfolded data (note the multiplication factors).

Table IV-2. Negative ions due to low-energy electron impact on i-$C_5F_{12}$, neo-$C_5F_{12}$, and c-$C_5F_{10}$

| Molecule | Negative ion[b] | Relative peak intensity | Energy of maximum ion intensity (eV)[c] | FWHM[a] (eV)[d] | Appearance onset (eV)[d] |
|---|---|---|---|---|---|
| i-$C_5F_{12}$ | $C_5F_{12}^{-*}$ | 1000(1000)[e] | 0.55±0.05(0.6) | 0.82(0.75) | ∿0 (∿0) |
| | $C_5F_{11}^-$ | 170(170)<br>200(200) | 1.7±0.1(1.65)<br>2.25±0.05(2.25) | 2.15[f](2.05)[f] | 0.4±0.2(0.65)<br><1.2±0.3( 1.65) |
| | $C_4F_9^-$ | 57(51)<br>67(66) | 1.6±0.1(1.7)<br>2.4±0.05(2.45) | 2.2[f](2.1)[f] | 0.5±0.1(0.8)<br><1.6(<2) |
| | $C_3F_7^-$ | 265(300)<br>180(280) | 1.5±0.05(1.65)<br>2.25±0.2(2.4) | 1.85[f](2.3)[f] | 0.7±0.2(0.9)<br><1.7(<2) |
| | $F^-$ | 25(80)<br>55(180) | 1.7 (shoulder)(2.5)<br>3.45±0.1(3.8) | 1.9[f](1.65) | 1.1±0.1(1.65)<br>(>2.5) |
| neo-$C_5F_{12}$ | $C_5F_{12}^{-*}$ | 15 | 0.55±0.05 | 0.7 | ∿0 |
| | $C_5F_{11}^-$ | 3<br>4 | 1.75±0.2<br>2.3±0.1 | 2.1[f] | 0.7±0.2<br><1.7 |
| | $C_4F_9^-$ | 1000 | 2.6±0.05 | 2.0 | 1±0.3 |
| | $C_3F_7^-$ | 5<br>3.5 | 1.5±0.1<br>2.3±0.2 | 2.0[f] | 0.6±0.3<br><2 |
| | $F^-$ | 60 | 4.5±0.1 | 2 | 1.9±0.1 |
| c-$C_5F_{10}$ | $C_5F_{10}^{-*}$ | 1000[1000][g] | ∿0 [∿0] | 0.22 | |
| | $F^-$ | 25[100]<br>60[60]<br>50[42] | 4.5±0.1[4.6]<br>7.8±0.1[8.2]<br>10.3±0.1[10.4] | 1.4<br>1.25<br>2.35 | 3.4±0.1<br>6.8±0.2<br>8.4±0.3 |

[a]Full width at half maximum of the respective negative ion intensity as a function of electron energy.

[b]An asterisk (*) indicates that the ion in long lived with respect to autodetachment.

[c]Energy scale calibration determined using for the $SF_5^-/SF_6$ resonance the value of 0.37 eV. The ± refers to the standard deviation from the average.

[d]Values listed are from the unfolded data.

[e]Numbers in parentheses refer to n-$C_5F_{12}$ (Chapter III).

[f]Includes both peaks.

[g]Numbers in brackets refer to c-$C_4F_8$ (P. W. Harland and J. L. Franklin, J. Chem. Phys. 61, 1621 (1974).

$C_4F_9^-$ and $C_3F_7^-$, for the two molecules are in agreement within the experimental uncertainty. The $F^-$ from i-$C_5F_{12}$ is weaker by a factor of three and its onset is lower by ∿0.6 eV as compared to $F^-$ from n-$C_5F_{12}$. The two peaks of $C_4F_9^-$ are better resolved for i-$C_5F_{12}$ rather than for n-$C_5F_{12}$.

The peaks of the various anions for i-$C_5F_{12}$, like the case for n-$C_5F_{12}$, are grouped at certain energies indicating the existence of common NISs, precursors of these anions at these energies. Four such NISs can be identified: one at ∿0.6 eV leading mostly to parent anion formation, one at 1.6±0.1 eV leading mostly to fragment anions, and a third and a fourth at 2.3±0.2 and 3.5±0.1 eV, respectively, leading exclusively to fragment anions.

3. neo-$C_5F_{12}$. The parent $C_5F_{12}^{-*}$ and four fragment $C_5F_{11}^-$, $C_4F_9^-$, $C_3F_7^-$, $F^-$ anions were observed in electron collision with neo-$C_5F_{12}$. The nonunfolded and unfolded cross sections as a function of $\varepsilon$ for all anions are shown, respectively, in Figures IV-4(a) and IV-4(b), whereas the relative peak intensities, energy of maximum ion intensity, FWHM and appearance onsets are listed in Table IV-2. The latter three quantities for the neo-$C_5F_{12}$ are with a few exceptions (the $C_4F_9^-$ resonance is asymmetric showing only one peak and the $F^-$ peaks at higher energies for this molecule) in agreement with those of n-$C_5F_{12}$ and i-$C_5F_{12}$. There is, however, a dramatic difference in the relative intensities of the various anions for neo-$C_5F_{12}$ as compared to n-$C_5F_{12}$ and i-$C_5F_{12}$. For neo-$C_5F_{12}$ the predominant ion is the fragment $C_4F_9^-$, all other anions being much weaker. This finding will be discussed in

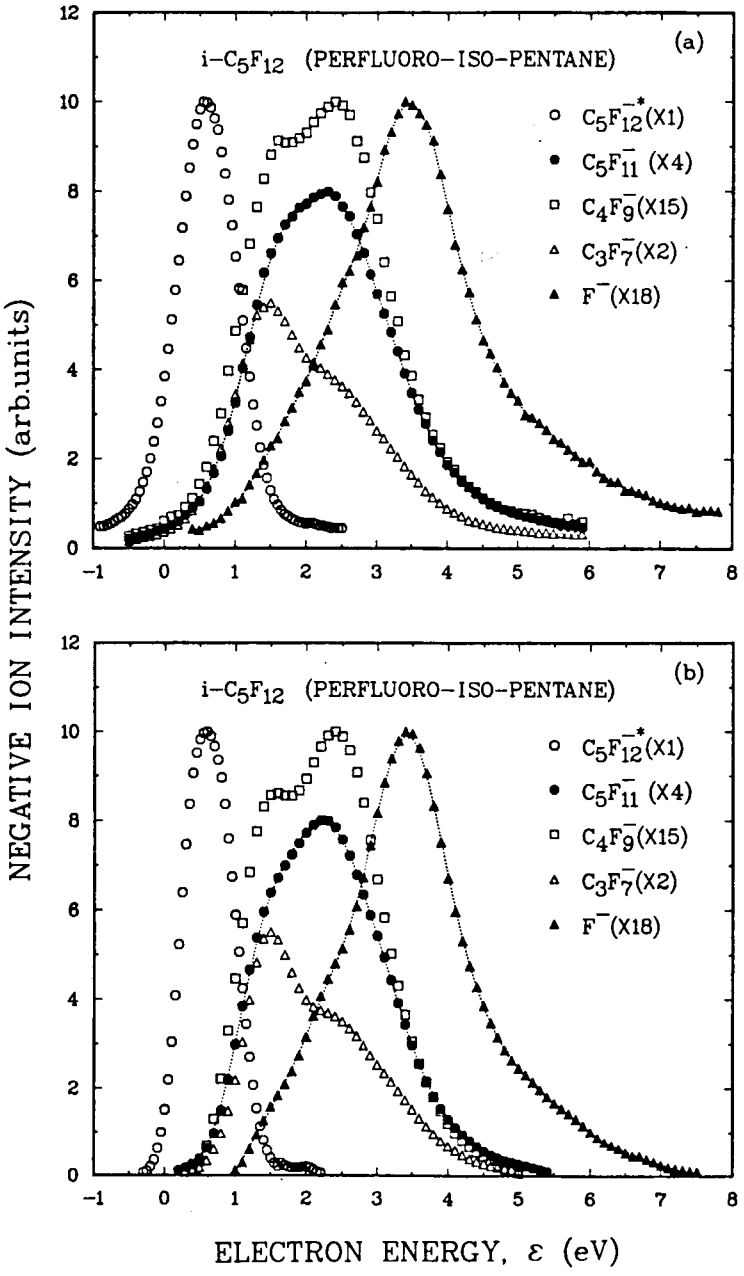


Figure IV-4. Negative ion intensity as a function of ε for neo-$C_5F_{12}$. (a) Nonunfolded data; (b) unfolded data (note the multiplication factors).

the next section. The formation of $C_3F_7^-$ from neo-$C_5F_{12}$ requires the severing of two C-C bonds in the parent molecule and the transfer of an atomic fluorine to the radical $(CF_3)_2C$. The analogous formation of $C_2F_5^-$ from i-$C_4F_{10}$ was not observed, however.

4. c-$C_5F_{10}$. Only two negative ions were observed in low-energy electron impact with c-$C_5F_{10}$: the parent anion $C_5F_{10}^{-*}$ and the fragment anion $F^-$. The relative cross sections for the two anions are shown, respectively, in Figures IV-5(a) and IV-5(b). The pertinent quantities are summarized in Table IV-2. In the same table are also listed for comparison the relative peak intensities and the energy of maximum intensity for the anions $C_4F_8^{-*}$ and $F^-$ observed from c-$C_4F_8$. There are distinct differences between the aliphatic and the cyclic perfluorocarbons in the way they attach low-energy electrons. The cyclic compounds form a strong parent anion peaking at thermal energies, and the $F^-$ from these molecules shows multiple, well resolved structure, being discussed in Section III.

B. Autodetachment Lifetimes, $\tau_a$

The parent anions of all four molecules i-$C_4F_{10}$, i-$C_5F_{12}$, neo-$C_5F_{12}$, and c-$C_5F_{10}$, were found to be long lived with $\tau_a > 10^{-6}$ s. The $\tau_a$ of the parent anions of i-$C_4F_{10}$, i-$C_5F_{12}$ and c-$C_5F_{10}$ were found to decrease with increasing $\varepsilon$. The intensity of the $C_5F_{12}^{-*}$/neo-$C_5F_{12}$ ion, however, was too weak to allow similar measurements to be made. The $\tau_a$ for this anion was estimated to be 89±13 μs. The variation of $\tau_a$ with $\varepsilon$ for the parent anions of i-$C_4F_{10}$, i-$C_5F_{12}$ and c-$C_5F_{10}$

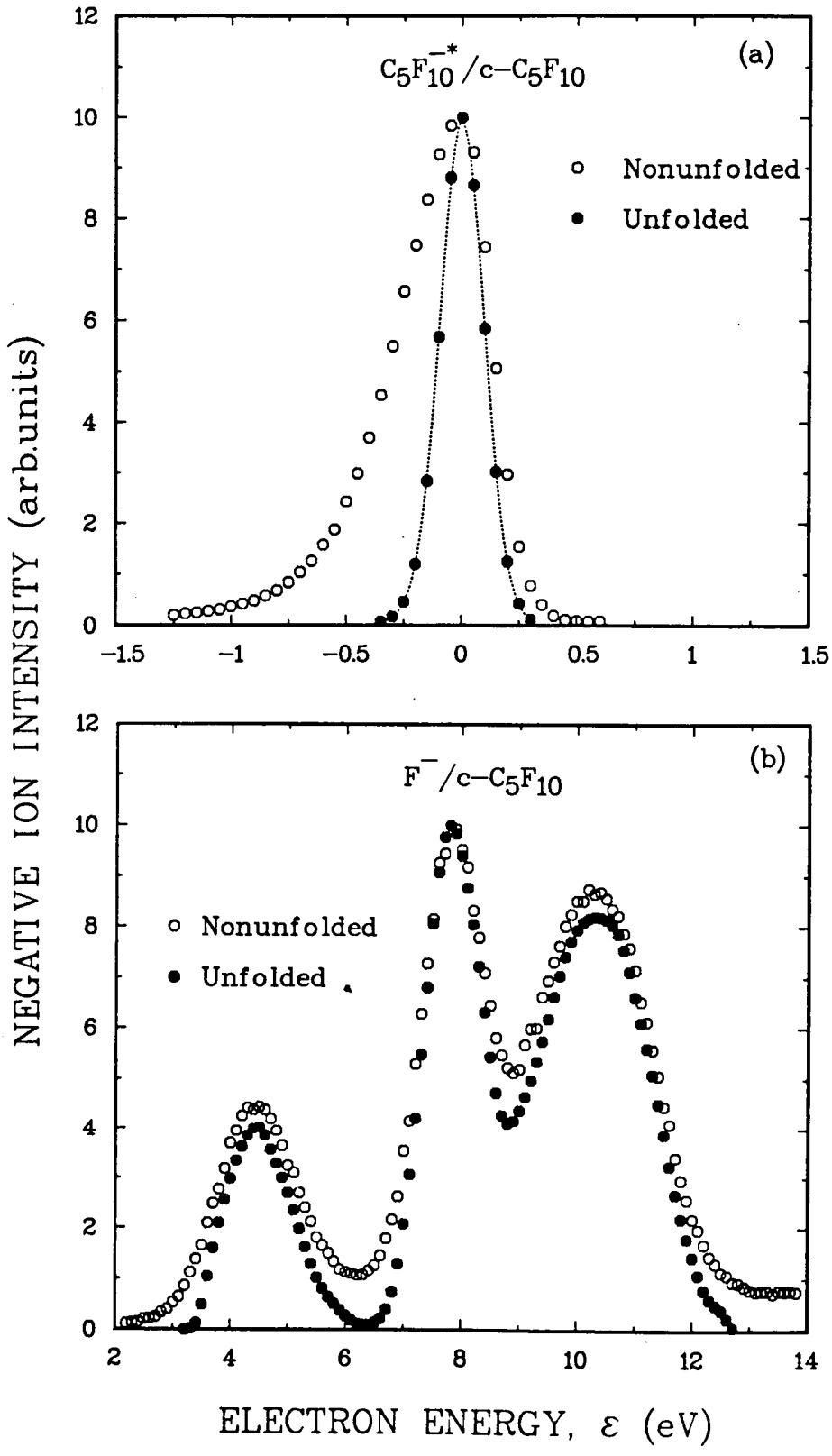


Figure IV-5. Negative ion intensity as a function of ε for c-$C_5F_{10}$.

(measured as described in Chapters II and III) is shown, respectively, in Figures IV-6(a) to IV-8(a). In Figures IV-6(b) to IV-8(b) the $\tau_a$ values determined at a number of energies by the slope method are shown. In Table IV-3 are listed the values of $\tau_a$ at the peak of the respective negative ion resonance.

## III. DISCUSSION

### A. Energetics of Dissociative Electron Attachment Processes

In the previous chapter we used energetic considerations to identify possible dissociative attachment processes leading to the formation of all observed negative ions. We have applied similar arguments to the fragment anions of the present chapter by making use of the energy balance equations of the previous chapter [Equations (III-2) to (III-4)] and the data of Table IV-4. The proposed fragmentation processes along with their estimated heats of reaction are summarized in Tables IV-5 and IV-6. A few remarks concerning the information in these two tables can be made.

The $F^-$ production (Table IV-5) from the c-$C_5F_{10}$ molecule is different from that from the molecules i-$C_4F_{10}$, i-$C_5F_{12}$ and neo-$C_5F_{12}$. For the latter molecules the $F^-$ formation at its lowest onset involves a direct cleavage of a C-F bond. This onset depends on whether the $F^-$ comes from a carbon connected to three other carbon atoms (tertiary carbon) or from a carbon connected to only one other carbon atom (primary carbon). Thus for i-$C_4F_{10}$ and i-$C_5F_{12}$ the onset is by $\sim$1 eV lower than that for neo-$C_5F_{12}$ and this reflects the fact that the tertiary C-F bond dissociation energy is lower by the same amount than

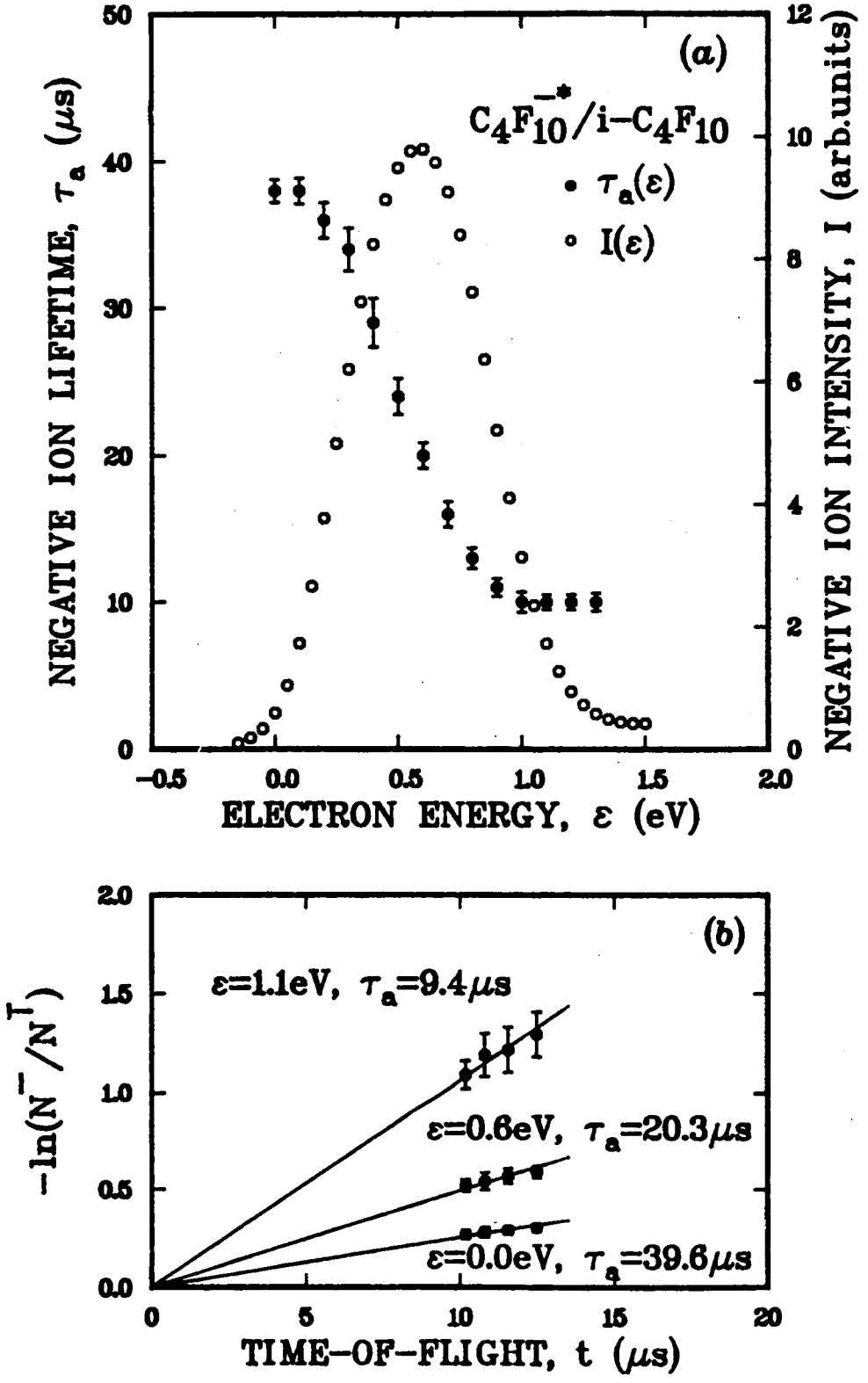


Figure IV-6. (a) Negative ion lifetime and negative ion intensity (unfolded results) for $C_4F_{10}^{-*}/i\text{-}C_4F_{10}$ as a function of electron energy. (b) Determination of $\tau_a$ for $C_4F_{10}^{-*}/i\text{-}C_4F_{10}$ at 0.0, 0.6, and 1.1 eV by the slope method.

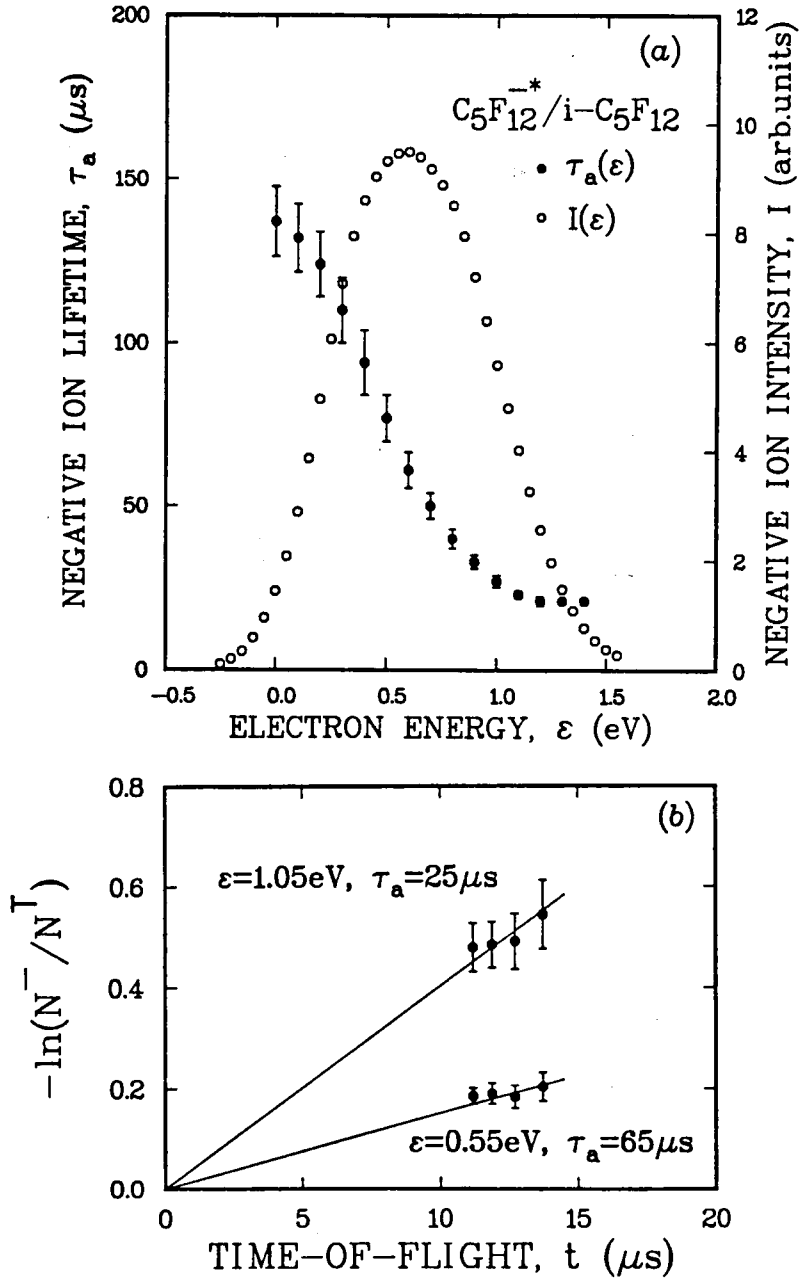


Figure IV-7. (a) Negative ion lifetime and negative ion intensity (unfolded results) for $C_5F_{12}^{-*}/i\text{-}C_5F_{12}$ as a function of electron energy. (b) Determination of $\tau_a$ for $C_5F_{12}^{-*}/i\text{-}C_5F_{12}$ at 0.55 and 1.05 eV by the slope method.

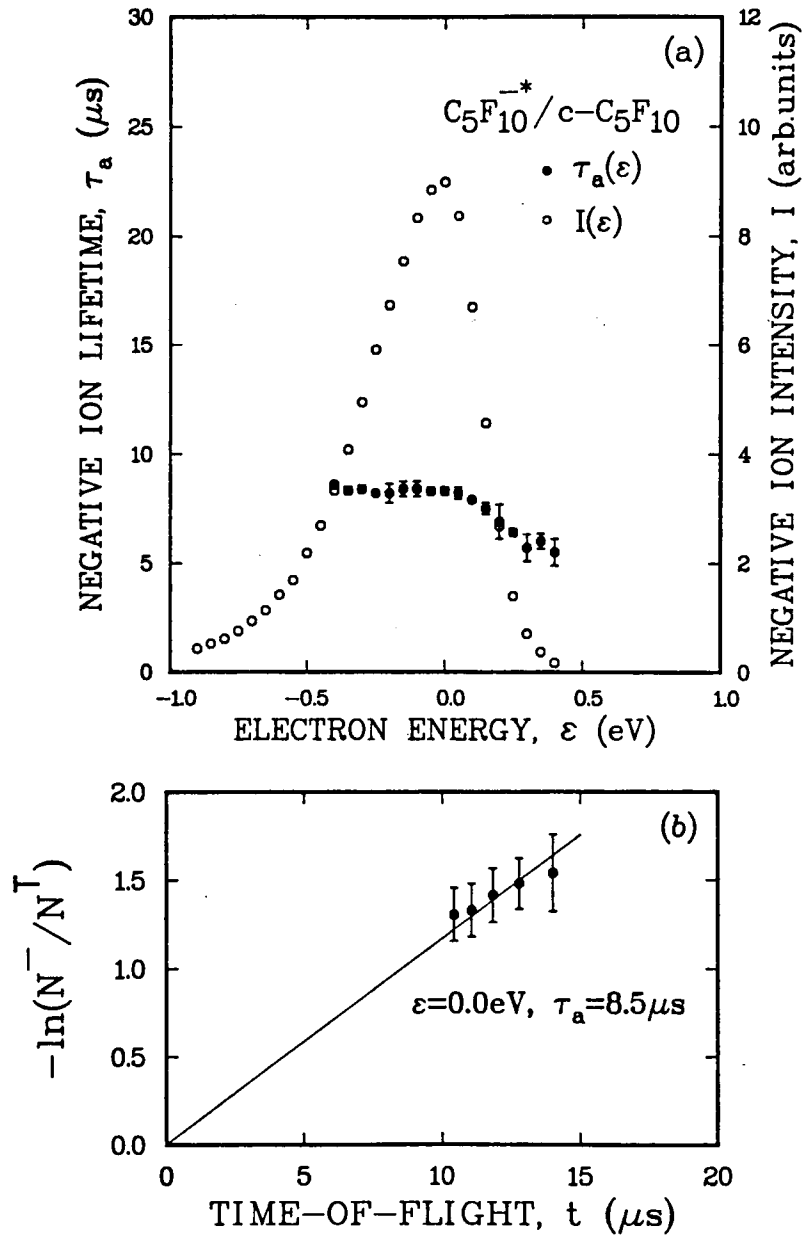


Figure IV-8. (a) Negative ion lifetime and negative ion intensity for $C_5F_{10}^{-*}/c-C_5F_{10}$ (nonunfolded results) as a function of electron energy. (b) Determination of $\tau_a$ for $C_5F_{10}^{-*}/c-C_5F_{10}$ at ~0.0 eV by the slope method.

Table IV-3. Lifetimes of long-lived negative ions observed in collisions of slow electrons with i-$C_4F_{10}$, i-$C_5F_{12}$, neo-$C_5F_{12}$ and c-$C_5F_{10}$

| Long-lived negative ion | Parent molecule | $\tau_a$ ($10^{-6}$ s) |
|---|---|---|
| $C_4F_{10}^{-*}$ | i-$C_4F_{10}$ | 20.3±0.7[a] |
| $C_5F_{12}^{-*}$ | i-$C_5F_{12}$ | 65±4[a] |
| $C_5F_{12}^{-*}$ | neo-$C_5F_{12}$ | 89±13[b] |
| $C_5F_{10}^{-*}$ | c-$C_5F_{10}$ | 8.5±0.5[a] |

[a]Lifetime decreases with increasing electron energy. The values listed in the table are the lifetimes at the resonance peak determined by the slope method.

[b]Determined from an average of over 150 separate measurements.

Table IV-4. Thermochemical data used in Chapter IV

| Quantity | Value (in eV) and reference | Quantity | Value (in eV) and reference |
|---|---|---|---|
| Heat of formation | | $i\text{-}C_4F_{10}$ | -22.35(c) |
| F | 0.82(a) | $c\text{-}C_5F_8$ | -15.5±0.2(e) |
| $CF_2$ | -1.72(b) | | |
| $CF_3$ | -4.94(a) | $(CF_3)_2CFC_2F_4$ | -21.92(c) |
| $C_2F_3$ | -1.99(c) | $CF_2C(CF_3)_3$ | -22.54(c) |
| $C_2F_4$ | -6.74(a) | $c\text{-}C_5F_{10}$ | -2..0±0.2(f) |
| $C_2F_5$ | -9.19(c) | $i\text{-}C_5F_{12}$ | -26.44(c) |
| $C_3F_5$ | -7.9(d) | $neo\text{-}C_5F_{12}$ | -27.07(c) |
| $C_3F_6$ | -11.22(c) | | |
| $(CF_3)_2CF$ | -13.87(c) | Electron affinity | |
| $c\text{-}C_4F_6$ | -10.1(b) | F | 3.45(g) |
| $c\text{-}C_4F_8$ | -15.7(b) | $CF_3$ | 2.1(h) |
| $C(CF_3)_3$ | -18.88(c) | | |
| $CF_2CF(CF_3)_2$ | -17.82(c) | | |

[a] J. L. Franklin, J. G. Dillard, H. M. Rosenstock, J. T. Herron, K. Draxl, and F. H. Field, NSRDS-NBS26 (1969).

[b] S. W. Benson and H. E. O'Neal, NSRDS-NBS21 (1970).

[c] W. M. Bryant, J. Polym. Sci. 56, 277 (1962).

[d] I. Sauers, L. G. Christophorou, and J. G. Carter, J. Chem. Phys. 71, 3016 (1979).

[e] Obtained using $c\text{-}C_5F_8 \rightarrow c\text{-}C_4F_6+CF_2$, with $\Delta H_r = D(C\text{-}C) = 3.7 \pm 0.2$ eV and the $\Delta H_f$ for $c\text{-}C_5F_8$, $c\text{-}C_4F_6$, and $CF_2$ from this table.

[f] The value listed is the average of the values obtained from the reactions $c\text{-}C_5F_{10} \rightarrow c\text{-}C_4F_8+CF_2$ and $c\text{-}C_5F_{10} \rightarrow C_3F_5+C_2F_5$ as in footnote e.

[g] R. S. Berry and C. W. Reimann, J. Chem. Phys. 38, 1540 (1963).

[h] H. H. Rosenstock, K. Draxl, B. W. Steiner, and J. T. Herron, J. Phys. Chem. Ref. Data 6, Suppl. No. 1 (1977).

Table IV-5. Possible dissociative attachment processes leading to the formation of $F^-$ from i-$C_4F_{10}$, $C_5F_{12}$, neo-$C_5F_{12}$ and c-$C_5F_{10}$ and thermochemical data deduced

| AO (eV) | Reaction | $\Delta H_r$[a] (eV) | Thermochemical data deduced (eV) |
|---|---|---|---|
| 1.2±0.1 | e + i-$C_4F_{10}$ → $F^-$ + $C(CF_3)_3$ | 0.85 | $D(F\text{-}C(CF_3)_3)$[b] ≤ 4.65±0.1 (4.3) |
| 2.1±0.2 | $F^-$ + $CF_2CF(CF_3)_2$ | 1.9 | $D(F\text{-}CF_2CF(CF_3)_2)$ ≤ 5.35±0.2 (5.35) |
| 1.1±0.1 | e + i-$C_5F_{12}$ → $F^-$ + $C(CF_3)_2C_2F_5$ | [1.1±0.1][c] | $D(F\text{-}C(CF_3)_2C_2F_5)$ ≤ 4.55±0.1; $\Delta H_f(C(CF_3)_2C_2F_5)$[c] = -22.7±0.1 |
| 1.9±0.1 | e + neo-$C_5F_{12}$ → $F^-$ + $CF_2C(CF_3)_3$ | 1.9 | $D(F\text{-}CF_2C(CF_3)_3)$ ≤ 5.35±0.1 (5.35) |
| 3.4±0.1[d] | e + c-$C_5F_{10}$ $\xrightarrow{1}$ $F^-$ + c-$C_5F_9$ | [1.9][e] | $E^*$[f] = 1.5 |
| | $\xrightarrow{2}$ $F^-$ + F + c-$C_5F_8$ | 3.7±0.4 | |
| | $\xrightarrow{3}$ $F^-$ + $C_2F_4$ + $C_3F_5$ | 3.7±0.2 | |
| 6.8±0.2[d] | $\xrightarrow{4}$ $F^-$ + $C_2F_3$ + $C_3F_6$ | 5.2±0.2 | $E^*$ = 1.4 |
| | $\xrightarrow{5}$ $F^-$ + $2CF_2$ + $C_3F_5$ | 7±0.2 | |
| 8.4±0.3[d] | → $F^-$ + (c-$C_5F_9$)[d] | | |

[a] Heat of reaction determined from Equation (III-2) and the data of Table IV-4, unless otherwise specified.

[b] Bond dissociation energy determined from Equation (III-4) using $E^* \geq 0$ eV and EA(F)=3.45 eV (Table IV-4). The numbers in parentheses are the values of Bryant (1962).

[c] Heat of formation determined from Equation (III-2) and the data of Table IV-4, using $\Delta H_r$=AO=1.1±0.1 eV.

[d] If $F^-$ from c-$C_5F_{10}$ is produced with thermal energy at the onset 3.4 eV and with excess energy at the onsets 6.8 and 8.4 eV (like the case of $F^-$ from c-$C_4F_8$; Harland and Franklin, 1974), then reactions (2) and (3) may account for the 3.4 eV onset and reactions (2) to (5) for the 6.8 and 8.4 eV onsets. The case of producing $F^-$ + c-$C_5F_9^*$ may not be excluded also for all three onsets.

[e] $\Delta H_r$ determined from Equations (III-3) and (III-4) using $D(F\text{-c-}C_5F_9)$=5.35 eV.

[f] Excess energy determined from Equation (III-3).

Table IV-6. Possible dissociative attachment processes leading to the formation of various anions from i-$C_4F_{10}$, i-$C_5F_{12}$ and neo-$C_5F_{12}$ and thermochemical data deduced

| Ion | AO (eV) | Reaction | $\Delta H_r$[a] (eV) | Thermochemical data deduced (eV) |
|---|---|---|---|---|
| $CF_3^-$ | 2.5 ± 0.1 | e + i-$C_4F_{10}$ → $CF_3^-$ + $(CF_3)_2CF$ | 1.45 | E* = 1.05 ± 0.1[b] |
| $C_3F_7^-$ | 0.9 ± 0.1 | e + i-$C_4F_{10}$ → $(CF_3)_2CF^-$ + $CF_3$ | [1.05 ± 0.3] | EA[$(CF_3)_2CF$] ≥ 2.65 ± 0.1[c] |
| | 2.2 ± 0.2 | → (d) | | E* = 1.15 ± 0.5 eV |
| | 0.7 ± 0.2 | e + i-$C_5F_{12}$ → $(CF_3)_2CF^-$ + $C_2F_5$ | [1 ± 0.4] | EA[$(CF_3)_2CF$] ≥ 2.7 ± 0.2[c] |
| | <1.7 | → (d) | | E* ≤ 0.7 ± 0.4 |
| | 0.6 ± 0.3 | e + neo-$C_5F_{12}$ → $(CF_3)_2CF^-$ + $C_2F_5$ | [0.6 ± 0.3][e] | EA[$(CF_3)_2CF$] = 3.4 ± 0.3[c,e] |
| | <2 | → (d) | | E* ≤ 1.4 ± 0.3 |
| $C_4F_9^-$ | 0.9 ± 0.1 | e + i-$C_4F_{10}$ → $(CF_3)C^-$ + F | [1.2 ± 0.3] | EA[$(CF_3)_3C$] ≥ 3.4 ± 0.1[c] |
| | 2.0 ± 0.3 | → $(CF_3)_2CFCF_2^-$ + F | (1.8 ± 0.5) | EA[$(CF_3)_2CFCF_2$] ≥ 3.55 ± 0.5[f] |
| | 0.5 ± 0.1 | e + i-$C_5F_{12}$ → $(CF_3)_2CFCF_2^-$ + $CF_3$ | [0.5 ± 0.3] | EA[$(CF_3)_2CFCF_2$] ≥ 3.2 ± 0.1[c] |
| | <1.6 | → (d) | | E* ≤ 1.1 ± 0.3 |
| | 1 ± 0.3 | e + neo-$C_5F_{12}$ → $(CF_3)C^-$ + $CF_3$ | (≈0) | E* ≈ 1 ± 0.3 |
| $C_5F_{11}^-$ | 0.4 ± 0.2 | e + i-$C_5F_{12}$ → $(CF_3)_2CC_2F_5^-$ + F | (0.4 ± 0.3)[g] | EA[$(CF_3)_2CC_2F_5$] ≥ 4.15 ± 0.3[f] |
| | <1.2 0.3 | → $(CF_3)_2CFC_2F_4^-$ + F | [1.2 ± 0.5] | EA[$(CF_3)_2CFC_2F_4$] ≥ 4.15 ± 0.3[c] |
| | 0.7 ± 0.2 | e + neo-$C_5F_{12}$ → $(CF_3)_3CCF_2^-$ + F | (0.7 ± 0.3) | EA[$(CF_3)_3CCF_2$] ≥ 4.65 ± 0.3[f] |
| | <1.7 | → (d) | | E* ≤ 1 ± 0.3 |

[a]Heat of reaction determined from Eqn. (III-2) and the data of Table IV-4. Values in parentheses were obtained using the EA values listed in the last column of this table. Values in brackets were determined from Eqns. (III-3) and (III-4), using the EA values listed in the last column of this table and the value 3.7 ± 0.2 eV for C-C bond, 5.3 ± 0.2 (Table III-7) for primary and secondary and 4.6 ± 0.2 eV (Table IV-5) for tertiary C-F bond dissociation energies.

[b]Excess energy determined from Eqn. (III-3).

[c]Electron affinity determined from Eqns. (III-2) and (III-3) with E* ≥ 0 and the data in Table IV-4.

[d]Reactions denoted by (d) correspond to the second AO of double-peak anions and it was assumed that they lead to identical products as the reactions corresponding to the first AO. Only the excess energy for these reactions is given in the table.

[e]The EA value found for $C_3F_7$ from neo-$C_5F_{12}$ is higher than that for $C_3F_7$ from either i-$C_4F_{10}$ and i-$C_5F_{12}$. See text for discussion. $\Delta H_r$ was taken to be equal to AO.

[f]Electron affinity determined from Eqn. (III-4) using the dissociation energy deduced from the complementary anion production.

[g]Heat of reaction determined as in footnote a of this table and using for $\Delta H_f[(CF_3)_2CC_2F_5]$ the value -22.7 ± 0.1 eV found in Table IV-5.

the primary C-F bond dissociation energy (Table IV-5). The $F^-$ from c-$C_5F_{10}$ is observed at higher energies (3.4 eV) and there is an indication that its formation involves multiple fragmentation of the parent molecule accompanied by possible formation of double bonds in the neutral fragments. The relative cross section function of the $F^-$ from the cyclic structures [see Figure IV-5(b) (p. 104) for c-$C_5F_{10}$ and also Table IV-2 (p. 100) for c-$C_4F_8$] shows a multipeak structure. The many peaks in the small fragment anion $F^-$ can be understood from a multiple fragmentation of the parent molecule, since such fragmentation may have many possible combinations and thus various asymptotic limits.

The other fragment anions observed from the three aliphatic molecules of this chapter are also produced in a direct cleavage of a single C-C or C-F bond of the respective parent molecules. The only exception is the $C_3F_7^-$ from neo-$C_5F_{12}$ whose formation involves breakage of more than one bond and fluorine transfer from one fragment to the other. The anions $C_3F_7^-$, $C_4F_9^-$ and $C_5F_{11}^-$ from the same molecules show two resonance peaks in their negative ion intensity functions, except for $C_4F_9^-$ from neo-$C_5F_{12}$ which is single peaked. It was found not possible to attribute the second peak to a reaction different from that describing the first peak. And since the energy difference in the onsets for the two peaks is small ($\sim$ 1 eV) (and thus not permitting to attribute the double peak structure as due to electronic excitation of the fragments), it was assumed that in general the two peaks originate from two separate NISs which lead to

the same asymptotic limits. The second peak is then accompanied by excess energy of the order of ∿ 1 eV distributed among the fragments (see footnote d of Table IV-6, p. 112).

The electron affinity (EA) values of the radicals $C_3F_7$, $C_4F_9$ and $C_5F_{11}$, determined and listed in the last column of Table IV-6, are consistent with themselves and also with the values determined in the previous chapter for the case of the normal perfluoralkanes. The present findings confirm the previous findings that the EA of the fluorocarbon radicals increase with increasing size of these radicals. The EA value determined for $C_3F_7$ from neo-$C_5F_{12}$ is higher by ∿ 0.7 eV than that from either i-$C_4F_{10}$ or i-$C_5F_{12}$ (see also footnote e of Table IV-6). This discrepancy may be attributed to uncertainty in the determination of the EA of $C_3F_7$ from neo-$C_5F_{12}$ due to the fact that this radical is formed from this molecule not directly but rather through multiple fragmentation and molecular rearrangement.

B. Energy Position of NISs. Types and Relative Intensities of Parent and Fragment Negative Ions

All four molecules [i-$C_4F_{10}$, i-$C_5F_{12}$, neo-$C_5F_{12}$, and c-$C_5F_{10}$] of the present chapter were found to attach low-energy electrons nondissociatively and dissociatively. It was found in the previous chapter that the parent anion cross sections for the normal perfluoroalkanes peak at the same energy of ∿ 0.6 eV independently of the size of the molecule. The results on the above first three molecules suggest that not only the size but also the geometrical structure of the molecule leaves unaffected the energy position of the parent anion formation, as long as the structure does not change from noncyclic to

cyclic or the change in the structure does not involve the introduction of double or triple bonds. However, for cyclic and unsaturated perfluorocarbons with four or more carbon atoms the parent anion is always formed at 0.0 eV (see also Sauers et al., 1979) and is generally very strong (Christodoulides et al., 1979). It has to be pointed out here that the energy position of the observed long-lived parent anion is a measure of the vertical attachment energy which is usually not a good measure of the EA of the molecule. Thus for the normal perfluoroalkanes n-$C_4F_{10}$, n-$C_5F_{12}$, and n-$C_6F_{14}$, for which it was indicated (Chapter III) that the EA increases with increasing size of the molecule, it was suggested that the equilibrium distance for the parent negative ion increases when the molecule becomes larger, so that the vertical attachment energy remains the same for the three molecules. The fact that the parent anions for the cyclic perfluorocarbons (e.g., c-$C_4F_8$ and c-$C_5F_{10}$) peak at lower energies compared to the noncyclic structures may suggest that the EA values for the former are larger than those for the latter, but may be due also to smaller equilibrium distances for the parent negative ions of the cyclic molecules as compared to the noncyclic structures.

The results of the previous chapter showed that for normal perfluoroalkanes the dissociating NISs shift to lower energies with increasing size of the molecule, and this was satisfactorily rationalized. There is, however, no obvious correlation between the geometrical structure of the molecules studied in the previous and in this chapter and the energy position of the dissociative NISs. The NISs for i-$C_4F_{10}$, for example, are lower by $\sim$ 1 eV compared to

those of n-$C_4F_{10}$ (Table IV-1, p. 98), whereas the NISs for i-$C_5F_{12}$ and neo-$C_5F_{12}$ are generally at the same position as those for n-$C_5F_{12}$. The dissociating NISs of c-$C_5F_{10}$ lie at higher energies than those of the aliphatic perfluoroalkanes and this was attributed to the fact that fragment negative ion formation in c-$C_5F_{10}$ proceeds through multiple fragmentation which as requiring more energy raises the asymptotic limits and the positions of the NISs to higher energies.

Concerning the types of the fragment anions observed, we notice that the small anion $CF_3^-$ is hardly observed from i-$C_4F_{10}$, whereas the anions $CF_3^-$ and $C_2F_5^-$ have not been observed from i-$C_5F_{12}$ and neo-$C_5F_{12}$. The small $F^-$ ion, however, has been observed from all molecules i-$C_4F_{10}$, i-$C_5F_{12}$, neo-$C_5F_{12}$, and c-$C_5F_{10}$. The absence of small anions over large anions from the aliphatic fluorocarbons can be attributed to two reasons. The first reason is based on energetic grounds. Larger fragments have larger electron affinities and therefore lower asymptotic limits, which result in more energy available during the dissociation. The second, and probably more important reason, has to do with the localization of the extra electron in the molecule upon capture. The fluorocarbon molecules do not have any particular electrophilic site for the extra electron to be preferentially located (like e.g., the fluorosulphides—see Chapter V), the entire molecule being an electrophilic site. The extra electron charge is distributed more or less uniformly in the whole molecule, and thus the probability is greater for the electron to be found on a larger rather than on a smaller fragment. Also the large number

of fluorine atoms in the molecule enhances the chance for the electron to be found on a n-orbital of a fluorine atom, thus explaining the observance of $F^-$ from all the above molecules.

The most interesting finding from the study of the molecules of this and the previous chapter is probably that pertaining to the relative intensities of the parent versus fragment anions. Let us summarize here these findings very briefly: For n-$C_4F_{10}$ the predominant anion is the $F^-$, all other anions (including the parent anion) being by more than a factor of ten weaker. For i-$C_4F_{10}$ the strongest ion is the parent anion but the intensity of the fragment anions is $\sim$ 50 to 80% that of the parent anion. For n-$C_5F_{12}$ and i-$C_5F_{12}$ the predominant ion is again the parent anion, with the fragment anions having intensities by a factor of $\sim$ 3 to 15 lower. For neo-$C_5F_{12}$ the fragment anion $C_4F_9^-$ is by far the most abundant ion with the other anions (parent and fragment) being by a factor of $\sim$ 15 to 250 times less intense. Energetic considerations (associated with the position of the NIS and/or the asymptotic limits for dissociative attachment) cannot account for these differences in the relative intensities of the various anions from each molecule, since from the data summarized in Tables IV-1, IV-2, IV-5 and IV-6 (pp. 98. 100, 111 and 112) these energetics do not vary too much from one molecule to another. Also, the types of the anions observed from the various isomers of each molecule are the same. The key factor determining the dramatic differences in the relative intensities of the fragment anions as compared between themselves and to the parent anions must be sought elsewhere. We propose that what affects crucially the

probabilities by which the transient anion decays to the various channels, is the way as well as how fast the excess energy (comprised of the incident electron kinetic energy and the EA of the molecule) is distributed among the various degrees of freedom of the molecule. It seems that the geometrical structure of the molecule and its symmetry affect these factors more heavily than does the size of the molecule. Thus for the symmetric molecule neo-$C_5F_{12}$ the excess energy should be distributed very rapidly and almost entirely in the mode leading to fragmentation along any of the four coordinates $CF_3$-$C_4F_9$, thus explaining why $C_4F_9^-$ is by far the strongest anion. On the other hand, for i-$C_4F_{10}$ which has an analogous structure to neo-$C_5F_{12}$, but not so symmetric, the excess energy is distributed among the various degrees of freedom of the molecule in such a way that the probability for this energy to be concentrated along any particular coordinate leading to dissociation is almost as high as to remain equally shared by all degrees of freedom, thus explaining the observed relative negative ion intensities for this molecule. It is obvious that the pictures described above involve dynamic considerations and so represent extra difficulties to be encountered by any theoretical approach attempted, although such approach would be very interesting and is suggested.

# CHAPTER V

## FRAGMENTATION OF FLUOROETHERS AND FLUOROSULPHIDES UNDER LOW-ENERGY ($\leq$ 10 eV) ELECTRON IMPACT

### I. INTRODUCTION

In this chapter the results of a TOF mass spectrometric study on the attachment of low-energy ($\leq$ 10 eV) electrons to four fluoroethers ($CF_3OCF_3$, $CF_3OCF_2H$, $CF_2HOCF_2H$, and $CF_3OCH_3$) and two fluorosulphides ($CF_3SCF_3$ and $CF_3SCH_3$) are presented and discussed. Electron attachment to these fluoroethers and fluorosulphides is of basic and practical interest. This group of molecules provides a basis to study the effect of atomic substitution in the molecule on its electron attaching properties. Additionally, since these molecules attach electrons dissociatively, and thus their attachment rate constants are expected to be pressure independent, they provide a straightforward comparison of the results obtained by the TOFMS and electron swarm techniques. The magnitude and energy dependence of the attachment rate constants for $CF_3OCF_3$ and $CF_3SCF_3$ are such as to make them excellent gas dielectrics, and also good candidates for additives in mixtures for diffuse-discharge switches (Christophorou and Hunter, 1983).

None of the molecules described in this chapter has been studied previously.

# II. RESULTS

## A. Negative Ion Fragments

The present TOF mass spectrometric study has shown that low-energy electrons attach dissociatively to the fluoroether and fluorosulphide molecules investigated. No parent anions were observed in any of these molecules.

1. Fluoroethers. The relative cross sections as a function of $\varepsilon$ for all fragment anions observed for the four fluoroether molecules studied are shown in Figure V-1. Each curve represents the average of at least four sets of data. Each set of data was deconvoluted and the averages of the corresponding unfolded functions are shown in Figure V-2. The relative peak intensities, energy of the maximum ion intensity, full width at half maximum (FWHM), and the appearance onsets for all the anions are listed in Table V-1. It is evident from these results that the types, relative intensities and energy positions of the maxima of the various anions depend strongly on the number and relative positions of the F atoms in the molecules. The molecules having one or both of the methyl groups partially fluorinated are more fragile upon electron impact compared with the molecules for which all the atoms of the methyl group are of one kind (H or F). Five anions: ($CF_3O^-$, $CFO^-$, $CF_3^-$, $HF_2^-$, $F^-$) and four anions ($CF_3O^-$, $CFO^-$, $HF_2^-$ and $F^-$) have been observed, respectively, for $CF_3OCF_2H$ and $CF_2HOCF_2H$. The formation of $CFO^-$ and $HF_2^-$ requires multiple molecular fragmentation and the formation of $CF_3O^-/CF_2HOCF_2H$ also requires strong molecular rearrangement. For both molecules

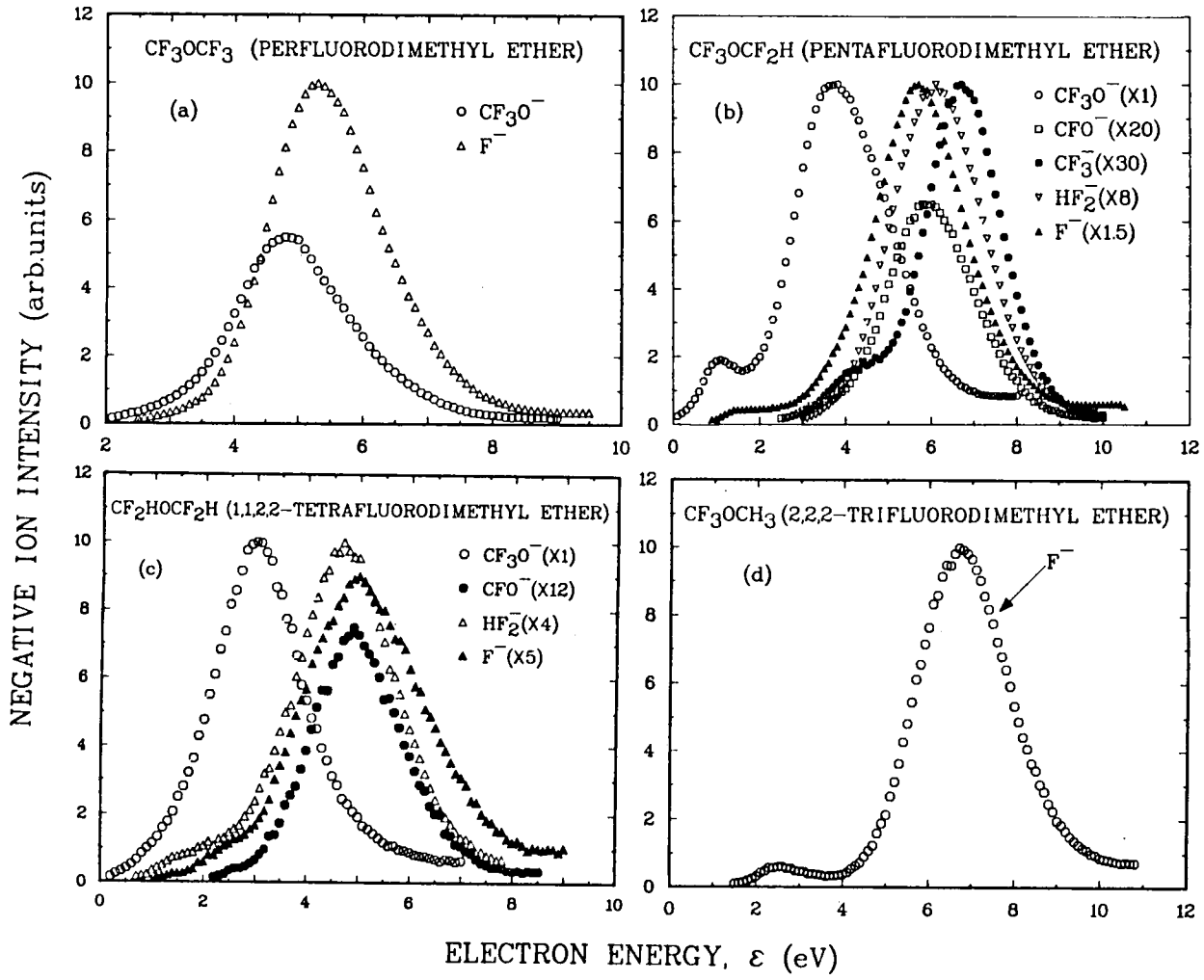


Figure V-1. Negative ion intensity as a function of ε (nonunfolded data) for (a) $CF_3OCF_3$, (b) $CF_3OCF_2H$, (c) $CF_2HOCF_2H$, (d) $CF_3OCH_3$.

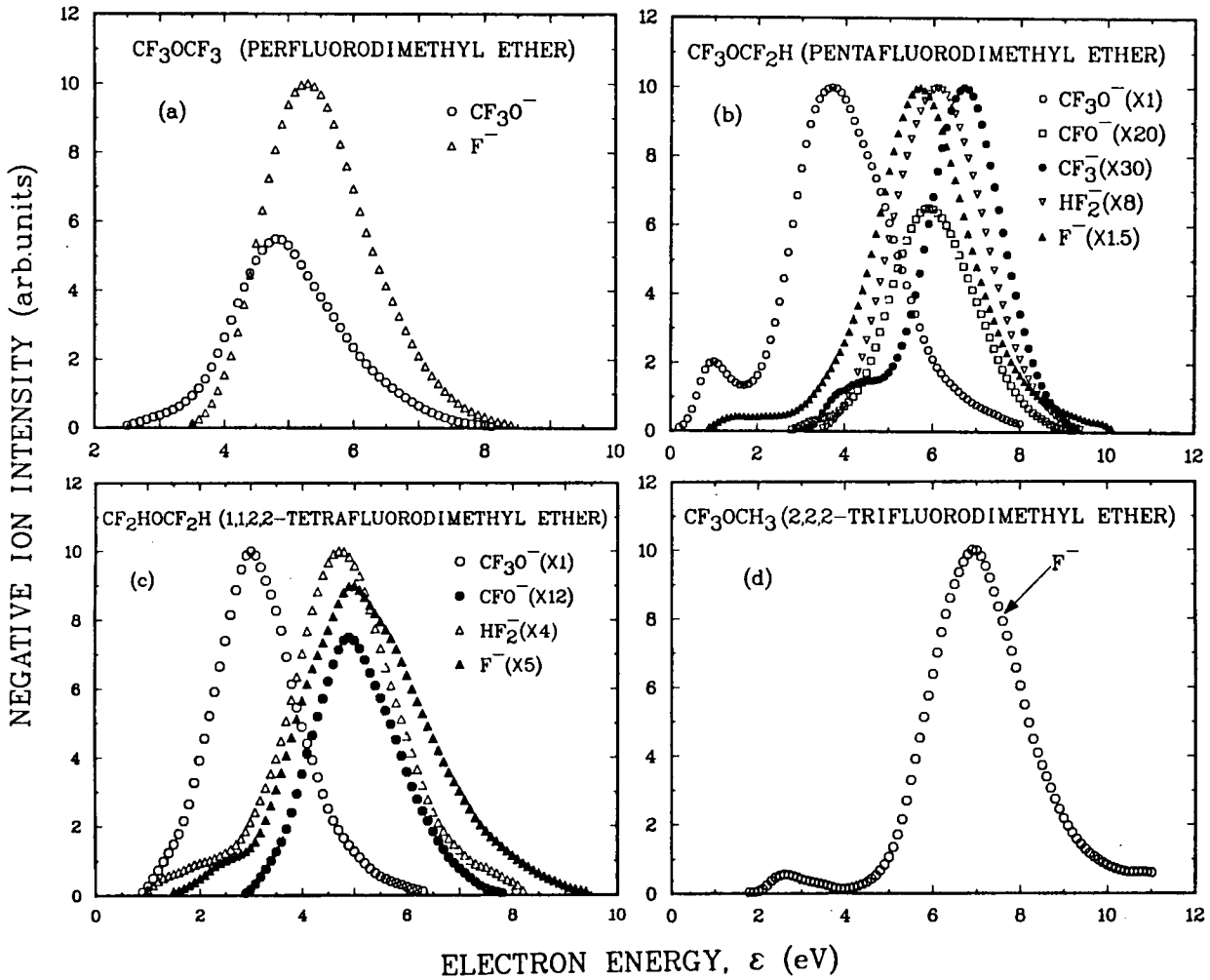


Figure V-2. Negative ion intensity as a function of ε (unfolded data) for (a) $CF_3OCF_3$, (b) $CF_3OCF_2H$, (c) $CF_2HOCF_2H$, (d) $CF_3OCH_3$.

Table V-1. Negative ions due to low-energy electron impact on $CF_3OCF_3$, $CF_3OCF_2H$, $CF_2HOCF_2H$, and $CF_3OCH_3$

| Molecule | Negative ion | Relative peak intensity | Energy of maximum ion intensity (eV)[b] | FWHM[a] (eV)[c] | Appearance onset (eV)[c] |
|---|---|---|---|---|---|
| $CF_3OCF_3$ | $CF_3O^-$ | 550 | 4.8 ± 0.05 | 1.85 | 2.5 ± 0.1 |
| | $F^-$ | 1000 | 5.3 ± 0.05 | 1.85 | 3.5 ± 0.2 |
| $CF_3OCF_2H$ | $CF_3O^-$ | 200 | 1.0 ± 0.2 | 1.0 | 0.2 ± 0.1 |
| | | 1000 | 3.7 ± 0.1 | 2.5 | 2.0 ± 0.3 |
| | $CFO^-$ | | d | | 2.8 ± 0.1 |
| | | 35 | 5.9 ± 0.05 | 2.3 | 4.0 ± 0.2 |
| | $CF_3^-$ | | d | | 3.1 ± 0.1 |
| | | 35 | 6.7 ± 0.05 | 2.0 | 4.8 ± 0.1 |
| | $HF_2^-$ | 125 | 6.1 ± 0.05 | 2.4 | 3.7 ± 0.2 |
| | $F^-$ | | d | | 1.0 ± 0.1 |
| | | 650 | 5.7 ± 0.05 | 2.35 | 2.8 ± 0.2 |
| $CF_2HOCF_2H$ | $CF_3O^-$ | 1000 | 3.0 ± 0.05 | 1.8 | 0.9 ± 0.1 |
| | $CFO^-$ | 60 | 4.9 ± 0.05 | 1.9 | 2.9 ± 0.1 |
| | $HF_2^-$ | | d | | 1.0 ± 0.2 |
| | | 250 | 4.7 ± 0.05 | 2.25 | 2.6 ± 0.3 |
| | $F^-$ | | d | | 1.7 ± 0.2 |
| | | 200 | 5.0 ± 0.05 | 2.75 | 2.8 ± 0.2 |
| $CF_3OCH_3$ | $F^-$ | 50 | 2.5 ± 0.1 | 1.0 | 1.8 ± 0.1 |
| | | 1000 | 6.7 ± 0.1 | 2.5 | 4.7 ± 0.3 |

[a]Full width at half maximum of the respective ion yield as a function of electron energy.

[b]Energy scale calibration determined using for the $SF_5^-/SF_6$ resonance the value of 0.37 eV. The ± refers to the standard deviation from the average.

[c]Values listed are from the unfolded data.

[d]Unresolved peak.

the predominant ion is $CF_3O^-$, with the other anions having an intensity up to thirty times less than that of $CF_3O^-$. On the other hand, for $CF_3OCF_3$ only two ($CF_3O^-$ and $F^-$) and for $CF_3OCH_3$ only one ($F^-$) ion have been detected. The relative intensity of $F^-$ to $CF_3O^-$ from $CF_3OCF_3$ is 2:1. A possible explanation for the absence (or extremely weak intensity) of $CF_3O^-$ from $CF_3OCH_3$ is given in the next section.

2. Fluorosulphides. The relative cross sections as a function of $\varepsilon$ for the two fluorosulphides are shown in Figure V-3, whereas the peak intensities, resonance maxima, FWHM and onsets for each negative ion are summarized in Table V-2. The types of the anions observed are analogous to the fluoroether counterparts: $CF_3S^-$ and $F^-$ from $CF_3SCF_3$ and $CF_3S^-$ from $CF_3SCH_3$. There is, however, a dramatic difference in the relative intensities of these ions and their energy positions as compared to those for the fluoroether counterparts. For the fluorosulphides the predominant ion is the $CF_3S^-$ peaking at 0.6 eV for $CF_3SCF_3$ and at thermal energies for $CF_3SCH_3$. For $CF_3SCF_3$ the $F^-$ ion is 300 times less intense than $CF_3S^-$, whereas for $CF_3SCH_3$, $F^-$ was not observed.

## B. Electron Attachment Rate Constants and Absolute Attachment Cross Sections

The results of the TOF mass spectrometric study on the molecules of this chapter can be compared with those obtained by the swarm technique (Spyrou et al., 1983). The electron attachment rate constants, $k_a$, measured by the swarm technique show that

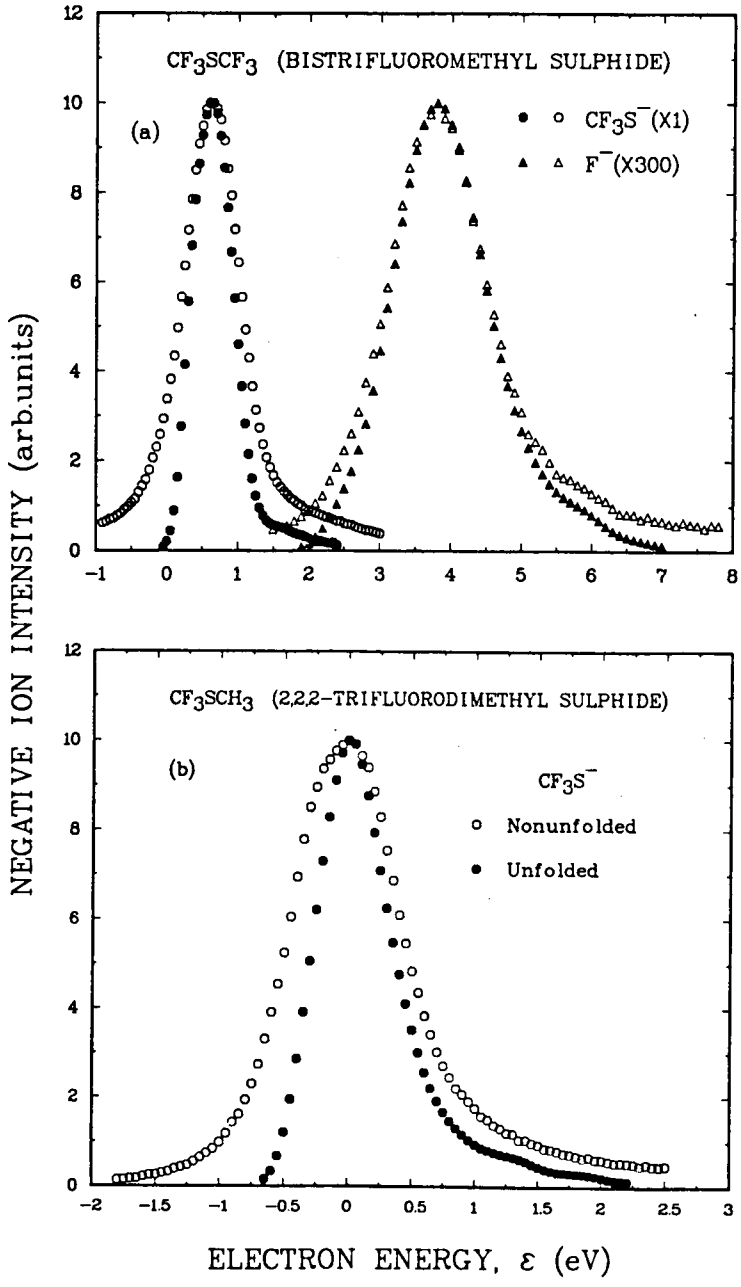


Figure V-3. Negative ion intensity as a function of $\varepsilon$ (open symbols: nonunfolded, solid symbols: unfolded data) for (a) $CF_3SCF_3$, (b) $CF_3SCH_3$.

Table V-2. Negative ions due to low-energy electron impact on $CF_3SCF_3$ and $CF_3SCH_3$

| Molecule | Negative ion | Relative peak intensity | Energy of maximum ion intensity (eV)[b] | FWHM[a] (eV)[c] | Appearance onset (eV)[c] |
|---|---|---|---|---|---|
| $CF_3SCF_3$ | $CF_3S^-$ | 1000 | 0.6 ± 0.05 | 0.7 | ∿0 |
| | $F^-$ | 3 | 3.8 ± 0.1 | 1.5 | 1.9 ± 0.1 |
| $CF_3SCH_3$ | $CF_3S^-$ | 1000 | ∿0 | 0.7 | |

[a]Full width at half maximum of the respective ion yield as a function of electron energy.

[b]Energy scale calibration determined using for the $SF_5^-/SF_6$ resonance the value of 0.37 eV. The ± refers to the standard deviation from the average.

[c]Values listed are from the unfolded data.

fluorosulphides attach lower energy electrons than do the fluoroethers, a finding consistent with the beam data. From the measured $k_a$, the total electron attachment cross sections, $\sigma_a$, were determined using the swarm unfolding technique and the swarm-beam technique analysis. In Figure V-4 are compared the $\sigma_a$ obtained by the two techniques for the case of $CF_3OCF_3$. In the swarm-beam analysis the shape for the $\sigma_a(\varepsilon)$ function was obtained by adding the relative cross sections of the $F^-$ and $CF_3O^-$ anions, and the magnitude and the energy scale calibration shift were calculated as described in Chapter II. The agreement between the cross sections as obtained by the two techniques is very good as far as the onset, FWHM and the peak energy position is concerned, but the agreement of the absolute magnitude of the two cross sections is not as good. The 20% discrepancy in the magnitude may be attributed to the fact that the swarm-unfolded $\sigma_a(\varepsilon)$ function has a higher edge tail which in turn is due to the fact that the unfolding analysis is trying to determine $\sigma_a$ in a region far beyond the region where the experimental $k_a$ lie (0-4.5 eV). This comparison shows the capability as well as the possible limitations of the swarm-unfolding technique. Similar analyses were made for the other fluoroether and fluorosulphide molecules investigated and they showed good agreement between the beam and the swarm data.

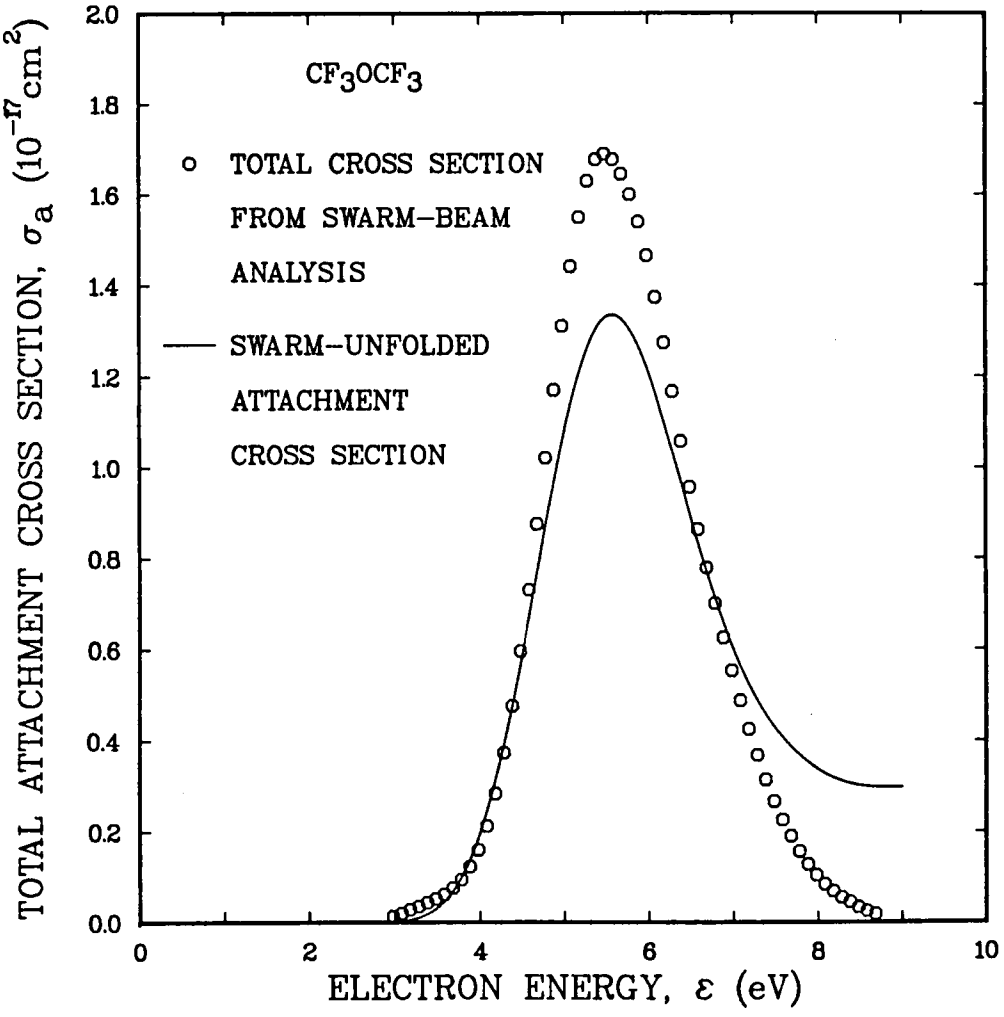


Figure V-4. Total electron attachment cross section for $CF_3OCF_3$ obtained by the swarm-beam (o) and the swarm unfolding (—) technique.

# III. DISCUSSION

## A. Energetics of Dissociative Electron Attachment Processes

The main difficulty encountered in considering the energetics of the fragmentation processes for the fluoroether and fluorosulphide molecules of this chapter was the lack of sufficient and accurate thermochemical data (e.g., heats of formation, bond dissociation energies and electron affinities of molecules and radicals) on the fluoroether and fluorosulphide molecules studied. The available literature thermochemical information necessary for the interpretation of the results of the present work is summarized in Table V-3. In the same table are also shown some values of the heats of formation of molecules and radicals and bond dissociation energies not available directly in the literature, but they were derived by us from the listed literature thermochemical information. The method of their derivation is explained in the footnotes of the table.

We used Eqns. (III-2) to (III-4) and the data of Table V-3 to identify possible dissociative attachment processes leading to the formation of all observed negative ions. The proposed fragmentation processes along with their estimated heats of reaction are summarized in Tables V-4 and V-5.

Some of the anions observed ($CFO^-$ and $HF_2^-$) can obviously be produced only in multiple-fragment reactions accompanied by intramolecular atomic rearrangement within the transient anion. In many cases, even the formation of the anions $F^-$ and $CF_3^-$, which can be

Table V-3. Thermochemical data used in Chapter V

| Quantity | Value (in eV) and reference | Quantity | Value (in eV) and reference |
|---|---|---|---|
| $\Delta H_f(F)$ | 0.82(a) | $\Delta H_f(COF_2)$ | -6.62(b) |
| $\Delta H_f(H)$ | 2.26(b) | $\Delta H_f(CF_3)$ | -4.94(a) |
| $\Delta H_f(O)$ | 2.58(b) | $\Delta H_f(CHF_3)$ | -7.22(b) |
| $\Delta H_f(CF)$ | 2.65(b) | $\Delta H_f(CH_2F_2)$ | -4.63(a) |
| $\Delta H_f(CO)$ | -1.15(b) | $\Delta H_f(CF_4)$ | -9.58(a) |
| $\Delta H_f(FO)$ | 1.13 ± 0.4(b) | $\Delta H_f(CF_3O)$ | [-6.6](d) |
| $\Delta H_f(HF)$ | -2.82(b) | $D(F_3C-O)$ | [3.9 ± 0.4](e) |
| $\Delta H_f(HF_2)$ | [-2](c) | $\Delta H_f(CF_3OCF_3)$ | [-15.4 ± 0.4](f) |
| $\Delta H_f(CFH)$ | 1.3 ± 0.3(b) | $\Delta H_f(CF_3OCF_2H)$ | [-13.5 ± 0.4](g) |
| $\Delta H_f(CFO)$ | -1.78 ± 0.65(b) | $\Delta H_f(CF_2HOCF_2H)$ | [-11.3 ± 0.4](h) |
| $\Delta H_f(HOF)$ | -1.02(b) | $\Delta H_f(CF_3OCH_3)$ | [- 9.0 ± 0.4](i) |
| $\Delta H_f(CH_3)$ | 1.51(b) | EA(F) | 3.45(j) |
| $\Delta H_f(CHF_2)$ | -3.04(a) | $EA(CF_3)$ | 2.1(k) |
| $\Delta H_f(CH_2F)$ | -0.3(a) | $EA(HF_2)$ | 3.0(k) |
| $\Delta H_f(CHFO)$ | -3.9(b) | EA(CFO) | 2.7, 3.3(l) |
| | | $D(F_3C-C)$ | 3.7 ± 0.2(m) |
| | | $D(F-CF_3)$ | 5.3 ± 0.2(m) |

[a]J. L. Franklin, J. G. Dillard, H. M. Rosenstock, J. T. Herron, K. Draxl, and F. H. Field, NSRDS-NBS 26 (1969).

[b]JANAF Thermochemical Table, edited by D. R. Stull (Dow Chemical Company, Midland, Michigan, 1969).

[c]This and all other values enclosed in brackets have been estimated using the data of this table as described in the footnotes of this table. The $\Delta H_f(HF_2)$, for example, was found using $HF_2 \rightarrow HF+F$ and Eqn. (III-2) and assuming that $\Delta H_r = D(HF-F) \simeq 0$ eV, since $HF_2$ is an unstable system, being detected only as a negative ion (P. N. Noble and R. N. Kortzeborn, J. Chem. Phys. 52, 5375 (1970).

[d]Obtained using $CF_3OF \rightarrow CF_3O + F$ and Eqn. (III-2), with $\Delta H_r = D(CF_3O-F) = 1.9$ eV [J. Czarnowski, E. Castellano, and H. J. Schumacher, Chem. Commun. 1255, 1968] and $\Delta H_f(CF_3OF) = -7.7$ eV [R. D. W. Kemmitt and D. W. Sharp, Adv. Fluorine Chem. 4, 216 (1965)].

[e]Obtained using $CF_3OF \rightarrow CF_3 + OF$ and Eqn. (III-2) with $D(CF_3-OF) = \Delta H_r$.

[f]Obtained using $CF_3OCF_3 \rightarrow CF_3 + OCF_3$ and Eqn. (III-2) with $\Delta H_r(F_3C-O) = 3.9 \pm 0.4$ eV.

[g]Obtained using $CF_3OCF_2H \rightarrow CF_2H + OCF_3$ and Eqn. (III-2) with $\Delta H_r(F_2HC-O) = 3.9 \pm 0.4$ eV.

[h]Obtained using $CF_2HOCF_2H \rightarrow CF_2H + O + CF_2H$ and Eqn. (III-2) with $\Delta H_r = 2D(F_2HC-O) = 7.8 \pm 0.4$ eV.

[i]Obtained using $CF_3OCH_3 \rightarrow CH_3 + OCF_3$ and Eqn. (III-2) with $\Delta H_r = D(H_3C-O) = 3.9 \pm 0.4$ eV).

[j]R. S. Berry and C. W. Reimann, J. Chem. Phys. 38, 1540 (1963).

[k]H. M. Rosenstock, K. Draxl, B. W. Steiner, and J. T. Herron, J. Phys. Chem. Ref. Data 6, Suppl. No. 1 (1977).

[l]K. A. G. MacNeil and J. C. J. Thynne, Int. J. Mass Spectrom. 3, 35 (1969) and P. W. Harland and J. C. Thynne, J. Phys. Chem. 74, 52 (1970), respectively.

[m]Table III-7.

Table V-4. Possible dissociative attachment processes leading to the formation of various anions from $CF_3OCF_3$, $CF_3OCF_2H$, $CF_2HOCF_2H$ and $CF_3OCH_3$

| Ion | AO (eV) | Reaction | $\Delta H_r$ [a] (eV) | Thermochemical data deduced (eV) |
|---|---|---|---|---|
| $CF_3O^-$ | 2.5 ± 0.1 | $e + CF_3OCF_3 \rightarrow CF_3O^- + CF_3$ | (0.2 ± 0.5) | $E^*$ [b] = 2.3 ± 0.6 |
| | 0.2 ± 0.1 | $e + CF_3OCF_2H \rightarrow CF_3O^- + CF_2H$ | (0.2 ± 0.5) | $EA(CF_3O) \geq 3.7 \pm 0.5$ [c] (1.35, ≥ 1.9, 3.86) |
| | 2.0 ± 0.3 | $\rightarrow CF_3O^- + (CF_2H)$ [d] | (0.2 ± 0.5) | $E^* = 1.8 \pm 0.8$ [d] |
| | 0.9 ± 0.1 | $e + CF_2HOCF_2H \rightarrow CF_3O^- + CH_2F$ | (0.9 ± 0.4) | $EA(CF_3O) \geq 3.5 \pm 0.5$ [e] |
| $F^-$ | 3.5 ± 0.2 | $e + CF_3OCF_3 \rightarrow F^- + CF_3 + OCF_2$ | 1.25 ± 0.4 | $E^* = 2.25 \pm 0.6$ |
| | | $\rightarrow F^- + CF_3OCF_2$ | [1.85 ± 0.1] | $E^* = 1.65 \pm 0.3$ |
| | 1.0 ± 0.1 | $e + CF_3OCF_2H \rightarrow F^- + COF_2 + CF_2H$ | 1.2 ± 0.4 | |
| | 2.8 ± 0.2 | $\rightarrow F^- + CF_3OCFH$ | [1.85 ± 0.1] | $E^* = 0.95 \pm 0.3$ |
| | 1.7 ± 0.2 | $e + CF_2HOCF_2H \rightarrow F^- + CFHO + CF_2H$ | 1.7 ± 0.4 | |
| | | $\rightarrow F^- + CFHOCF_2H$ | [1.85 ± 0.1] | |
| | 2.8 ± 0.2 | $\rightarrow F^- + (CFHOCF_2H)$ [d] | | $E^* = 0.95 \pm 0.3$ |
| | 1.8 ± 0.1 | $e + CF_3OCH_3 \rightarrow F^- + CH_3 + OCF_2$ | 1.25 ± 0.4 | |
| | | $\rightarrow F^- + CF_2OCH_3$ | [1.85 ± 0.1] | |
| | 3.7 ± 0.3 | $\rightarrow F^- + (CF_2OCH_3)$ [d] | | $E^* = 2.85 \pm 0.4$ |
| $CFO^-$ | 2.8 ± 0.1 | $e + CF_3OCF_2H \rightarrow CFO^- + CF_3 + HF$ | 0.95 ± 1 | $E^* = 1.85 \pm 1$ |
| | | $\rightarrow CFO^- + CF_4 + H$ | 1.4 ± 1 | $E^* = 1.4 \pm 1$ |
| | | $\rightarrow CFO^- + CHF_3 + F$ | 2.3 ± 1 | $E^* = 0.4 \pm 1$ |
| | 4.0 ± 0.2 | $\rightarrow CFO^- + (CHF_3 - F)$ [d] | | $E^* = 1.7 \pm 1$ |
| | 2.9 | $e + CF_2HOCF_2H \rightarrow CFO^- + CHF_2 + HF$ | 0.7 ± 1 | $E^* = 2.2 \pm 1$ |
| | | $\rightarrow CFO^- + CHF_3 + H$ | 1.6 ± 1 | $E^* = 1.3 \pm 1$ |
| | | $\rightarrow CFO^- + CH_2F_2 + F$ | 2.7 ± 1 | $E^* = 0.2 \pm 1$ |
| $HF_2^-$ | 3.7 ± 0.2 | $e + CF_3OCF_2H \rightarrow HF_2^- + CO + CF_3$ | 2.4 ± 0.4 | $E^* = 1.3 \pm 0.6$ |
| | 1.0 ± 0.2 | $e + CF_2HOCF_2H \rightarrow HF_2^- + ?$ | | |
| | 2.6 ± 0.3 | $\rightarrow HF_2^- + CO + CF_2H$ | 2.1 ± 0.4 | |
| $CF_3^-$ | 3.1 ± 0.1 | $e + CF_3OCF_2H \rightarrow CF_3^- + CF_2HO$ | [1.8 ± 0.4] | $E^* = 1.3 \pm 0.5$ |
| | | $CF_3^- + CFO + HF$ | 1.85 ± 1 | $E^* = 1.25 \pm 1.1$ |
| | 4.8 ± 0.1 | $\rightarrow CF_3^- + (CF_2HO)$ [d] | | $E^* = 3$ |

[a] Heat of reaction determined using Eqn. (III-2) and the data of Table V-3. Values in parentheses were obtained using the EA values listed in the last column of this table. Values in brackets were found from Eqns. (III-3) and (III-4) and the data in Table V-3.

[b] Excess energy determined from Eqn. (III-3).

[c] Electron affinity determined from Eqn. (III-4) using $D(F_3CO-CF_2H) = 3.9 \pm 0.4$ eV (Table V-3). It was assumed that $E^* \geq 0$ eV. The first two numbers in parentheses are values found, respectively, by F. M. Page and G. C. Goode, Negative Ions and the Magnetron, Wiley Interscience, New York, 1969, and J. C. J. Thynne and K. A. G. MacNeil, Int. J. Mass Spectrom. Ion Phys. 5, 95 (1970). The third number is the result of MNDO calculations by M. J. S. Dewar and H. S. Rzepa, J. Am. Chem. Soc. 100, 784 (1978).

[d] Fragmentation of these radicals additional to those listed in this table and described in the corresponding proceeding reactions would lead to a reaction whose $\Delta H_r$ is much higher than the AO under consideration (see also text for discussion). The E* values listed refer to the proceeding reaction with $\Delta H_r$ closest to the AO under consideration.

[e] Electron affinity determined from Eqns. (III-2) and (III-3) using the data in Table V-3 and assuming that $E^* \geq 0$ eV.

Table V-5. Possible dissociative attachment processes leading to the formation of $CF_3S^-$ and $F^-$ from $CF_3SCF_3$, and $F^-$ from $CF_3SCH_3$

| Ion | AO (eV) | Reaction | $\Delta H_r$ (eV) | Thermochemical data deduced (eV) |
|---|---|---|---|---|
| $CF_3S^-$ | 0 | $e + CF_3SCF_3 \rightarrow CF_3S^- + CF_3$ | a | $EA(CF_3S) \geq 3.2^b$ $(1.8)^c$ |
| | 0 | $e + CF_3SCH_3 \rightarrow CF_3S^- + CH_3$ | a | $EA(CF_3S) \geq 3.2^b$ |
| $F^-$ | 1.9 | $e + CF_3SCF_3 \rightarrow F^- + CF_2SCF_3$ | $1.85 \pm 0.1^d$ | |

[a]A value $\leq 0$ e.g., equal or less than the corresponding AO can be assigned to these reactions.

[b]Electron affinity determined from Eqn. (III-4) and assuming that the dissociation energy $D(CF_3S\text{-}CF_3)$ is equal to $D(CH_3S\text{-}CH_3 = 3.17$ eV (T. L. Cottrell, The Strengths of Chemical Bonds, Butterworth Scientific Publications, London, 1958, 2nd ed.) and $E^* \geq 0$ eV.

[c]Value found by F. M. Page and G. C. Goode, Negative Ions and the Magnetron, Wiley Interscience, New York, 1969.

[d]Heat of reaction determined from Eqn. (III-4) using $D(F\text{-}CF_2SCF_3) = 5.3 \pm 0$ eV. (Table III-8) and EA(F) = 3.45 eV (Table V-3), and assuming $E^* \geq 0$ eV.

produced via two-fragment reactions, was found necessary to be attributed to multiple-fragment reactions. In all cases only reactions with $\Delta H_r$ lying below the corresponding AO of the negative ion have been listed in Table V-4. A comparison of the respective $\Delta H_r$ and AO [Eqn. (III-3)] shows that most of the processes describing the formation of the anions from the fluoroethers are characterized by considerable excess energy, being listed in the last column of Table V-4. The energetics, as described in Table V-4, are useful for understanding the NISs of the four fluoroether molecules studied. The energy dependencies of the relative cross sections of the various anions produced from these molecules (Figures V-1 and V-2, pp. 121 and 122) suggest that there may be two main NISs for each molecule: a low-energy lying and a high-energy lying one. For the symmetric molecule $CF_3OCF_3$ (symmetry $C_{2v}$) the two states are degenerate, while for the asymmetric molecule $CF_3OCF_2H$ there is an indication for a third low-energy lying NIS. The first NIS leads mostly to the production of $CF_3O^-$ (this anion was not observed for $CF_3OCH_3$) and its position shifts to higher energies with increasing F substitution. A similar observation can be made for the two fluorosulphides studied.

Figure V-5 summarizes the energy dependencies of the relative cross section for $CF_3O^-$ and $CF_3S^-$ produced, respectively, from the fluoroether and fluorosulphide molecules of this study. Whenever these two [and other anions (like $F^-$ and possibly $CFO^-$)], have as precursor the low-energy NIS are formed with no excess energy. On the other hand, formation of anions associated with the high-energy NIS is accompanied by excess energy.

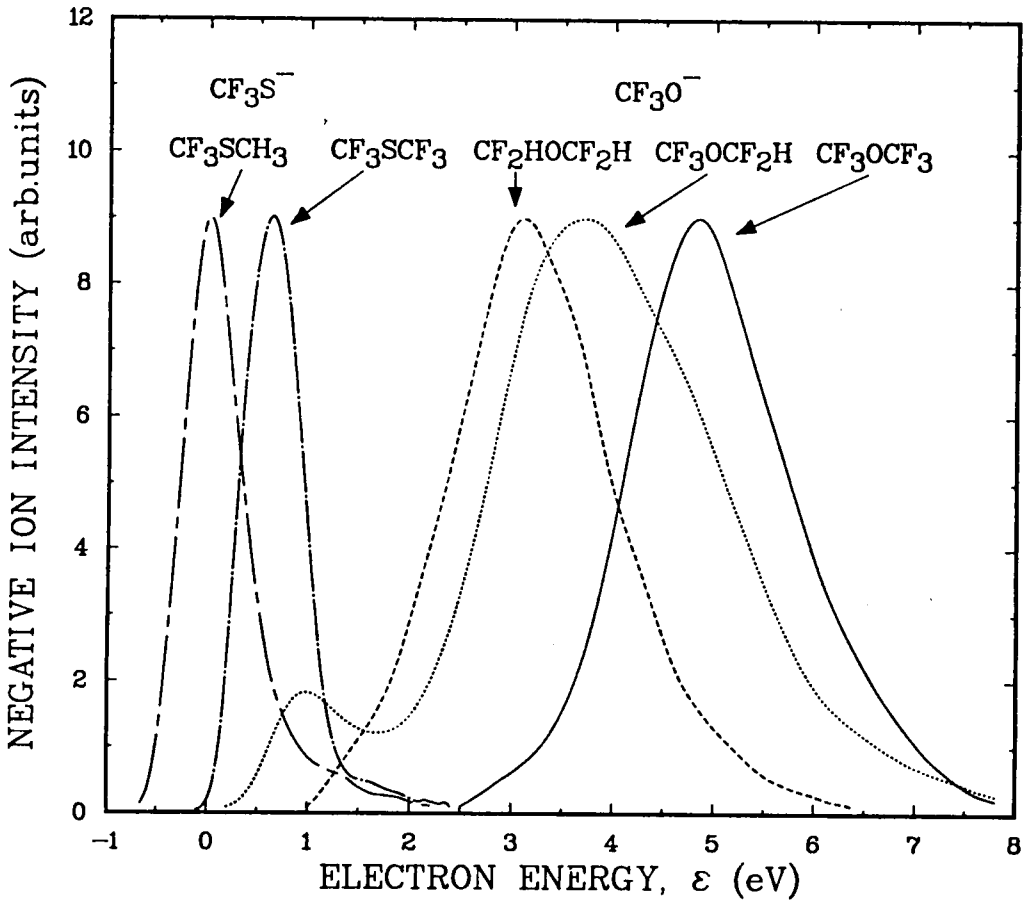


Figure V-5. Negative ion intensity as a function of ε for $CF_3O^-$ from $CF_3OCF_3$, $CF_3OCF_2H$, $CF_2HOCF_2H$, and $CF_3S^-$ from $CF_3SCF_3$, $CF_3SCH_3$.

It is seen from Table V-4 that we were unable to identify specific reactions responsible for the production of some anions at certain energies. This was the case for anions which exhibit two maxima in their relative cross sections. We may consider these maxima as originating from two separate NISs which, however, converge to the same asymptotic limit. This will explain the formation of $CF_3O^-$, $CFO^-$ and $CF_3^-$ from $CF_3OCF_2H$, and $F^-$ from $CF_2HOCF_2H$ and $CF_3OCH_3$ at their high-energy maxima (see footnote d of Table V-4), but it leaves unanswered the problem of the low-energy peak of $HF_2^-/CF_2HOCF_2H$.

In addition to the determination of the E* of the various reactions which are listed in Tables V-4 and V-5, we were able to estimate the EA of the radicals $CF_3O$ and $CF_3S$ listed in the last column of these tables. It is not unreasonable for these EA to be high (>3 eV). These values as derived from the various molecules show good consistency between themselves and also good agreement with a MNDO calculated EA value of $CF_3O$. Support for the high EA values of the radicals $CF_3O$ and $CF_3S$ comes also from the observation that $CH_3O$ and $CH_3S$ were found by photon impact techniques to have EA equal, respectively, to 1.59 and 1.86 eV (Christodoulides et al., 1983), and furthermore H to F substitution will increase the EA value even more [e.g., EA($CH_3$) = 0.08 eV, EA($CF_3$) = 2.0 eV and EA(CH) = 1.24 eV, EA(CF) > 3.2 eV; Christodoulides et al., 1983].

B. Results of CNDO/2 Calculations

In addition to the energetic considerations described in Section IIIA of this chapter, as a second step to relationalize the

findings of this study concerning the types, relative intensities and energy positions of the various anions observed, we have performed CNDO/2 molecular orbital calculations (Pople and Beveridge, 1970). A general point regarding the application of molecular orbital theory for the present case has to be made. As it has been already pointed out (Section II) all molecules of the present study attach electrons dissociatively. The dissociative attachment processes are known (see Section IIB in Chapter I) to take place in two steps: a very fast ($10^{-16}$ s) initial step where the electron is captured by the neutral molecule to form a transient negative ion in a vertical transition, and a later step where the transient anion either loses the electron by autodetachment or it dissociates moving along a dissociative potential energy curve (surface). It is expected that the results of the present CNDO/2 calculations can be used in conjunction with only the first step, since in these calculations no account was taken of any possible changes in the geometry of the neutral molecule upon formation of the transient negative ion, and obviously CNDO calculations do not address the question of the possible decay channels of the transient NIS.

Despite these limitations, CNDO calculations can provide information on: (i) energies of the virtual (empty) molecular orbitals, and (ii) charge distribution in the neutral molecules and negative ions. We tried to find any possible correlation between the experimental results on the position of the NISs and the CNDO virtual orbital energies. Using Koopmans' theorem (Koopmans, 1933) we assumed the resonance energies to be given by the energies of the

first virtual orbitals. The CNDO calculations did show that the orbital energies of the fluorosulphide molecules are much lower than those of their fluoroether counterparts, a fact consistent with the experimental findings. The calculations, however, were poor in showing any correlation between the virtual orbital energies and the observed NISs for each group of molecules. This may be attributed to inappropriate assumptions in using Koopmans' theorem, limitations of the CNDO method, as well as to other factors neglected in the calculations, such as reorganization and correlation energies. The CNDO calculations were more promising when used to find charge density distributions. The charge density distributions for each neutral molecule and for its corresponding negative ion were calculated and the differences between these distributions were used to find how the extra electron charge is distributed in the molecule. These calculations showed again a distinct difference between the fluoroether and fluorosulphide molecules in the way the charge of the attached electron is distributed in the molecule. In the fluorosulphide molecules $\sim$ 50% of the extra electron charge is localized on the S atom. This suggests that the $CF_3S^-$ formation from either $CF_3SCF_3$ or $CF_3SCH_3$ is associated preferentially with the S atom rather than the F or C atoms. This may explain why for $CF_3SCF_3$ the $CF_3S^-$ ion is $\sim$ 300 times stronger than $F^-$, and why for $CF_3SCH_3$ the $F^-$ was not observed or if formed was too weak to be detected. On the other hand, for the fluoroether molecules no preferred localization of the extra electron to any particular atom was found. For these molecules the

electron attachment seems to be associated with the molecule as a whole. Support for this comes from the fact that for the two molecules $CF_3OCF_2H$ and $CF_2HOCF_2H$ negative ions have been observed whose formation implies considerable molecular fragmentation and rearrangement. For the molecules $CF_3OCF_3$ and $CF_3OCH_3$ (H and F atoms are not found on the same C atom), no indication for such a rearrangement was observed. For these molecules the dissociation is direct and the formation of $F^-$ is favored over the formation of $CF_3O^-$ for the reason that the electron once captured has statistically increased probability to be found on any F atom. This is consistent with the observation that for $CF_3OCF_3$ the $F^-$ is twice as strong as $CF_3O^-$, while for $CF_3OCH_3$, $CF_3O^-$ is so weak (or not formed at all) to be detected.

The results of the above calculations, although when combined with the discussion in the previous section provide some qualitative rationalization of the experimental results, still are inadequate for an exact interpretation.

## IV. CONCLUSION

The results of the present study in combination with the molecular orbital calculations have revealed some important aspects of electron attachment to polyatomic molecules. They showed that the types, relative intensities and energy positions of the negative ions formed from a molecule under low-energy electron impact are very sensitive to the substitution of even one atom by another of a different kind in the molecule. The substituent atom apart from changing the energy positions of the NISs of the molecule, may introduce preferred

electrophilic sites in the molecule, thus affecting the way the molecule attaches the electron and dissociates. Electron attachment to even relatively small polyatomic molecules, as those of the present study, may be accompanied by extensive molecular fragmentation and rearrangement.

# CHAPTER VI

# EFFECT OF TEMPERATURE ON ELECTRON ATTACHMENT TO THE FREON $CClF_3$

## I. INTRODUCTION

In this chapter the results of a swarm study on the temperature dependence of electron attachment to the freon $CClF_3$ are first presented and discussed. For comparison are also presented the results of a room temperature TOF mass spectrometric study of the same molecule. In this section a brief survey of the dissociative electron attachment processes to "hot" molecules is given. In Section II the present results are given and in Section III a discussion of the results is given.

The study of the effects of temperature on electron attachment to molecules is of intrinsic as well as of practical interest. Vibrational and/or rotational excitation of the molecule affect the magnitude and the energy dependence of the cross section for negative ion production. Therefore, accurate determination of thermochemical data (see Chapters III to V) which use appearance onsets for dissociative electron attachment processes are expected to be dependent on the internal excitation of the molecule. A knowledge of the temperature dependence of electron attachment to molecules may be also helpful in the determination of various parameters relating to the neutral and the negative ion states of the molecule. Similar knowledge is valuable to many applied areas which employ temperatures higher than ambient (e.g., combustion, flames, circuit breakers, etc.). The effects

of temperature on electron attachment processes have been investigated (see Christophorou, 1980, and Christophorou et al., 1983 for a review) by both the electron beam (Hickam and Berg, 1958; Fite and Brackmann, 1963; Fite et al., 1965; Mahan and Young, 1966; Henderson et al., 1969; Spence and Schulz, 1969, 1973; Chantry, 1969; Chen and Chantry, 1972, 1979; Allan and Wong, 1978, 1981) and the electron swarm (Compton et al., 1966; Wentworth et al., 1967, 1969; Chaney and Christophorou, 1969; Fehsenfeld, 1970; Warman and Sauer, 1971; Shimamori and Fessenden, 1979; McCorkle et al., 1982; Hunter et al., 1983) methods; the former extended to T = 3000 K and the latter have been restricted to $T \lesssim 500$ K.

Of all these works, here we refer only to the early experimental results of Fite et al. (1963) on the temperature dependence of dissociative attachment to $O_2$ producing $O^-$. The theoretical work developed for the interpretation of these results will be helpful in the understanding of the results of the present work as well. It was found that for $O^-/O_2$ as T increases the threshold energy decreases (it shifts from $\sim$ 4 eV at $\sim$ 300 K to $\sim$ 1.2 eV at 1970 K), the energy position of the resonance maximum decreases, while the magnitude of the cross section and the resonance width increase. To explain these data O'Malley (1967) assumed that the direct effect of T on $O_2$ is to produce a Maxwellian distribution of vibrational (v) and rotational (j) states. The effective cross section $\sigma_{da}(T, \varepsilon)$ for dissociative attachment, then, is the Boltzmann average of the cross section $\sigma_{da}^{v,j}(\varepsilon)$ from each of the individual states, i.e.,

$$\sigma_{da}(T, \varepsilon) = \sum_{v=v_{min}}^{\infty} \sum_{j=j_{min}}^{\infty} N e^{-(E_v + E_j)/kT} \sigma_{da}^{v,j}(\varepsilon) \qquad \text{(VI-1)}$$

where

$$N = \left( \sum_{v=v_{min}}^{\infty} \sum_{j=j_{min}}^{\infty} e^{-(E_v + E_j)/kT} \right)^{-1}$$

and $v_{min}$ and $j_{min}$ are subject to the energy threshold requirement $\varepsilon + E_v + E_j \geq E_{threshold} = D(0 - 0) - EA(0) = 5.08 - 1.46 = 3.62$ eV. The cross section $\sigma_{da}^{v,j}(\varepsilon)$ is (O'Malley, 1966, 1967)

$$\sigma_{da}^{v,j}(\varepsilon) = \frac{4\pi^2 g}{k^2} \frac{\Gamma_{a,X}}{\Gamma_d} \left| \tilde{\chi}_v \left( R_\varepsilon - i \frac{\Gamma_a}{\Gamma_d} \right) \right|^2 e^{-\rho} \qquad \text{(VI-2)}$$

where $\tilde{\chi}_v$ is the initial vibrational wave function, k is the electron's momentum, $\Gamma_{a,X}$ is the partial autodetachment width for the state X and the rest of the symbols as defined in Eqns. (I-6) and (1-7). In his treatment O'Malley considered the effect of rotational states to be negligible and the excellent agreement of his predictions on the threshold, magnitude, width, and energy position of the $O^-/O_2$ resonance with the experimental results justifies this assumption. As T increases, higher vibrational levels are populated, the internuclear distances increase (and hence the Franck-Condon region broadens and thus the resonance width increases, whereas the resonance maximum and threshold energy decrease) significantly and although at 2000 K there is only a limited amount of vibrational excitation, there is a profound change in the survival factor $e^{-\rho}$ in Eqn. (VI-2) which dominates the temperature dependence of the cross section.

# II. RESULTS

## A. Electron Attachment Rate Constants

In Figure VI-1 are shown the total electron attachment rate constants, $k_a(\langle\varepsilon\rangle)$, as a function of $\langle\varepsilon\rangle$ for the molecule $CClF_3$ at the temperatures 300, 400, 500, and 600 K, measured in the high temperature swarm apparatus as described in Section III of Chapter II. All measurements were performed using Ar as the buffer gas. Measurements in $N_2$ were not done because of lack of knowledge of $f(\varepsilon, \langle\varepsilon\rangle)$ and the drift velocities for this gas at temperatures higher than ambient. For the monatomic gas Ar, however, there are no inelastic processes in the electron-molecule interaction over the energy range of interest and it is possible to calculate $f(\varepsilon, \langle\varepsilon\rangle)$ at every temperature, since T will then affect only the translational energy. Within the temperature and E/N range studied it was reasonable to assume that the $f(\varepsilon, \langle\varepsilon\rangle)$ functions at the higher temperatures are well approximated by the $f(\varepsilon, \langle\varepsilon\rangle)$ at room temperature. The total number densities employed were $8.86 \times 10^{19}$ molecules $cm^{-3}$ for the temperatures 300 and 400 K and $6.44 \times 10^{19}$ molecules $cm^{-3}$ for 500 and 600 K (these densities correspond to pressures at room temperature equal, respectively, to 2750 and 2000 Torr). Measurements at all temperatures were performed over a range of partial pressures of the attaching gas. In Figure VI-2 are shown typical examples of $k_a$ vs. $N_a/N_t$ (ratio of the attaching gas number density, $N_a$, over the total number density, $N_t$) for a number of $\langle\varepsilon\rangle$ and T. To remove any possible effect of the presence of the attaching gas on the $f(\varepsilon, \langle\varepsilon\rangle)$ describing the pure buffer gas (see Section III in Chapter II), the $k_a$ were extrapolated to zero $N_a$, and

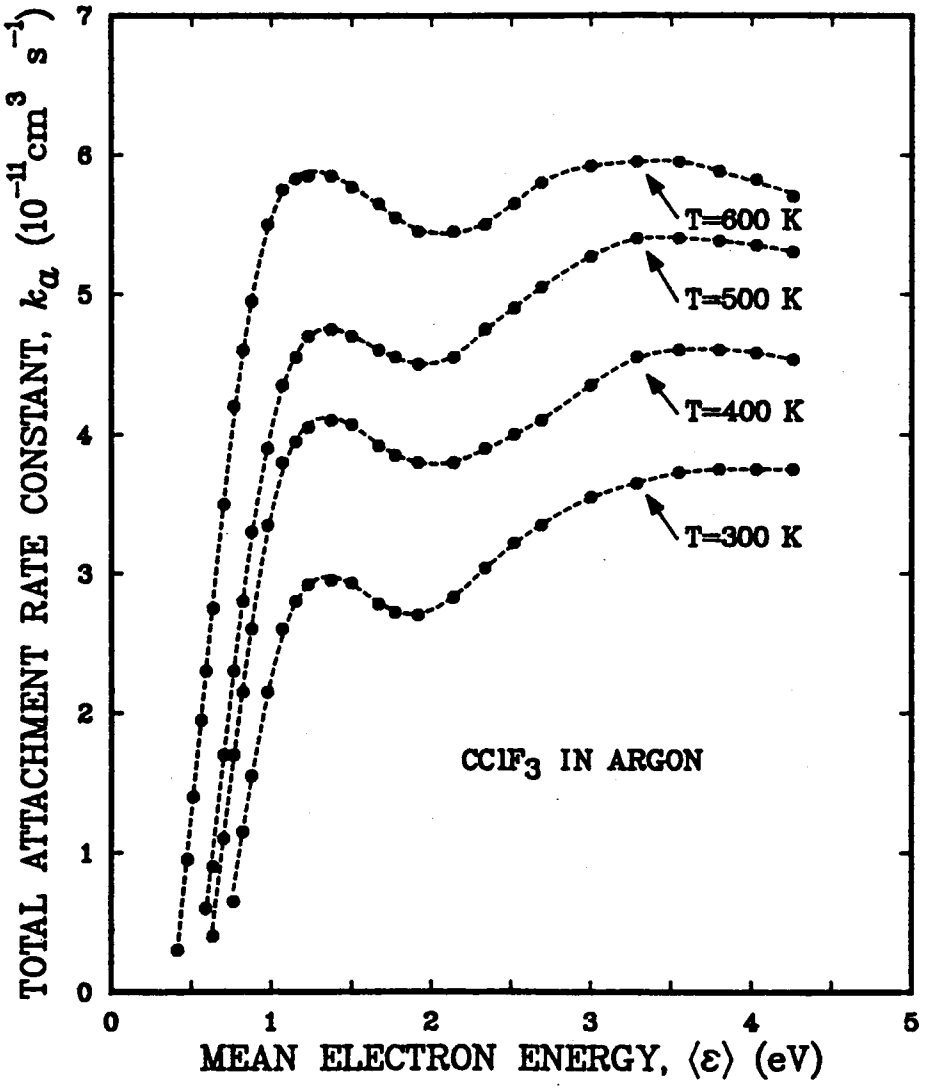


Figure VI-1. Total electron attachment rate constant, $k_a$, as a function of the mean electron energy <ε> for $CClF_3$ at 300, 400, 500, and 600 K.

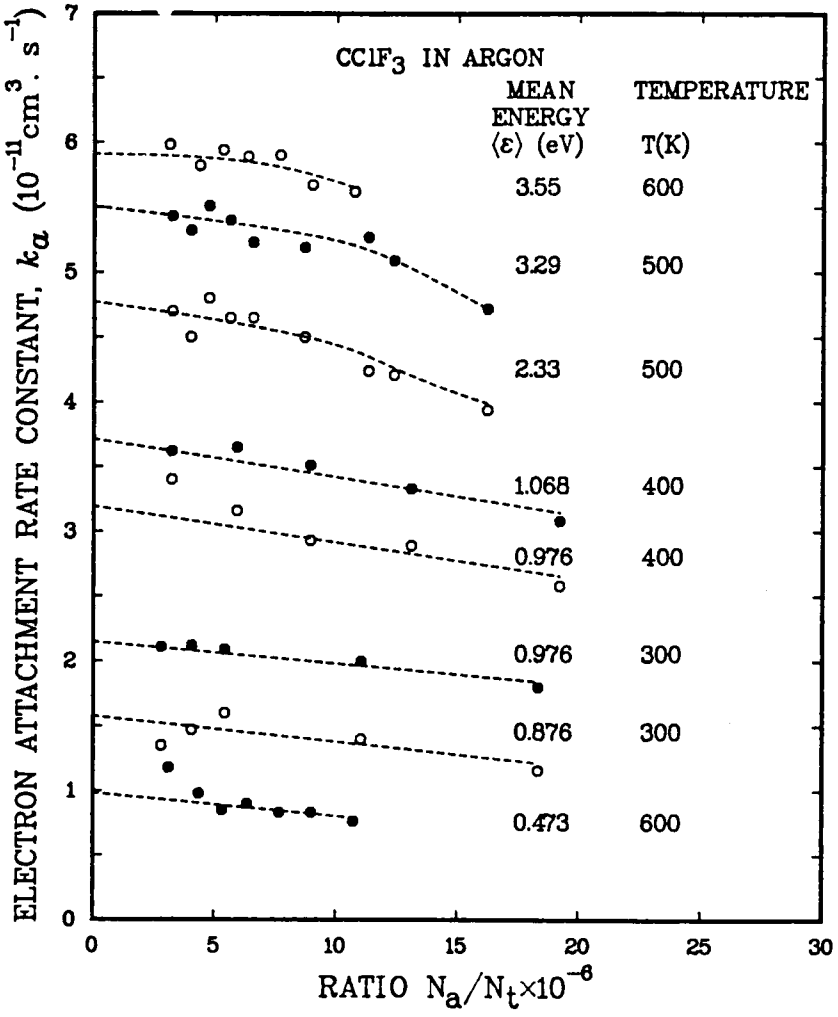


Figure VI-2. The electron attachment rate constant, $k_a$, for $CClF_3$ as a function of the ratio of the attaching gas number density, $N_a$, to the total gas number density, $N_t$, for a number of $\langle\varepsilon\rangle$ and T, extrapolated to zero $N_a$.

these are the values used in Figure VI-1 and listed in Table VI-1. It was not possible in the present study to extend the measurements to as low values of $N_a/N_t$ as $1:10^8$. The reason for this was the fact that $CClF_3$ is a very weak electron attacher, its $k_a$ ($\sim 10^{-11}$ $cm^3$ $s^{-1}$) being by four orders of magnitude less compared to the maximum value of $\sim 10^{-7}$ $cm^3$ $s^{-1}$.

B. Swarm Unfolded Cross Sections

The swarm unfolding technique (Section IIIC in Chapter II) was applied to the measured $k_a(<\varepsilon>)$ data for $CClF_3$ to obtain the total electron attachment cross section $\sigma_a(\varepsilon)$. The $\sigma_a(\varepsilon)$ for the four temperatures studied are shown in Figure VI-3 and are also tabulated in Table VI-2. These functions were obtained after 1000 unfolding iterations. Two resonance peaks are observed in the $\sigma_a(\varepsilon)$ functions shown in Figure VI-3. The magnitude and the width of the low-energy lying peak increase with increasing T and its position shift to lower energies (from 1.7 eV at 300 K to 1.3 eV at 600 K). For the high energy peak, the magnitude and position do not change noticeably with increasing T, but its lower tail becomes progressively larger. A few remarks concerning the present unfolded functions have to be made. As it was pointed out in Section IIIC, Chapter II, the swarm unfolded results should be considered with certain precautions. This is particularly true whenever there are two peaks in the unfolded cross section function, as in the present case. The unfolding procedure may then give poor results on the relative magnitude of the two peaks, depending on how close the two peaks are. An additional

Table VI-1. Electron attachment rate constant for $CClF_3$ in argon at T = 300, 400, 500, and 600 K

| E/N ($10^{-18}$ V cm$^2$) | $\langle\varepsilon\rangle_{T=300K}$ (eV) | $W_{T=300K}$ ($10^5$ cm s$^{-1}$) | $k_a$ ($10^{-11}$ cm$^3$ s$^{-1}$) T(K) | | | |
|---|---|---|---|---|---|---|
| | | | 300 | 400 | 500 | 600 |
| 0.217 | 0.412 | 1.097 | | | | 0.30 |
| 0.311 | 0.473 | 1.200 | | | | 0.95 |
| 0.373 | 0.509 | 1.258 | | | | 1.40 |
| 0.466 | 0.559 | 1.335 | | | | 1.95 |
| 0.528 | 0.590 | 1.38 | | | 0.60 | 2.30 |
| 0.621 | 0.634 | 1.44 | | 0.40 | 0.90 | 2.75 |
| 0.777 | 0.702 | 1.53 | | 1.13 | 1.70 | 3.50 |
| 0.932 | 0.764 | 1.61 | 0.65 | 1.70 | 2.30 | 4.20 |
| 1.09 | 0.822 | 1.68 | 1.15 | 2.15 | 2.80 | 4.60 |
| 1.24 | 0.876 | 1.75 | 1.58 | 2.60 | 3.30 | 4.95 |
| 1.55 | 0.976 | 1.87 | 2.15 | 3.35 | 3.90 | 5.50 |
| 1.86 | 1.068 | 1.95 | 2.60 | 3.80 | 4.35 | 5.75 |
| 2.17 | 1.152 | 2.03 | 2.80 | 3.95 | 4.55 | 5.83 |
| 2.49 | 1.23 | 2.10 | 2.92 | 4.05 | 4.70 | 5.85 |
| 3.11 | 1.37 | 2.22 | 2.95 | 4.10 | 4.75 | 5.85 |
| 3.73 | 1.50 | 2.33 | 2.93 | 4.07 | 4.70 | 5.77 |
| 4.66 | 1.67 | 2.46 | 2.78 | 3.92 | 4.60 | 5.65 |
| 5.28 | 1.77 | 2.54 | 2.72 | 3.85 | 4.55 | 5.55 |
| 6.21 | 1.92 | 2.64 | 2.70 | 3.80 | 4.50 | 5.45 |
| 7.77 | 2.14 | 2.79 | 2.83 | 3.90 | 4.55 | 5.45 |
| 9.32 | 2.33 | 2.92 | 3.04 | 4.00 | 4.75 | 5.50 |
| 10.87 | 2.52 | 3.04 | 3.22 | 4.15 | 4.90 | 5.65 |
| 12.4 | 2.69 | 3.14 | 3.35 | 4.25 | 5.05 | 5.80 |
| 15.5 | 3.00 | 3.33 | 3.57 | 4.45 | 5.27 | 5.92 |
| 18.6 | 3.29 | 3.49 | 3.67 | 4.55 | 5.40 | 5.95 |
| 21.7 | 3.55 | 3.63 | 3.73 | 4.58 | 5.40 | 5.95 |
| 24.9 | 3.80 | 3.76 | 3.72 | 4.58 | 5.38 | 5.88 |
| 27.9 | 4.03 | 3.88 | 3.70 | 4.55 | 5.35 | 5.86 |
| 31.1 | 4.26 | 3.99 | 3.67 | 4.53 | 5.30 | 5.70 |

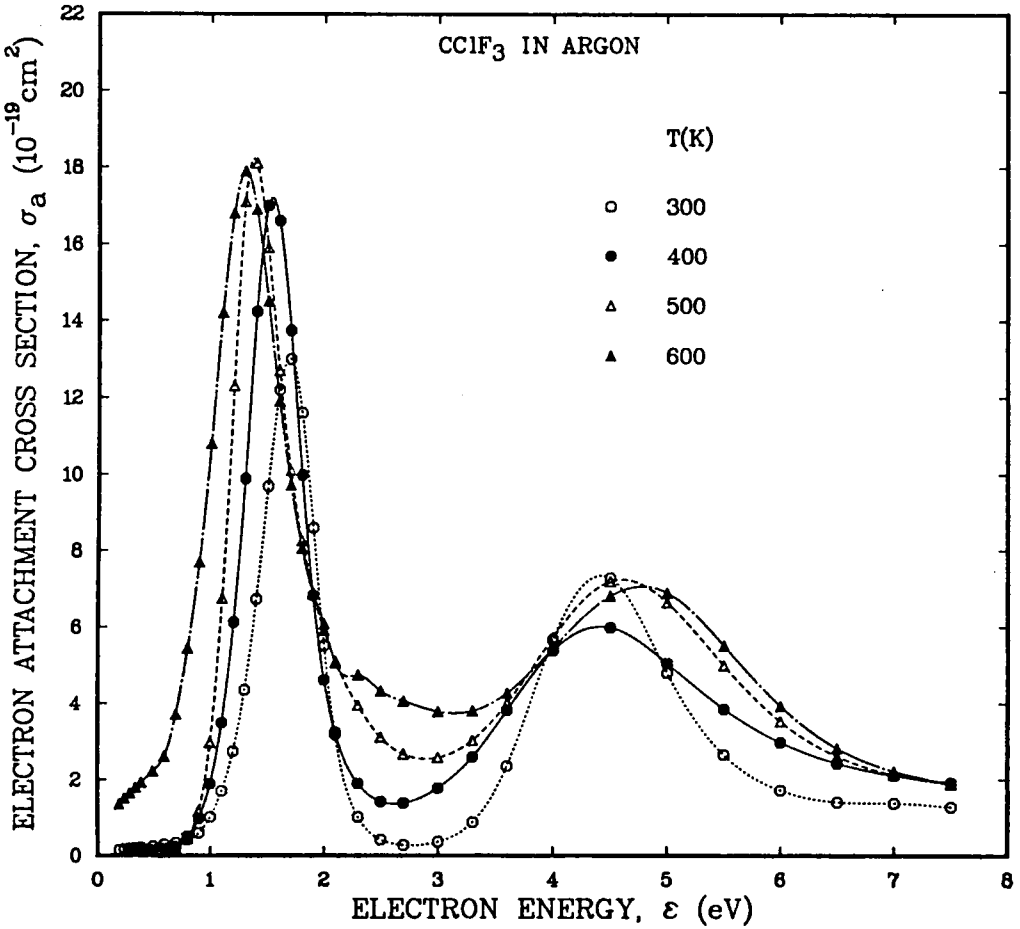


Figure VI-3. Swarm unfolded total electron attachment cross section as a function of $\varepsilon$ for $CClF_3$ at 300, 400, 500, and 600 K.

Table VI-2. Electron attachment cross section for $CClF_3$ at T = 300, 400, 500, and 600 K

| ε (eV) | $\sigma_a(\varepsilon)$ ($10^{-18}$ cm$^2$) T(K) 300 | 400 | 500 | 600 |
|---|---|---|---|---|
| 0.20 | 0.015 | | | 0.135 |
| 0.25 | 0.017 | | | 0.151 |
| 0.30 | 0.019 | 0.09 | | 0.164 |
| 0.35 | 0.020 | 0.012 | | 0.179 |
| 0.40 | 0.021 | 0.013 | | 0.192 |
| 0.5 | 0.024 | 0.015 | | 0.222 |
| 0.6 | 0.029 | 0.019 | 0.008 | 0.261 |
| 0.7 | 0.034 | 0.024 | 0.017 | 0.370 |
| 0.8 | 0.042 | 0.051 | 0.045 | 0.544 |
| 0.9 | 0.060 | 0.099 | 0.117 | 0.769 |
| 1.0 | 0.102 | 0.191 | 0.297 | 1.08 |
| 1.1 | 0.170 | 0.353 | 0.674 | 1.42 |
| 1.2 | 0.274 | 0.619 | 1.23 | 1.68 |
| 1.3 | 0.435 | 1.00 | 1.71 | 1.79 |
| 1.4 | 0.672 | 1.44 | 1.81 | 1.69 |
| 1.5 | 0.969 | 1.72 | 1.59 | 1.45 |
| 1.6 | 1.22 | 1.68 | 1.27 | 1.19 |
| 1.7 | 1.30 | 1.39 | 1.01 | 0.972 |
| 1.8 | 1.16 | 1.01 | 0.826 | 0.805 |
| 1.9 | 0.860 | 0.690 | 0.690 | 0.686 |
| 2.0 | 0.551 | 0.467 | 0.591 | 0.607 |
| 2.1 | 0.318 | 0.328 | 0.510 | 0.505 |
| 2.3 | 0.102 | 0.192 | 0.394 | 0.474 |
| 2.5 | 0.042 | 0.144 | 0.311 | 0.432 |
| 2.7 | 0.028 | 0.140 | 0.267 | 0.405 |
| 3.0 | 0.037 | 0.180 | 0.258 | 0.378 |
| 3.3 | 0.088 | 0.263 | 0.303 | 0.380 |
| 3.6 | 0.236 | 0.386 | 0.400 | 0.427 |
| 4.0 | 0.568 | 0.545 | 0.573 | 0.545 |
| 4.5 | 0.728 | 0.606 | 0.719 | 0.681 |
| 5.0 | 0.480 | 0.511 | 0.664 | 0.689 |
| 5.5 | 0.266 | 0.390 | 0.479 | 0.551 |
| 6.0 | 0.172 | 0.302 | 0.353 | 0.393 |
| 6.5 | 0.141 | 0.246 | 0.262 | 0.283 |
| 7.0 | 0.138 | 0.213 | 0.213 | 0.222 |
| 7.5 | 0.128 | 0.194 | 0.189 | 0.188 |
| 8.0 | 0.117 | 0.186 | 0.182 | 0.165 |

difficulty associated with the present $k_a$ is related to the increased random errors in the measurements. These errors are due to increased uncertainty in the measurement of the individual $k_a$ at each attaching gas number density, because of the weak attachment in $CClF_3$, and also to an uncertainty in the extrapolated values of $k_a$ to zero $N_a$. We feel that these two sources of error were the most serious in the present study. Taking into account the effect of these errors on the unfolded $\sigma_a(\varepsilon)$ it can be said that the energy position and the widths of the resonance peaks are more accurately determined rather than their magnitude. The high leading tail of the first peak in the $\sigma_a(\varepsilon)$ function at 600 K most probably is not real but is rather associated with the unfolding procedure.

C. Comparison of the Swarm with the Beam Results

The $CClF_3$ was also studied in the TOFMS to identify the negative ions produced in low-energy electron impact with this molecule. The nonunfolded and unfolded relative cross section as a function of $\varepsilon$ for the four anions $Cl^-$, $F^-$, $ClF^-$, and $CClF_2^-$ observed for $CClF_3$ are shown in Figures VI-4(a) and VI-4(b), respectively. Pertinent quantities on the relative peak intensities, energy of maximum ion intensity, FWHM and appearance onset for these anions are listed in Table VI-3, where a comparison is made with literature data. The agreement of the present results with those of Illenberger et al. (1979) is good, but with a few exceptions: Illenberger et al. reported the magnitude of the second peak in the $Cl^-$ cross section to be $\sim$ 10 times larger than that of the first peak. The beam results of Verhart et al. (1978)

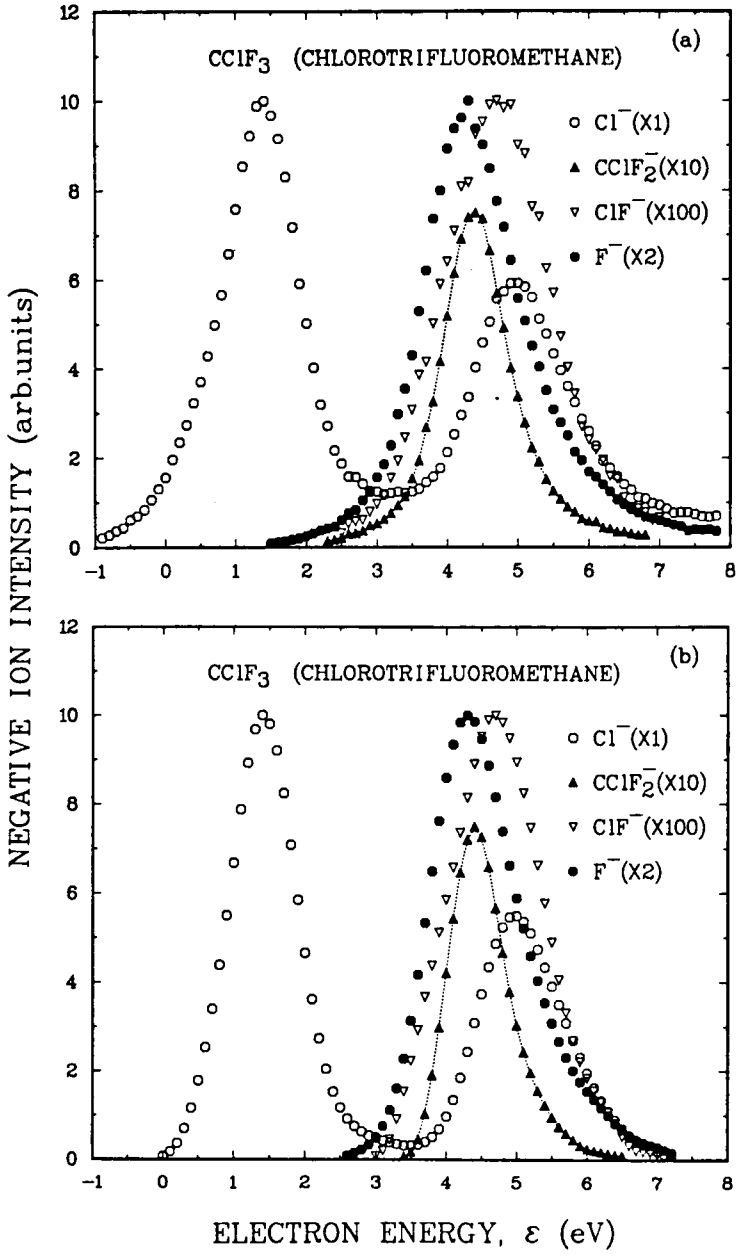


Figure VI-4. Negative ion intensity as a function of $\varepsilon$ for $CClF_3$. (a) Nonunfolded data, (b) unfolded data (note the multiplication factors).

Table VI-3. Negative ions due to low-energy electron impact on $CClF_3$

| Negative ions | Relative peak intensity | Energy of maximum ion intensity (eV)[b] | FWHM[a] (eV)[c] | Appearance onset (eV)[c] |
|---|---|---|---|---|
| $CClF_2^-$ | 75 | 4.4 ± 0.1 (4.2)[c] | 0.9 | 3.5 ± 0.15 (3.5 ± 0.3)[d] |
| $ClF^-$ | 10 | 4.7 ± 0.1 (3.9)[d] | 1.55 | 3.0 ± 0.15 (3.0 ± 0.3)[d] |
| $F^-$ | 500 | 4.3 ± 0.05 (4.1)[d] (4.3)[e] | 1.4 | 2.8 ± 0.2 (3.0 ± 0.2)[d] |
| $Cl^-$ | 1000 | 1.4 ± 0.1 (1.3)[d] (1.4)[e] | 1.1 | 0.3 ± 0.3 (0.7 ± 0.3)[d] |
| | 550 | 5.0 ± 0.1 (4.8)[d] (5.0)[e] | 1.45 | 3.8 ± 0.2 (3.4 ± 0.3)[d] |

[a]Full width at half maximum of the respective ion intensity as a function of electron energy.

[b]Energy scale calibration determined using for the $SF_5^-/SF_6$ resonance the value of 0.37 eV. The ± refers to the standard deviation from the average.

[c]Values listed are from the unfolded data.

[d]Results of E. Illenberger, H. V. Scheunemann and H. Baumgartel, Chem. Phys. 37, 21 (1979), using a trochoidal monochromator electron source. In their paper these authors report the relative energy integrated intensities.

[e]Results of C. J. Verhaart, W. J. Van der Hart and H. H. Brongersma, Chem. Phys. 34, 161 (1978), using an electron transmission experiment.

and the present beam as well as the swarm results suggest that the first $Cl^-$ resonance process is stronger than the second one. The 0.7 ± 0.3 eV onset for the low-energy process for $Cl^-$ measured by Illenberger et al. (1979) lies higher than the ∿ 0.3 ± 0.3 eV onset of the present beam study. This onset was not well reproducible in the present study and it was found to be dependent on the electron source conditions and the filament temperature. The swarm unfolded cross section supports also a higher onset for $Cl^-$.

The 3.9 eV peak position of the $ClF^-$ resonance measured by Illenberger et al. (1979) is lower by ∿ 0.8 eV compared to the 4.7 eV value of the present work, although the appearance onset for this anion was found by both studies to be the same. The present 4.7 eV value, however, is more consistent with a grouping of the peak resonance maxima of all anions observed for $CClF_3$ at 4.5 ± 0.2 eV, indicating the existence at this energy of a NISs precursor of the observed fragment anions.

The total swarm unfolded and the beam relative electron attachment cross sections for $CClF_3$ agree reasonably well in revealing the positions and the relative magnitudes of the two negative ion resonances for this molecule. From this comparison it can be said that the swarm determined $\sigma_a(\varepsilon)$ should be associated with $Cl^-$ formation at its low-energy peak, and with $Cl^-$, $F^-$, $ClF^-$, and $CClF_2^-$ formation at its second peak. The first resonance maximum in the $\sigma_a(\varepsilon)$ function (at 1.7 eV) lies by 0.3 ± 0.1 eV higher than the beam determined value of 1.4 ± 0.1 eV, but this is within the experimental

uncertainty and the accuracy of the swarm unfolding technique. The low-lying resonance as determined from the swarm study is narrower compared to the $Cl^-$ cross section function from the beam study.

## III. DISCUSSION

### A. Energetics of Dissociative Electron Attachment Processes for $CClF_3$

Before discussing the effect of T on the electron attachment processes for $CClF_3$ it is worth considering the energetics of these processes. In Table VI-4 are summarized possible fragmentation processes along with their heats of reaction leading to the formation of the four anions observed in low-energy electron impact with $CClF_3$. In the last column of the same table are also listed the excess energy, E*, of some of the proposed reactions, and the electron affinity, EA, of the radicals CCl and $CClF_2$ and are compared with literature data whenever available. All quantities were determined using the energy balance Eqns. (III-2) to (III-4) of Chapter III, as described in the footnotes of Table VI-4.

### B. Temperature Dependence of Electron Attachment to $CClF_3$

From the results presented in Section II it is apparent that the temperature does affect the $k_a(\langle\varepsilon\rangle)$ for $CClF_3$. By increasing T an overall increase in $k_a(\langle\varepsilon\rangle)$ is observed. The increase is progressively toward lower energies (Figure IV-1, p. 95). For the cross section the effect of T is more pronounced for the low-energy process, as expected. As T increases the energy position of the first resonance maximum decreases, while the resonance width and generally the magnitude

Table VI-4. Possible dissociative attachment processes leading to the formation of various anions from $CClF_3$ and thermochemical data deduced

| Ion | AO (eV) | Reaction | $\Delta H_r$[a] (eV) | Thermochemical data deduced (eV) |
|---|---|---|---|---|
| $Cl^-$ | 0.3 ± 0.3 | $e + CClF_3 \rightarrow Cl^- + CF_3$ | 0.05 | $E^* \approx 0.3 \pm 0.3$[b] (≈0.7) |
| | 3.8 ± 0.2 | $\rightarrow Cl^- + F + CF_2$ | 4.1 | |
| | | $\rightarrow Cl^- + CF_3^*$[c] | 0.05 | $E^* = 3.75 \pm 0.2$ |
| $F^-$ | 2.8 ± 0.2 | $e + CClF_3 \rightarrow F^- + CClF_2$ | 1.9 ± 0.1 | $E^* = 0.9 \pm 0.3$ (≈0.0) |
| $ClF^-$ | 3.0 ± 0.15 | $e + CClF_3 \rightarrow ClF^- + CF_2$ | (3.0 ± 0.15)[d] | $EA(ClF) \geq 2.1 \pm 0.15$[d] (1.5 ± 0.3, 1.5 ± 0.4, 2.37 ± 0.21) |
| $CClF_2^-$ | 3.5 ± 0.15 | $e + CClF_3 \rightarrow CClF_2^- + F$ | (3.6 ± 0.25) | $EA(CClF_2) \geq 1.8 \pm 0.35$[e] (1.6 ± 0.3) |

[a]Heat of reaction determined from Eqn. (III-2) using EA(Cl) = 3.61 eV, EA(F) = 3.45 eV [R. S. Berry and C. W. Reimann, J. Chem. Phys. 38, 1540 (1963)] and the following values (in eV) for the $\Delta H_f$ of $CClF_3$ (-7.34) [S. S. Chen, R. C. Wilhoit and B. J. Zwolinski, J. Phys. Chem. Ref. Data 5, 571 (1976)], Cl (1.26), F( 0.82), $CF_4$ (-4.94)[J. L. Franklin, J. G. Dillard, H. M. Rosenstock, J. T. Herron, K. Draxl and F. H. Field, NSRDS-NBS26 (1969)], $CClF_2$ (-2.79 ± 0.1) [L. M. Leyland, J. R. Majer and J. C. Robb, Trans. Faraday Soc. 66, 898 (1970)], ClF (-0.54) [A. G. Gaydon, Dissociation Energies and Spectra of Diatomic Molecules, 3rd ed. (Chapman and Hall, London, 1968)]. Numbers in parentheses were obtained using the EA values listed in the last column of this table.

[b]Excess energy determined from Eqn. (III-3). Numbers in parentheses are values measured by E. Illenberger, Ber. Bunsenges. Phys. Chem. 86, 252 (1982).

[c]Asterisk indicates internal excitation of the $CF_3$ radical.

[d]Electron affinity determined from Eqn. (III-2) using $\Delta H_r$ = AO($ClF^-$) = 3.0 ± 0.15 eV and the $\Delta H_f$ values given in footnote a of this table. Numbers in parentheses are, respectively, the values of H. Dispert and K. Lacmann, Int. J. Mass Spectrom. Ion Phys. 28, 49 (1978), J. C. J. Thynne, Dyn. Mass Spectrom. 3, 67 (1972) and A. V. Dudin, L. N. Gorokhov and A. V. Baluev, Bull. Acad. Sci. USSR Div. Chem. Sci. Engl. Transl. 28, 2227 (1979).

[e]Electron affinity determined from Eqn. (III-4) using for the dissociation energy D(F-$CClF_2$) the value of 5.3 ± 0.2 eV (Table III-8). The number in parentheses is the value of H. Dispert and K. Lacmann, Int. J. Mass Spectrom. Ion Phys. 28, 49 (1978).

of the cross section increase (Figure VI-3 (p. 148). This behavior is analogous to that of $O^-/O_2$ discussed in Section I. It can thus be understood in the framework of O'Malley's (1967) theoretical treatment. From the results in Section II it was clear that the first peak in the $\sigma_a(\varepsilon)$ is associated exclusively with $Cl^-$ production. We may then consider that in the energy range below $\sim$ 2.5 eV, the $Cl^-$ formation from $CClF_3$ can be described by a diatomic-like molecule picture. The CCl stretching vibrational frequency is 781 $cm^{-1}$ (0.097 eV) Shimanouchi, 1972). Assuming a Boltzmann distribution describing the population of internally excited states in the $CClF_3$ molecule, even at 300 K, 2% of the molecules are in the first vibrational state, whereas at 600 K, $\sim$ 15% of the molecules are excited to the same state. Therefore the effect of increasing T on the electron attachment to $CClF_3$ can be attributed to population of higher vibrational levels and hence broadening of the Franck-Condon region (compared with similar discussion for $O_2$ at the end of Section I). The effect of rotational excitation cannot be excluded but its contribution cannot be assessed.

In Figure VI-5(a) the log $k_a$ versus 1/T is plotted for five mean electron energies $\langle\varepsilon\rangle$. Within the accuracy of the data [see error bars in Figure VI-5(a)] and over the temperature range studied (300 to 600 K) the plots are seen to be straight lines. Similar straight lines [not shown in Figure VI-5(a)] were obtained for other values of $\langle\varepsilon\rangle$. From these results the $k_a(\langle\varepsilon\rangle)$ as a function of $\langle\varepsilon\rangle$ and T can be well described by the Arrhenius expression

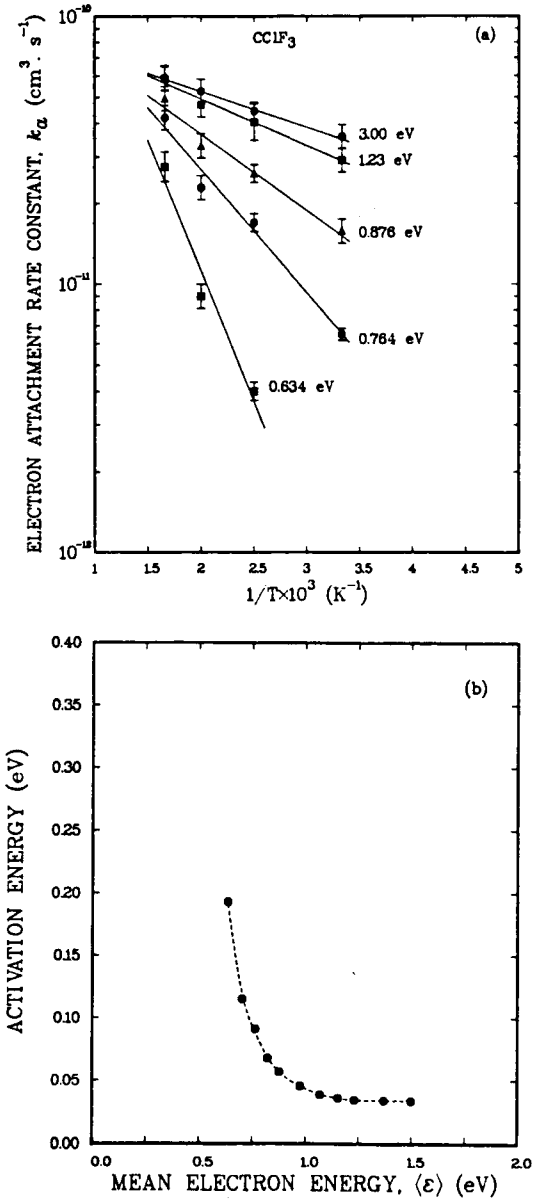


Figure VI-5. (a) Plot of the electron attachment rate constant, $k_a$, versus 1/T for a number of mean electron energies, $\langle\varepsilon\rangle$; (b) plot of the activation energy, $D(\langle\varepsilon\rangle)$, versus $\langle\varepsilon\rangle$ in dissociative electron attachment to $CClF_3$.

$$k_a(\langle\varepsilon\rangle, T) = C(\langle\varepsilon\rangle) \exp[-D(\langle\varepsilon\rangle)/kT] \ . \qquad \text{(VI-3)}$$

The value of the pre-exponential factor $C(\langle\varepsilon\rangle)$ and the $D(\langle\varepsilon\rangle)$ were calculated from straight lines similar to those shown in Figure VI-5(a). In Figure VI-5(b) values of $D(\langle\varepsilon\rangle)$ are plotted against $\langle\varepsilon\rangle$. Henderson et al. (1969) used an expression similar to that in Eqn. (VI-3) for the cross section of $O^-/O_2$ and they argued that such description is expected when the energy levels are sufficiently closed spaced. O'Malley, in his treatment of the same dissociative process for $O^-/O_2$, gave a physical interpretation of the activation energy $D(\langle\varepsilon\rangle)$. He interpreted the $D(\langle\varepsilon\rangle)$ as the average internal energy (vibrational and rotational) of the molecule which maximizes the cross section in Eqn. (VI-1). A similar interpretation can be given to the $D(\langle\varepsilon\rangle)$ plotted in Figure VI-5(b). From the discussion presented in Section II we concluded that a reliable value for the $Cl^-$ onset is $0.7 \pm 0.3$ eV, although the asymptotic limit for this process lies at $\sim 0.05$ eV (Table VI-4). Figure VI-5(b) does show that when the mean electron energy is 0.7 eV, an activation (internal) energy of $\sim 0.1$ eV is necessary to raise the system above the threshold. As $\langle\varepsilon\rangle$ becomes progressively lower then $D(\langle\varepsilon\rangle)$ becomes progressively larger [see Figure VI-5(b)].

These findings confirm the correctness of the diatomic-like picture adopted for the low-energy dissociation process observed in $CClF_3$. They also confirm the assumption of the Arrhenius dependence of $k_a(\langle\varepsilon\rangle)$ on $\langle\varepsilon\rangle$ and T. Studies of the same molecule at higher T are recommended and they will be undertaken in the very near future.

# CHAPTER VII

## SUMMARY AND CONCLUSIONS

Attachment of low-energy electrons (0-10 eV) to three series of polyatomic molecules has been studied using a time-of-flight mass spectrometer. The mass spectrometric study of each molecule included mass identification of the negative ions formed from the molecule, measurement of the intensity of each observed negative ion as a function of electron energy, and measurement of the autodetachment lifetime, $\tau_a$, of the long-lived ($\tau_a$ > 1 μs) metastable anions. The effect of the broad electron energy distribution on the measured relative cross sections was removed by an unfolding procedure. In addition, a high temperature electron swarm apparatus was constructed and used to study the effect of temperature on electron attachment to the $CClF_3$ molecule. The results obtained by both experiments provided the basis of investigating various aspects of the attachment of low-energy electrons to polyatomic molecules.

In the first series of molecules, including the normal perfluoralkanes (PFAs) n-$C_NF_{2N+2}$ (N = 1-6), the effect of molecular size on negative ion formation was investigated. It was found that low-energy electrons attach to these molecules dissociatively and/or nondissociatively. Which mode of electron attachment predominates depends on the size of the molecule. For the lower PFAs ($CF_4$, $C_2F_6$ and $C_3F_8$) only fragment negative ions were observed, $F^-$ being the

most abundant. For n-$C_4F_{10}$ a weak parent ion was detected, but again the predominant anion was $F^-$. For the higher members of the series (n-$C_5F_{12}$, n-$C_6F_{14}$) the parent anions were formed and were most intense than any of the fragment negative ions with relative cross sections peaking at $\sim$ 0.6 eV. The $\tau_a$ of the long-lived parent anion of n-$C_4F_{10}$, n-$C_5F_{12}$, and n-$C_6F_{14}$—21, 49, and 53 μs at 0.6 eV, respectively—was found to increase with increasing molecular size and to decrease with increasing electron energy. In slow-electron-PFA molecule collisions, in addition to $F^-$, other fragment anions were observed of the form $C_NF^-_{2N+1}$, $C_NF^-_{2N}$, and $C_NF^-_{2N-1}$ with N = 1-6. The position of the dissociating negative ion states (NISs) shifted to lower energies with increasing size of the molecule. Energetic considerations were used to identify possible fragmentation mechanisms of the NISs leading to the production of the observed fragment anions. From the appearance onsets of a number of fragment negative ions, various C-C and C-F bond dissociation energies, heats of formation, and electron affinities, EA, of certain fragments have been determined and reported. It was found that the EA of perfluorocarbon radicals increases with increasing size of these radicals, and similar behavior was indicated also for the perfluoroalkane molecules themselves. The separation times of the dissociating fragments and the autodetachment lifetimes of the extremely short-lived ($\sim 10^{-15}$ s) and dissociating NISs of $CF_4$ and $C_2F_6$ were estimated. The energy position of the dissociating NISs and the relative intensities of the fragment negative ions were rationalized on the basis of the present work and relevant data from electron swarm data measurements.

In the second series of molecules, i-$C_4F_{10}$, i-$C_5F_{12}$, neo-$C_5F_{12}$, and c-$C_5F_{10}$, the possible effect(s) of geometrical structure of a molecule on its electron attaching properties was investigated. All four molecules were found to attach slow electrons dissociatively and non-dissociatively. For the first three above molecules, the parent anion cross section, as in the case of the normal PFAs, was found to peak at the same energy of $\sim$ 0.6 eV independently of the size or geometry of the molecule. However, for c-$C_5F_{10}$ [and generally for cyclic and unsaturated perfluorocarbons with four or more carbon atoms [see also Sauers et al. (1979)] the parent anion was found to peak at $\sim$ 0.0 eV. No obvious correlation was found between the geometrical structure of the molecule and the energy position of the dissociating NISs. But a dramatic effect was observed of the structure of the molecule on the relative intensity of the fragment anions as compared between themselves and to the parent anions. To understand these differences, we proposed that what affects crucially the probability by which the transient anion intermediate decays to the various channels, is the way as well as how fast the excess energy (comprised of the incident electron kinetic energy and the EA of the molecule) is distributed among the various degrees of freedom of the molecule. It is expected that these two latter factors depend strongly on the symmetry of the molecule.

The third series of molecules, four fluoroethers ($CF_3OCF_3$, $CF_3OCF_2H$, $CF_2HOCF_2H$, and $CF_3OCH_3$) and two fluorosulphides ($CF_3SCF_3$ and $CF_3SCH_3$), provided the basis to study the effect of atomic substitution in the molecule on its electron attaching properties. All

six molecules were found to attach electrons dissociatively. The types and relative intensities of these fragment anions were found to depend strongly on the number and relative position of the F atom in the molecule and on the O to S substitution. The molecules having one or both of the methyl groups partially fluorinated were more fragile upon electron impact compared with the molecules for which all the atoms of the methyl group are of one kind (H or F). The fluorosulphides attached lower energy electrons than did the fluoroethers. The magnitudes of the total attachment cross sections (determined by the swarm-beam method) increased with increasing F substitution. Energetic considerations were used to identify possible fragmentation mechanisms of the dissociating NISs leading to the production of the observed fragment anions and to deduce EA of the radicals $CF_3O$ and $CF_3S$. CNDO/2 calculations were performed in an effort to rationalize the findings of this study concerning the types, relative intensities and energy positions of the various anions observed. It was found that the S atom lowered the energy position of the NISs of the molecule and it introduced preferred electrophilic sites in the molecule, thus affecting the way the molecule attached the electron and dissociated.

The electron attachment rate constant, $k_a$, for $CClF_3$ in the buffer gas Ar in the mean electron energy range $\sim$ 0.5 to 4.26 eV was measured at the temperatures 300, 400, 500, and 600 K, using the high temperature swarm apparatus. From the measured $k_a$, the electron attachment cross section, $\sigma_a$, at each temperature studied was calculated by applying the swarm-unfolding technique. Two peaks at $\sim$ 1.5

and 4.5 eV, respectively, were found in the unfolded $\sigma_a$. From a comparison of the swarm and the beam results, the first peak was attributed to $Cl^-$ formation. The width and the onset of the first resonance peak increased with increasing T, whereas its position shifted to lower energies. These findings were understood in the framework of O'Malley's (1967) theory as due to population of excited vibrational (and/or rotational) levels. The Arrhenius dependence of $k_a$ on T was invoked to calculate activation energies for the $Cl^-$ production at various mean energies.

The present work indicated the need for further theoretical and experimental work. The theoretical work should be extended to tackle problems in negative ion formation in polyatomic molecules. In this regard, measurements of the autodetachment lifetimes as a function of electron energy (using energy resolution down to 100 mV) and as a function of T and/or the internal excitation of the molecule will be helpful.

# LIST OF REFERENCES

## LIST OF REFERENCES


Allan, M. and Wong, S. F. (1978). Phys. Rev. Lett. 41, 1791.

Allan, M. and Wong, S. F. (1981). J. Chem. Phys. 74, 1687.

Allen, J. D. and Grimm, F. A. (1979). Chem. Phys. Lett. 66, 72.

Bardsley, J. N. and Mandl, F. (1968), Rep. Prog. Phys. 31, 471.

Bardsley, J. N., Herzenberg, A., and Mandl, F. (1964). In Atomic Collision Processes. (M. R. C. McDowell, ed.), North Holland Publishing Co., Amsterdam.

Bardsley, J. N., Herzenberg, A., and Mandl, F. (1966). Proc. Phys. Soc. (London) 89, 321.

Bennett, C. L., Beukens, R. P., Clover, M. R., Gove, H. E., Liebert, R. B., Litherland, A. E., Purser, K. H., and Sondheim, W. E. (1977). Science 198, 508.

Benson, S. W. and O'Neal, H. E. (1970). NSRDS-NBS 21.

Berry, R. S. and Reimann, C. W. (1963). J. Chem. Phys. 38, 1540.

Bibby, M. M. and Carter, G. (1963). Trans. Faraday, Soc. 59, 2455.

Bortner, T. E. and Hurst, G. S. (1958). Health Phys. 1, 39.

Bryant, W. M. d. (1962). J. Polym. Sci. 56, 277.

Burns, J. F. (1964). In Atomic Collision Processes. (M. R. C. McDowell, ed.), North Holland Publishing Co., Amsterdam.

Castelman, A. W. and Keesee, R. C. (1981). In Electron and Ion Swarms (L. G. Christophorou, ed.). Pergamon Press, New York.

Chaney, E. L. and Christophorou, L. G. (1969). J. Chem. Phys. 51, 883.

Chantry, P. J. (1969). J. Chem. Phys. 51, 3369.

Chen, J. C. Y. (1967). Phys. Rev. 156, 12.

Chen, J. C. Y. and Peacher, J. L. (1967). Phys. Rev. 163, 103.

Chen, C. L. and Chantry, P. J. (1970). Bull. Am. Phys. Soc. 15, 418.

Chen, C. L. and Chantry, P. J. (1972). Bull. Am. Phys. Soc. 17, 1133.

Chen, C. L. and Chantry, P. J. (1979). J. Chem. Phys. 71, 3897.

Chen, S. S., Wilhoit, R. C., and Zwolinski, B. J. (1976). J. Phys. Chem. Ref. Data 5, 571.

Christodoulides, A. A. and Christophorou, L. G. (1970). Oak Ridge National Laboratory Report ORNL/TM-3163.

Christodoulides, A. A., Christophorou, L. G., Pai, R. Y., and Tung, C. M. (1979). J. Chem. Phys. 70, 1156.

Christodoulides, A. A., McCorkle, D. L., and Christophorou, L. G. (1983). In Electron-Molecule Interactions and Their Applications (L. G. Christophorou, ed.). Academic Press, New York (in press).

Christophorou, L. G. (1971). Atomic and Molecular Radiation Physics. Wiley-Interscience, New York.

Christophorou, L. G. (1978). Adv. Electron. and Electron Phys. 46, 55.

Christophorou, L. G. (1980). Environ. Health Perspect. 36, 3.

Christophorou, L. G., ed. (1983). Electron-Molecule Interactions and Their Applications, Vols. I and II. Academic Press, New York (in press).

Christophorou, L. G. and Siomos, K. (1983). In Electron-Molecule Interactions and Their Applications (L. G. Christophorou, ed.). Academic Press, New York (in press).

Christophorou, L. G. and Hunter, S. R. (1983). In Electron-Molecule Interactions and Their Applications (L. G. Christophorou, ed.). Academic Press, New York (in press).

Christophorou, L. G., McCorkle, D. L., and Carter, J. G. (1971a). J. Chem. Phys. 54, 253.

Christophorou, L. G., McCorkle, D. L., and Anderson, V. E. (1971b). J. Phys. B 4, 1163.

Christophorou, L. G., Hadjiantoniou, A., and Carter, J. G. (1973). J. Chem. Soc. Faraday Trans. II 69, 1713.

Christophorou, L. G., Gant, K. S., and Anderson, V. E. (1977). J. Chem. Soc. Faraday Trans. II 73, 804.

Christophorou, L. G., McCorkle, D. L., Maxey, D. V., and Carter, J. G. (1979). Nucl. Instr. Meth. 163, 141.

Christophorou, L. G., James, D. R., and Pai, R. Y. (1982a). In Applied Atomic Collision Physics—Special Topics, Vol. 5 (H. S. W. Massey, E. W. McDaniel, and B. Bederson, eds.). Academic Press, New York.

Christophorou, L. G., McCorkle, D. L., and Sauers, I. (1982b). Analytica. Chem. Acta 135, 179.

Christophorou, L. G., James, D. R., Sauers, I., Pace, M. O., Pai, R. Y., and Fatheddin, A. (1982c). In Gaseous Dielectrics III (L. G. Christophorou, ed.). Pergamon Press, New York, 151.

Christophorou, L. G., Hunter, S. R., Carter, J. G., and Mathis, R. A. (1982d). Appl. Phys. Lett. 41, 147.

Christophorou, L. G., McCorkle, D. L., and Christodoulides, A. A. (1983). In Electron-Molecule Interactions and Their Applications (L. G. Christophorou, ed.). Academic Press, New York (in press).

Chutjian, A. (1981). Phys. Rev. Lett. 46, 1511.

Coburn, J. W. and Winters, H. F. (1979). J. Vac. Sci. Technol. 16, 391.

Collins, P. M., Christophorou, L. G., and Carter, J. G. (1973). Oak Ridge National Laboratory Report ORNL/TM-2614.

Compton, R. N., Christophorou, L. G., Hurst, G. S., and Reinhardt, P. W. (1966). J. Chem. Phys. 45, 4634.

Cottrell, T. L. (1958). The Strength of Chemical Bonds. Butterworths Scientific Publications, London.

Creitz, E. C. (1961). J. Res. Nat. Bur. Stand. 65A (No. 4), 389.

Czarnowski, J., Castellano, E., and Schumacher, H. J. (1968). Chem. Commun., 1255.

Danilov, A. D. (1970). Chemistry of the Ionosphere (Translated from the Russian). Plenum Press, New York.

Darwent, B. (1970). NSRDS-NBS 31.

DeCopro, J. J. and Franklin, J. L. (1971). J. Chem. Phys. 54, 1885.

DeCopro, J. J., Bafus, D. A., and Franklin, J. L. (1971). J. Chem. Phys. 54, 1592.

Dewar, M. J. S. and Rzepa, H. S. (1978). J. Am. Chem. Soc. 100, 784.

Dispert, H. and Lacmann, K. (1978). Int. J. Mass Spectrom. and Ion Phys. 28, 49.

Dougherty, R. C. (1981). Anal. Chem. 53, 628A.

Dudin, A. V., Gorokhov, L. N., and Buluev, A. V. (1979). Bull. Acad. Sci. USSR. Div. Chem. Sci. Engl. Transl. 28, 2227.

Fehsenfeld, F. C. (1970). J. Chem. Phys. 53, 2000.

Ferguson, E. E. (1968). In Advances in Electronics and Electron Physics, Vol. 24. Academic Press, New York.

Ferguson, E. E. (1969). Can. J. Chem. 47, 1815.

Ferguson, E. E. (1974). Revs. Geophys. Space Phys. 12, 703.

Field, F. H. (1980). Proc. 28th Annual Conf. on Mass Spectr. Allied Topics, May 25-30, 1980, New York, American Society for Mass Spectrometry, 2.

Fite, W. L. and Brackmann, R. T. (1963). Proc. Sixth Int. Conf. on the Ionization Phen. in Gases, Paris, 1, 21.

Fite, W. L., Brackmann, R. T., and Henderson, W. R. (1965). Proc. Fourth Int. Conf. on the Phys. of Electron and Atomic Coll. Science, Bookcrafters, Inc., Hastings-on-Hudson, New York, 100.

Forst, W. (1973). Theory of Unimolecular Reactions. Academic Press, New York.

Fox, R. E., Hickam, W. H., Grove, D. J., and Kjeldaas, T. (1955), Rev. Sci. Instr. 26, 1101.

Franklin, J. L. (1976). Science 193, 725.

Franklin, J. L., Dillard, J. G., Rosenstock, H. M., Herron, J. T., Draxl, K., and Field, F. H. (1969). NSRDS-NBS 26.

Gaydon, A. G. (1968). Dissociation Energies and Spectra of Diatomic Molecules, 3rd ed. Chapman and Hall, London.

Greene, D. B., Halprin, E. A., and Skofronick, J. G. (1975). Rev. Sci. Instr. 46, 136.

Greenhaus, H. L. (1965). "Negative Ion Formation by Electron Impact in Some Perfluoroalkanes," University Microfilms, Ann Arbor, Michigan.

Gordon, S. M., Haarhoff, P. C., and Krige, G. J. (1969). Int. J. Mass Spectrom. Ion Phys. 3, 13.

Hadjiantoniou, A., Christophorou, L. G., and Carter, J. G. (1973). Oak Ridge National Laboratory Report ORNL/TM-3990.

Hammond, P. R. (1970). J. Chem. Phys. 55, 3468.

Harland, P. W. and Thynne, J. C. L. (1969). J. Phys. Chem. 74, 52.

Harland, P. W. and Thynne, J. C. J. (1972). Int. J. Mass Spectrom. Ion Phys. 9, 253.

Harland, P. W. and Thynne, J. C. J. (1973). Int. J. Mass Spectrom. Ion Phys. 11, 445.

Harland, P. W. and Franklin, J. L. (1974). J. Chem. Phys. 61, 1621.

Hastie, J. W. and Hargrave, J. L. (1969). J. Phys. Chem. 73, 1105.

Henderson, W. R., Fite, W. L., and Brackmann, R. T. (1969). Phys. Rev. 183, 157.

Hickam, W. M. and Fox, R. E. (1956). J. Chem. Phys. 25, 642.

Hickam, W. M. and Berg, D. (1958). J. Chem. Phys. 29, 517.

Hunter, S. R. and Christophorou, L. G. (1983). J. Chem. Phys. (to be published).

Hunter, S. R., Christophorou, L. G., McCorkle, D. L., Sauers, I., Ellis, H. W., and James, D. R. (1983). J. Phys. D 16, 573.

Illenberger, E. (1982). Ber. Bunsenges. Phys. Chem. 76, 252.

Illenberger, E., Scheunemann, H. U., and Baumgartel, H. (1979). Chem. Phys. 37, 21.

James, D. R., Christophorou, L. G., and Mathis, R. A. (1980). In Gaseous Dielectrics II (L. G. Christophorou, ed.). Pergamon Press, New York.

JANAF Thermochemical Tables. (1969) (D. R. Stull, ed.). Dow Chemical Company, Midland, Michigan.

Johnson, J. P. (1977). Ph.D. Dissertation, University of Tennessee, Knoxville.

Johnson, J. P., Christophorou, L. G., and Carter, J. G. (1977). J. Chem. Phys. 67, 2196.

Kemmitt, R. D. W. and Sharp, D. W. (1965). Adv. Fluorine Chemistry 4, 216.

Klots, C. E. (1967). J. Chem. Phys. 46, 1197.

Koopmans, T. (1933). Physica 1, 104.

Kopp, M. K., Valentine, K. H., Christophorou, L. G., and Carter, J. G. (1982). Nucl. Instr. Meth. 201, 395.

Lane, N. F. (1980). Rev. Mod. Phys. 52, 29.

Leyland, L. M., Majer, J. R., and Robb, J. C. (1970). Trans. Faraday Soc. 66, 898.

Lifshitz, C. and Crajower, R. (1969). Int. J. Mass Spectrom. Ion Phys. 3, 211.

Luft, P. E. (1975). "Description of a Backward Prolongation Program for Computing Transport Coefficients." JILA Report No. 14, University of Colorado, Boulder, Colorado.

MacNeil, K. A. G. and Thynne, J. C. J. (1969). Int. J. Mass Spectrom. Ion Phys. 3, 35.

MacNeil, K. A. G. and Thynne, J. C. J. (1970). Int. J. Mass Spectrom. Ion Phys. 3, 455.

Mahan, B. H. and Young, C. E. (1966). J. Chem. Phys. 44, 2192.

Marmet, P. (1974). Can. J. Phys. 42, 2102.

Massey, H. W. W. (1976). Negative Ions. Cambridge University Press, London.

Massey, H. S. W., McDaniel, E. W., and Bederson, B., eds. (1982). Applied Atomic Collision Physics—Special Topics, Vols. 1-5. Academic Press, New York.

McConnell, J. C. and Schiff, H. I. (1978). Science 199, 174.

McCorkle, D. L. and Christophorou, L. G. (1972). Oak Ridge National Laboratory Report ORNL/TM-3839.

McCorkle, D. L., Szamrej, I., and Christophorou, L. G. (1982). J. Chem. Phys. 77, 5542.

Mills, R. M. (1968). Combustion and Flame 12, 513.

Naff, W. T. (1972). Oak Ridge National Laboratory Report ORNL/TM-3410.

Noble, P. N. and Kortzeborn, R. N. (1970). J. Chem. Phys. 52, 5375.

O'Malley, T. F. (1966). Phys. Rev. 150, 14.

O'Malley, T. F. (1967). Phys. Rev. 155, 59.

Page, F. M. and Goode, G. C. (1969). Negative Ions and the Magnetron. Wiley-Interscience, New York.

Phelps, A. V. (1979). In Electron-Molecule Scattering (S. C. Brown, ed.). Wiley-Interscience, New York.

Pople, J. A. and Beveridge, D. L. (1970). Approximate Molecular Orbital Theory. McGraw-Hill, New York.

Rademacher, J. F. (1974). Ph.D. Dissertation, University of Tennessee, Knoxville.

Reese, R. M., Dibeler, V. H., and Mohler, F. L. (1956). J. Res. Nat. Bur. Stand. 57, 367..

Robin, M. B. (1974). Higher Excited States of Polyatomic Molecules, Vol. I. Academic Press, New York.

Robinson, P. J. and Holbrook, K. A. (1972). Unimolecular Reactions. Wiley-Interscience, New York.

Rosenstock, H. M., Draxl, K., Steiner, B. W., and Herron, J. T. (1977). J. Phys. Chem. Ref. Data 6, Suppl. No. 1.

Sauers, I., Christophorou, L. G., and Carter, J. G. (1979). J. Chem. Phys. 71, 3016.

Schulz, G. J. (1960). J. Appl. Phys. 31, 1134.

Schulz, G. J. (1973). Rev. Mod. Phys. 45, 378.

Shimamori, H. and Fessenden, R. W. (1979). J. Chem. Phys. 70, 1137.

Shimanouchi, T. (1972). Tables of Molecular Vibrational Frequencies, Vol. I. NSRDS-NBS 39.

Simpson, J. A. (1961). Rev. Sci. Instr. 32, 1283.

Spence, D. and Schulz, G. J. (1969). Phys. Rev. 188, 280.

Spence, D. and Schulz, G. J. (1973). J. Chem. Phys. 58, 1800.

Spyrou, M. S., Hunter, S. R., and Christophorou, L. G. (1983). J. Chem. Phys. (to be published).

Szent-Gyorgyi, A. (1968). Bioelectronics. Academic Press, New York.

Thynne, J. C. J. In Dynamic Mass Spectrometry, Vol. 3. (D. Price, ed.). Herden and Son, Ltd., London.

Thynne, J. C. J. and MacNeil, K. A. G. (1970). Int. J. Mass Spectrom. Ion Phys. 5, 95.

Verhaart, C. J., Van der Hart, W. J., and Brongersma, H. H. (1978). Chem. Phys. 34, 161.

Warman, J. M. and Sauer, M. C., Jr. (1971). Int. J. Radiat. Phys. Chem. 3, 273.

Wegener, P. P. (1974). Molecular Beams and Low Density Gasdynamics. Marcel-Dekker, New York.

Wentworth, W. E., Becker, R. S., and Tung, R. (1967). J. Phys. Chem. 71, 1652.

Wentworth, W. E., George, R., and Keith, H. (1969). J. Chem. Phys. 51, 1791.

Wiley, W. C. and McLaren, I. H. (1955). Rev. Sci. Instr. 26, 1150.

# VITA

Spyros M. Spyrou was born in Omodhos, Limassol, Cyprus, on January 12, 1954. He graduated from high school in 1972. After two years of service in the Cyprus army, he entered the University of Athens, Greece, in September 1974. He received a Bachelor of Science degree in Physics from that University in July 1978.

In September 1978 he began graduate studies in the Department of Physics at The University of Tennessee, Knoxville. He received the degree of Doctor of Philosophy in Physics in December 1983.

He is married to Chrysanthi of Athens, Greece, and he has two daughters, Marina and Sophia.